Imperial College of Science, Technology and Medicine
Department of Physics

# Probing the response of quantum plasmonic systems: from the macroscopic to the microscopic

Kyle McEnery

Submitted in part fulfilment of the requirements for the degree of
Doctor of Philosophy in Physics of the Imperial College London August 2014

# Abstract

In this thesis we investigate the response of plasmonic systems in a quantum optics setting. This work can be grouped into two sub-investigations, the study of macroscopic and microscopic responses. The narrative of the thesis comprises three principal parts. First, we give an in-depth review of the field of quantum plasmonics as it is an important theme that runs through the work contained in this thesis. In particular, we focus on outlining the cutting edge research that is being done on the intense interactions between plasmonic systems and quantum emitters. This leads naturally to the first investigation into the macroscopic response of quantum plasmonic systems in a metamaterial setting. We outline how complex hybrid systems of plasmonic metal nanoparticles (MNP) and two-level quantum dots (QD) can be used to create a quantum plasmonic metamaterial. Metamaterials are structures composed of periodic lattices of identical subwavelength unit cell scatterers, each of which governs completely the electromagnetic properties of the entire bulk material. We theorize the use of MNP-QD nanorings as a unit cell in order to control the macroscopic magnetic properties of the metamaterial. We outline how such a metamaterial can have a tunable, and saturable, magnetic permeability. In the last part of the thesis we consider the model of a single light mode interacting ultrastrongly with a collection of emitters, in the anticipation that quantum plasmonic systems can be brought into this ultrastrong-coupling regime (USC). In particular we study the emission of the system after the coupling between the light mode and the emitters is non-adiabatically switched-on. We find evidence that for both two-level, and multi-level, emitters in the USC, *both* the counter-rotating terms and the diamagnetic term must be included to prevent qualitative errors.

## Acknowledgements

I would first like to thank my two supervisors, Myungshik Kim and Stefan Maier. I have benefited greatly from their vast experience and their generous support. I am deeply indebted to you both for all the opportunities you have given me. I would also like to express my gratitude to my other collaborators Mark Tame and Tommaso Tufarelli. Mark mentored me through the first steps into PhD-dom and was instrumental to my development. I cannot thank him enough for all the time he gave to me. It is impossible to know how to begin to thank Tomasso. So in no particular order I thank him for providing me with; deep scientific insight, unwavering enthusiasm, limitless curiosity, questionable humour, friendship, swimming advice and a Nintendo Wii.

I have been incredibly lucky with my colleagues in the controlled quantum dynamics theory group. I thank my quantum optics brother Jake Illes-Smith, my PhD guru Ben Brown and of course my desk mate Howard Dale. Our corner was dark, our mood sometimes belligerent but we were rarely without a twinkle in our eyes. You better all miss me as much as I will miss you. I would also like to thank some other who have made my time so special, Vignesh Venkataraman, Kate Hughes, Marco Genoni, Doug Plato and Chuanqi Wan.

I would like to thank Rob Hogan and Ally O'Sullivan for being so ridiculously nice to me during the tough times and Ronan Gleeson for always being there. Thanks to my sister Kate for being on the other end of the phone when I needed to unload.

A special mention to V and A who provided me with, and put up with, the most.

Finally, to my Mum and Dad, to whom I owe the most. I simply would not be the person I am without you. I am a very lucky lad and I know it. Thank you for the unwavering love, support and guidance. I love you guys!

## Declaration

The following thesis was written solely by me. It presents my own work, and work by others is appropriately referenced.

Kyle McEnery

‘Expect problems and eat them for breakfast.’

*Alfred A. Montapert*

# Contents

# List of Figures

# Chapter 1

# Introduction

## 1.1 Motivation and objectives

The endeavour to understand how light and matter interact has been a long running theme in physics. From classical scattering theories, that explain the colour of the sky, to the development of quantum electrodynamics, this study has been wildly successful in helping us understand the world around us as well as developing technology that is essential to our everyday lives. In this thesis we examine how light-matter systems interact at the macroscopic and microscopic level. Specifically we examine two fields which have come to define modern research in this area.

At the macroscopic scale we study the burgeoning field of metamaterials [CS10]. The optics of materials is an immensely interesting, yet complex, area of research. A bulk material, such as a metal or a dielectric, is known to have characteristic optical properties. For example, we know that a metal is opaque to light as opposed to a dielectric which is transparent to it. Such characteristics are relatively simple to define but the process through which they occur is hugely complicated. A material is composed of a macroscopic collection of atoms and electrons and the material's optical response is dependent on how light interacts with these complex systems.

Nature has provided us with a finite number of materials, each of which has an electronic structure which dictates how the material responds to light. Some of these responses are unique while others are universal. What if we were not satisfied with this? How would we go about creating novel optical effects not found in nature? The first idea that springs to mind is to build your own material, electron by electron, atom by atom, ensuring that it has the optical response desired. Unfortunately this would be exceedingly difficult and we do not have this type of control at the quantum level, yet. However the rapidly developing field of metamaterials circumvents this problem. These man-made designer materials are composed of periodic arrays of identical unit cell scatterers. As long as the wavelength of the incident light is much greater than the size of the unit cell, then the individual optical response of a unit scatterer governs that of the entire material [CS10]. These unit cells are on the micro- or nano- scale and their fabrication is certainly feasible. Intriguingly the response is often based on the geometry of the unit cell as opposed to its component material. Such control allows us to construct materials whose optical properties are not found in nature, such as the negative refractive index metamaterial [PBS06]. This field is also developing exciting applications such as the super lens [Pen00] and the invisibility cloak [CCS10].

At the microscopic scale we investigate the prospect of intense interactions between a collection of quantum emitters and a single light mode. In the rest of this thesis we define a quantum emitter as a quantum system with a discrete energy level structure, for example atoms or quantum dots. In order to control light-matter interactions at the quantum scale it is essential that quantum emitters and light couple strongly. Unfortunately this is not often the case and we must provide encouragement for the interaction to take place. The most successful method to achieve this is to increase the interaction time, which is employed in the field of cavity quantum electrodynamics [WM08, RBH01]. Here the emitter is placed in a cavity with highly reflective boundaries. If the light mode does not interact with the emitter initially

it will just bounce off the boundary and attempt the interaction again, boosting the chances of coupling. The other method is to decrease the spatial mode volume of the light, this reduces the size mismatch between light and the emitter and encourages coupling. Lately, through further innovations of experimentalists, the interaction between light and quantum emitters has become unprecedentedly strong [NDH$^+$10, ALT$^+$10]. We have arrived at a point where the coupling frequency has become comparable to the resonance frequency of both the emitter and the light mode. This regime is known as the ultrastrong-coupling regime and it has sparked a flurry of research interest within the quantum optics community [Bra11].

It would appear that these two fields are unrelated. However there is a common theme in this work that links them both together; quantum plasmonics. Plasmonics is the theory of light-metal interactions at the nano-scale [Mai07]. Plasmonic modes are hybrid excitations, part electromagnetic wave, part electron plasma oscillation. Quantum plasmonics seeks to understand these processes at the quantum scale. Importantly quantum plasmonics plays a significant role in our study of both metamaterials and intense light-matter interactions and it has been the inspiration behind all the work completed in this thesis. In fact, we begin this thesis in chapter 2 by providing a thorough background on quantum plasmonics which is based on a review article co-written by the present author [TMÖ$^+$13].

The early work in metamaterials occurred in the infrared regime. Increasingly plasmonic components have been incorporated into metamaterial designs in order to bring them into the visible regime. In chapter 3 we investigate if we can incorporate the unique interaction between quantum plasmonic systems into a metamaterial design. Specifically we take a composite system of a two-level quantum dot and a silver metal nanoparticle which supports a highly confined plasmonic mode. The strong interaction between the plasmonic mode and the quantum emitter produces a Fano interference in the light scattered off the system. We attempt to mani-

fest this interference effect into a negative permeability metamaterial to introduce dynamic tunability and nonlinearity. The main results of chapter 3 are published in [MTMK14a].

Plasmonic modes are characterized by their highly confined fields. We have already highlighted how small mode volumes can facilitate intense interactions with quantum emitters. In this regard plasmonic modes interacting with a collection of quantum emitters can be considered a possible candidate for achieving ultrastrong interactions. In chapter 4 we theoretically examine the model of a single mode interacting with a collection of emitters in the ultrastrong-coupling regime. In particular we examine the effect the diamagnetic term, regularly neglected in light-matter models, has in this regime. We believe that such work will be useful to understand the behaviour of quantum plasmonic systems in the future. The main results of chapter 4 are contained in [MTMK14b], which is under review for publication.

## 1.2 Publications

Parts of this thesis are based on material published in the following papers:

- M. S. Tame, K. R. McEnery, S. K. Ozdemir, J. Lee, S. A. Maier, and M. S. Kim. Quantum plasmonics. *Nature Physics,*, **9**, 329-340 (2013).
- K. R. McEnery, M. S. Tame, S. A. Maier, and M. S. Kim. Tunable permeability in a quantum plasmonic metamaterial. *Physical Review A*, **8**9, 013822 (2014).
- K. R. McEnery, Tommaso Tuffareli, S. A. Maier, and M. S. Kim. Non-adiabatic emission of ultrastrongly-coupled oscillators: signatures of the $A^2$ term. *arXiv:1407.7446* (2014).

# Chapter 2

# Quantum plasmonics

## 2.1 Introduction

We begin by introducing the reader to the new field of quantum plasmonics [TMÖ+13, JS11], which is the study of the quantum properties of light, and its interaction with matter, at the nanoscale. Quantum plasmonics is the result of a cross-pollination of knowledge between the fields of plasmonics [Mai07] and quantum optics [WM08]. Quantum plasmonics is a rich area of study with many research opportunities. In this thesis we will specifically concentrate on the study of how plasmonic modes interact with discrete-level quantum emitters. In order to help the readers understand the context of this work we provide a thorough background in both classical, and quantum, plasmonics.

We start by introducing the theory of plasmonics, which is the study of the interaction between electromagnetic radiation and free electrons at metallic interfaces or in metallic nanostructures [SBW+10]. Plasmonics is a sub-field of nanophotonics which, as the name suggests, is the study of electromagnetic waves which are confined to nanoscale dimensions. Plasmonics is concerned with the confinement of light through metals, thus we give a short review on the optics of metals. We also

emphasise that plasmonic research is underpinned by two main excitation modes, the surface plasmon polariton (SPP) and the localized surface plasmon (LSP), both of which are discussed in detail. Following this we shift our focus away from the classical elements of plasmonics and towards investigating plasmonics at the quantum level. Initially we concentrate on the fundamental aspects of plasmonic excitations and we ask ourselves, what are the inherent quantum properties present? Finally we investigate the interesting, and most relevant, scenario where quantum emitters possessing finite energy levels, such as atoms, are coupled to plasmonic modes. The highly confined fields, associated with the plasmonic modes, couple strongly with the emitters, providing a fruitful platform to study extreme light-matter interactions.

## 2.2 Plasmonics: the basics

### The optical properties of metals

The information on how a metal, or any other material, responds to an electric field is encapsulated in its electric permittivity $\epsilon(\omega)$ [Gre98],

$$D = \epsilon(\omega)E. \tag{2.1}$$

Where $D$ is the displacement field, which is a linear combination of the incident external electric field (E) as well as the material's polarization field (P). This P field is a consequence of the polarization of all the material's atoms in response to the stimuli of the external field. We will discuss this macroscopic parameter, along with the magnetic version, the permeability $\mu(\omega)$, in greater detail in chapter 3. For the moment it will suffice to know that the permittivity is a complex value. The real part defines the dispersion of light in the metal, while the imaginary component describes the absorption of light by the metal. Let us investigate a simple model which can be used to derive an approximate expression for the permittivity of a

typical metal.

### Drude model

For a wide range of frequencies the Drude model provides an accurate description of the optical properties of metals [Mai07, KV95]. The model treats the electrons within the metal as a plasma, such that a sea of free electrons of number density $n$ oscillates against a fixed background of positive ions when subjected to a driving field of amplitude $E_0$. The electrons in the plasma experience collisions with themselves and the ions which dampen the oscillations of the plasma at a rate $\gamma$. For a harmonic driving field, we can write the oscillation of an electron, of mass $m$ and charge $e$, in the plasma as,

$$m\ddot{x} + m\gamma\dot{x} + eE_0\mathrm{e}^{-i\omega t} = 0. \tag{2.2}$$

If we also assume a harmonic time dependence for the position of the electron $x_0\mathrm{e}^{-i\omega t}$, then we can solve for the amplitude of the position as

$$x_0 = \frac{e}{m(\omega^2 + i\gamma\omega)}E_0. \tag{2.3}$$

We can now derive an expression for the amplitude of the polarization field set up by the oscillating electrons. To do so we substitute Eq. (2.3) into the formula for the polarization amplitude $P_0 = -nex_0$, which gives

$$P_0 = -\frac{ne^2}{m(\omega^2 + i\gamma\omega)}E_0. \tag{2.4}$$

As mentioned earlier the displacement field is a linear combination of the electric and polarization fields, $D = \epsilon_0 E + P$, where $\epsilon_0$ is the permittivity of free space. If we combine this form of the D field with Eq. (2.1) and Eq. (2.4) then we are left

with the following expression for the metallic permittivity,

$$\epsilon(\omega) = 1 - \frac{\omega_p^2}{\omega^2 + i\gamma\omega}, \tag{2.5}$$

where $\omega_p$ is the plasma frequency of the electron sea, $\omega_p = \sqrt{ne^2/\epsilon_0 m}$. What information can we derive from this permittivity expression? First it is useful to separate this complex expression into its real and imaginary components,

$$\mathsf{Re}[\epsilon(\omega)] = 1 - \frac{\omega_p^2/\gamma^2}{1 + \omega^2/\gamma^2}, \tag{2.6}$$

$$\mathsf{Im}[\epsilon(\omega)] = \frac{\omega_p^2/\gamma}{\omega(1 + \omega^2/\gamma^2)}. \tag{2.7}$$

Let us examine the region around $\omega_p$, where the frequencies tend to be much larger than the damping rates ($\omega \gg \gamma$). In such a case $\mathsf{Im}[\epsilon]$, which accounts for damping, is negligible and we can rewrite the real part as

$$\mathsf{Re}[\epsilon(\omega)] = 1 - \frac{\omega_p^2}{\omega^2}. \tag{2.8}$$

Writing the permittivity in this form emphasises the importance of the plasma frequency in regards the defining characteristics of metals. If the frequency of the light incident on the metal is less than $\omega_p$, then $\mathsf{Re}[\epsilon(\omega)] < 0$ and the metal reflects light. On the other hand it is clear that for frequencies greater than $\omega_p$, $\mathsf{Re}[\epsilon(\omega)] > 0$, the metal loses its 'metallic properties' as it becomes transparent to light. We should note that the Drude model has limitations, especially for noble metals where intersubband transitions in the regime $\omega > \omega_p$ are not taken into account. In this particular case the Drude model can be used without error if the following phenomenological correction is used,

$$\epsilon(\omega) = \epsilon_\infty - \frac{\omega_p^2}{\omega^2 + i\gamma\omega}, \tag{2.9}$$

where the metal dependent ultraviolet permittivity ($\epsilon_\infty$) is usually constrained by $1 \leq \epsilon_\infty \leq 10$.

In this section we have shown how a very simple plasma model can be used to learn about some of the optical properties inherent in metals. We will now move onto the more complex processes that can take place at metal-dielectric interfaces, namely the excitation of plasmonic modes.

**Surface plasmon polaritons**

We have just shown that a metal, for frequencies below its plasma frequency, will have a negative permittivity which is the key ingredient in exciting plasmonic modes [Mai07]. The first plasmonic we will discuss is the SPP, which is a propagating surface wave that is excited on the interface between a negative permittivity material and a positive one. An SPP on a metal-dielectric interface can be thought of as a photonic mode coupled to the collective oscillation of the free electron plasma in the metal. The hybrid nature of the SPP, shown in Fig. 2.1, restricts the mode volume, normal to the interface, to subwavelength dimensions [SBW$^+$10]. Researchers have long been aware of these plasmonic surface waves. The subject experienced a rebirth, however, when the photonic community became aware of the possibility of using SPPs to confine light below the diffraction limit [TYT$^+$97, GB10]. The diffraction limit imposes the following constraint on the spatial spread of a light mode

$$\Delta_i = \frac{\lambda_0}{2\eta}, \tag{2.10}$$

where $i \in \{x, y, z\}$, $\lambda_0$ is the wavelength of the light mode in free space and $\eta = \sqrt{\epsilon}$ is the refractive index of the non-magnetic material guiding the light [TMÖ$^+$13]. It is clear that materials that are bound to respect the diffraction limit can still provide subwavelength confinement, for example dielectric waveguides with a large

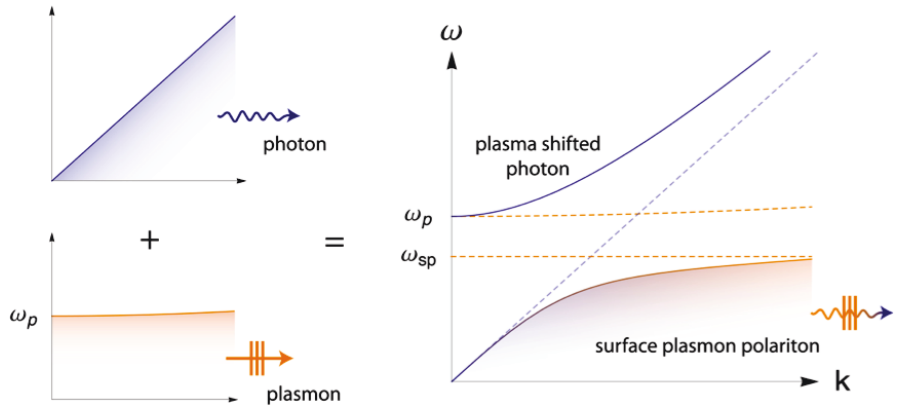


Figure 2.1: The coupling of a photon and a plasmon at the interface of a material with a negative dielectric permittivity (for example, a metal) and one with a positive dielectric permittivity (for, example air) leads to a splitting of the ($\omega$ - k) dispersion curves (solid lines) for the excitations, which form a plasma shifted photon and a SPP as the joint state of light (photon) and matter (surface plasmon).

positive permittivity. Significantly, SPP modes can achieve both subwavelength *and* subdiffraction confinement.

Let us reflect, for a moment, on why this property has made the study of SPP's so relevant. Let us examine the current state of information processing where the use of miniaturized electronic devices is problematic as their bandwidth and speed limitations become saturated [GB10]. The obvious advancement is to transport information with light, however there is a severe limitation on the capacity to integrate optical devices into miniaturized circuits. The reason for this is due to the diffraction limit, if the size of photonic waveguides is reduced past a certain size the guided light mode is no longer confined and all the information is lost. In this regard the SPP provides a convenient hybrid in which broadband light can be guided and manipulated at nanoscale lengths. Unfortunately, this high confinement comes at a price; namely high losses in plasmonic modes [Mai07]. To understand this, let us remind ourselves that we have defined a SPP as a hybrid excitation, part electromagnetic wave, part oscillation of the free electron plasma. If more of the SPP energy is confined within the metal's plasma then the mode will have a greater

confinement, but at the same time it will be more vulnerable to the ohmic damping that occurs when the electrons crash off each other.

### Localized surface plasmons

The LSP is the plasmonic mode associated with the resonance of the free electron plasma in a small metallic structure due to an external electric field [Mai07]. The strong resonance is a direct result of the nanoscale dimensions of the structure, the metallic surface serves as a restoring force for the oscillating electrons. The LSP acts to absorb and scatter incident light into the radiative far-field, however it is primarily characterized by an intense electric field both within the structure and in its near-field. Due to this property metallic nanoparticles (MNP) supporting LSPs can be used as an efficient antennas for small emitters, for example atoms [GFDHM11].

LSPs have, in fact, been exploited by humans since ancient times. The mechanism by which stained glass obtains its vibrant colour is in fact based on the resonant properties of the LSP. The exact colour of the glass depends on the resonant frequency of the embedded MNP. The obvious question is what defines the resonant frequency of a particular MNP. While the geometry of the structure has an effect, the main factor is the material in which the MNP is embedded [Mai07, KV95]. To understand this better let us take the example of a subwavelength spherical MNP which will be the subject of investigation in chapter 3. Due to the size of the MNP we can take the dipole approximation. In this thesis we will not consider the case of particles whose size is of the order of the incident light wavelength, such a case can be tackled, however, using Mie theory [BH83]. Within this dipole approximation the MNP has a dipole moment of

$$p_{\mathsf{MNP}} = \epsilon_0 \epsilon_b \alpha E_0. \tag{2.11}$$

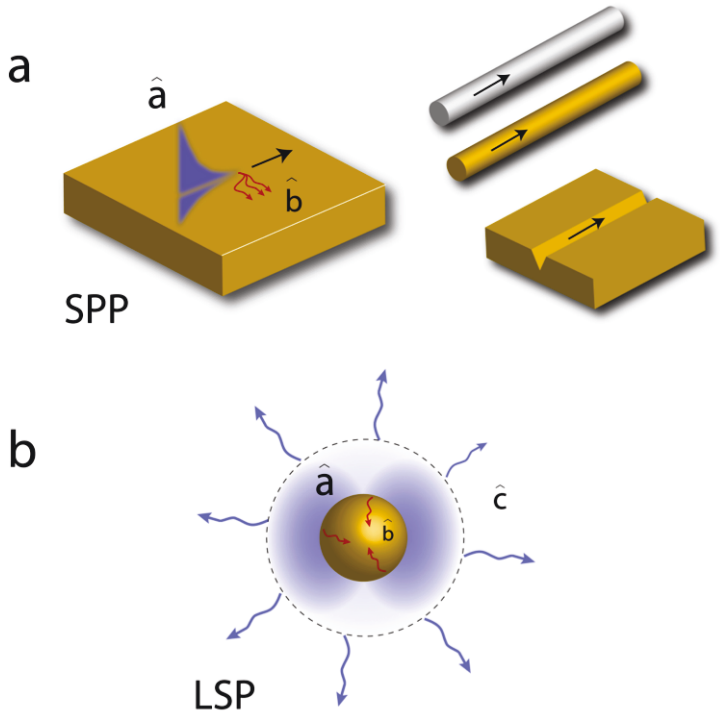


Figure 2.2: (**a**) Conceptual schematic of an SPP excited on the interface between gold (negative permittivity) and air (positive permittivity), we see that the propagating wave is evanescently confined in the direction perpendicular to the interface. We also show specific examples of SPP waveguides, such as gold and silver nanowires as well as a V-groove waveguide. We also introduce annihilation operators representing the quantized fields. $\hat{a}$ represents the SPP mode, while $\hat{b}$ represents the reservoir of phonon modes to which the SPP loses energy via ohmic damping. In (**b**) we show a conceptual schematic of a LSP mode excited in a gold spherical nanoparticle. Here $\hat{a}$ represents the LSP mode, while $\hat{b}$ and $\hat{c}$ represent reservoirs that account for ohmic and radiative damping respectively.

Where the strength of the MNP's dipole response is governed by the polarizability,

$$\alpha = 4\pi r^2 \frac{\epsilon(\omega) - \epsilon_b}{\epsilon(\omega) + 2\epsilon_b}. \tag{2.12}$$

Here $r$ is the radius of the MNP, $\epsilon(\omega)$ is the frequency dependent permittivity of the MNP's composite metal, while $\epsilon_b$ is the permittivity of the material in which the particle is embedded. Resonance occurs at the frequency for which the polarizability is maximized, this scenario is well expressed by the Frohlich condition [KV95]

$$\mathsf{Re}[\epsilon(\omega_0)] = -2\epsilon_b. \tag{2.13}$$

This dependency of the LSP frequency on the surrounding material makes MNPs an efficient sensing tool, as changes in a material's permittivity are observed in the light scattered by a MNP embedded in the material [GFDHM11].

## 2.3 Quantum plasmonic properties

The investigation into quantum plasmonics can be distilled into three main goals. First, to exploit the highly localized electric fields associated with plasmonic modes to stimulate intense interactions with single quantum emitters. Two, to manipulate quantum information at the nanoscale. Finally, from a more fundamental point of view, to understand exactly what quantum properties are retained by these complex quasi-particles. The first goal is the main concern of the thesis and will be covered in more detail in section 2.4.

To begin, let us briefly elaborate on how both the LSP and the SPP are quantized. In general we wish to quantize the near-field of the LSP. Fortunately, LSP near-field is analogous to a leaky cavity mode and can be quantized in the standard way [WS10, RSF$^+$10]. The SPP is more complex and it is best described by Hopfield's polariton model [Hop58]. The polariton is a joint state of light and

matter, and was originally used to describe the polarization field in matter. When described in this manner a single SPP excitation will exhibit bosonic quantum statistics [WM08, AMY$^+$07]. Initially the quantum nature of the SPP was doubted as typically quantum effects are associated with microscopic, isolated quantum objects, such as single atoms or photons. In contrast, the SPP mode is composed of a macroscopic collection of electrons ($\sim 10^6$ electrons) and it was thought that the collisions between electrons would cause decoherence and a subsequent loss of quantum effects. A huge milestone in proving that SPPs do indeed retain their quantum properties was the experimental observation of the preservation of entanglement. In the experiment by Altewischer *et* al, a polarization-entangled pair of photons were converted into SPPs on gold films perforated by subwavelength holes, then back into photons, and the entanglement survived [AvEW02]. Many of the incident photons were lost due to ohmic and surface-scattering losses, however the photons that survived were found to be entangled. Further entanglement experiments have been carried out using different degrees of freedom, such as energy-time entanglement [FRM$^+$05] and the entanglement of orbital angular momentum [RGH$^+$06]. In all cases the entanglement was preserved. This indicates that the quantum information is encoded into the overall oscillation of the electrons, which explains the preservation of quantum effects despite the macroscopic scale. This ability to encode quantum information into the SPP mode may prove very useful for the quantum information community. It could open the door to integrate optical components with microscopic, on-chip, quantum circuits, something which is not possible with conventional dielectric waveguides.

The LSP modes associated with metal nanoparticles have some interesting quantum properties aside from their ability to interact strongly with emitters. For single particles there is the quantum size effect [Hal86, GMK75, KXB93, HLC$^+$11]. Depending on the size of the nanoparticle, quantum effects can be significant in the description of its electrodynamics. The continuous electronic conduction band, valid

at macroscopic scales, breaks up into discrete states when the dimensions are small enough, making the use of the Drude model unsatisfactory. This quantum size effect manifests itself as a shift and broadening of the LSP resonance, in addition to a fine structure which corresponds to transitions between the discrete energy levels [Hal86, HLC+11]. For a collection of interacting nanoparticles there is the effect of quantum tunneling [ZPN09]. If the distance $d$ between two nanoparticles is $d < 1$ nm then electron tunneling has a profound impact on the two particle resonance. For even smaller distances ($d < 0.5$ nm) the two nanoparticles (dimer) enter a conductive regime where a charge transfer plasmon appears involving electrons travelling back and forth between the two particles [lMLWX09].

## 2.4 Quantum emitters coupled to plasmonic modes

The large size mismatch between light and single emitters ensures that their light-matter interaction is inherently weak. This is a problem as strong, coherent coupling between single photons and emitters is critical for developing future quantum technology [Mon02]. There are several strategies to circumvent this problem. High quality cavities have been used to boost interaction times and encourage stronger coupling. However the use of cavities places a restriction on the bandwidth and the size of devices. An alternative strategy is to use an interface to bridge the size gap. Confining the light field to small effective volumes in this way enables stronger coupling with the emitter. Plasmonic modes can be squeezed into volumes far below the diffraction limit, and therefore provide an excellent interface between single photons and emitters [CSHL06].

Cavity QED (CQED) has been a popular platform for proof-of-principle implementations of quantum information processing [Mon02]. However, the diffraction-limited optical cavities place a lower bound on the size of these systems. The drive to bring CQED down to the nanoscale has opened the door to plasmonic CQED. Here, both

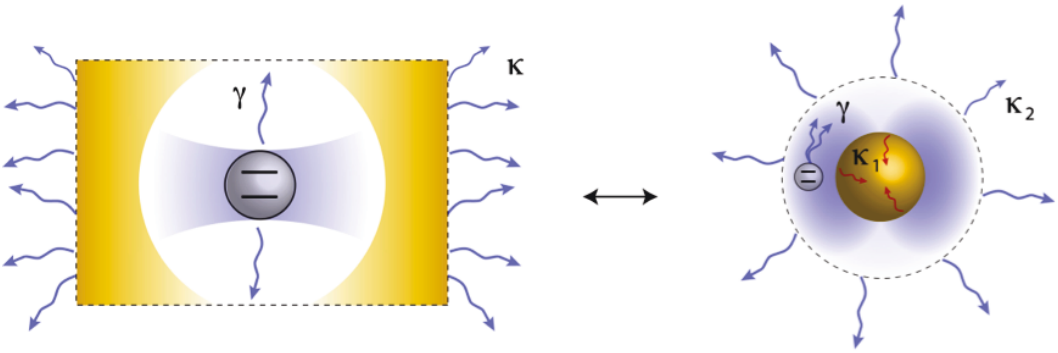


Figure 2.3: Analogy between an atom in a single mode leaky cavity (left) and an atom residing in the near-field of a resonant LSP mode supported by a MNP (right). The principle difference between the two is their dissipation channels. The cavity loses photons by transmission through its side walls ($\kappa$). The LSP mode, on the other hand, dissipates through ohmic ($\kappa_1$) and radiative ($\kappa_2$) channels associated with the MNP. In both cases the atom can radiate via spontaneous emission ($\gamma$).

SPP and LSP plasmonic modes offer subwavelength and subdiffraction field confinement that enables extreme light-matter coupling. In particular, the resonant LSP modes supported by metal nanoparticles can be described effectively as a leaky cavity in quantum optics formalism [WS10, RSF$^+$10], as shown in Fig. 2.3. Recent work on adding resonators to waveguide SPP systems brings these types of modes into the quasimode regime of CQED as well [LSY$^+$12, GV07, MOS$^+$09, HFJGVZ13].

Light-matter interactions can be split into two principal regimes, the weak-coupling and the strong-coupling regime. The strength of the interaction between the emitter and the field is characterized by a coupling frequency which is inversely related to the effective volume of the light mode

$$g \propto \frac{1}{V_{\text{eff}}}. \tag{2.14}$$

The boundary between the strong-coupling and weak-coupling regimes is dependent on the relative value of $g$ in relation to the damping rates of the plasmonic mode $(\kappa_1, \kappa_2)$ and the emitter $(\gamma)$. If $g \ll \gamma, \kappa_1, \kappa_2$ then we are working in the weak-coupling regime, while if $g \gg \gamma, \kappa_1, \kappa_2$ we have reached the strong-coupling regime.

**Weak-coupling: Purcell enhancement**

In the weak-coupling regime the excitation within the emitter-light system is irreversibly lost to the outside environment before any coherent exchange of energy can occur. In this case the light field has a perturbative effect on the emitter, which manifests itself as a modification of the emitter's decay rate, a phenomena known as Purcell enhancement of spontaneous emission [Pur46]. The level of modification can be quantified by the Purcell factor,

$$F_p = \frac{\gamma_{\mathsf{modified}}}{\gamma_{\mathsf{freespace}}} \propto \frac{Q}{V_{eff}}. \tag{2.15}$$

$F_p$ is simply the ratio between the emitter's modified decay rate, due to the presence of the strongly coupled light mode, and the decay rate the emitter would have if placed in an electromagnetic vacuum. Here Q stands for the quality of the light mono-mode.

Plasmonic modes are particularly suitable in enhancing the fluorescence of emitters despite having low quality factors due to ohmic losses. This enhancement is due to two simultaneous processes [ABN06]. First, the intense plasmonic field increases the excitation rate of the emitter. Second, the subwavelength confinement of the light field enhances the decay rate of the emitter into the plasmonic mode via the Purcell effect [Pur46]. The fluorescent enhancement, however, can be tempered by the non-radiative excitation of lossy surface waves at the metal surface [ABN06]. This process, known as fluorescence quenching, occurs close to the surface and therefore leads to an optimal distance for coupling the emitter into a plasmonic mode. The high quality factors, Q, or long interaction times associated with traditional cavities limits the speed at which photons can be emitted once collected into the cavity. Plasmonics does not suffer from this problem and thus promises single-photon sources at optical frequencies with high operation speed. This plasmon-induced Purcell

enhancement can also be used to encourage quantum interference between the transitions of a multi-leveled emitter, leading to an enhancement in phenomena such as electromagnetic-induced transparency, coherent population trapping and lasing without inversion [YPV09, HS10].

In 2007, Akimov *et* al demonstrated a 2.5-fold enhancement in the emission of an ensemble of quantum dots into an SPP mode of a silver nanowire[AMY+07]. Moreover, they observed that the light scattered from the end of the nanowire was anti-bunched, confirming that the SPP mode could collect and radiate single photons from the quantum dots. Subsequent experiments have showed Purcell enhancements of single emitters coupled to SPP [KGB+09, HKSA11] and LSP [ABN06, KHRS06] modes. Further efforts have also been made recently to exploit more advanced designs to improve collection and control. One example is hybrid SPPs [JKWB08], where a waveguide gap is used to achieve Purcell factors as high as 60. The growing use of nanoantenna to control the emission direction of the collected light is another example [CVT+10]. These efforts point towards the exciting prospect of single-photon antennas that can efficiently absorb light from emitters and subsequently emit the photons in a well-controlled manner [CWrK11].

**Intermediate-coupling: the bad cavity limit**

While confined plasmonic modes couple very strongly to matter, unfortunately because of large ohmic losses it is not easy to enter the strong-coupling regime in plasmonic systems, where light-matter interactions must be dealt with non-perturbatively. There is, however, a regime where the coupling frequency is intermediate between the decay rates of the plasmonic mode and the emitter. This is known as the bad-cavity limit in CQED and displays interesting physics, such as cavity-induced transparency [RB95]. A similar effect has been studied in coupled MNP-emitter systems, where very large enhancements in response have been predicted [RSF+10, WS10, ZGB06].

### Strong-coupling

In general, the strong-coupling regime is characterized by the reversible exchange of energy between the light field and the emitter, known as the Rabi oscillations. These oscillations manifest themselves in an energy splitting of the light-matter energy levels. There have been experimental observations of these splittings in the spectra of ensembles of molecules due to plasmonic interactions [DKB+05, VWP+13]. Experimental evidence for strong-coupling between a single emitter and a plasmonic mode, however, is still elusive. Classical predictions have suggested strong-coupling could be achieved between an emitter and a metallic dimer antenna [SSR+10]. There have also been theoretical examinations of the strong-coupling regime based on a fully quantum mechanical framework [TH08, VKH12]. These works take into consideration higher-order modes whose relevance cannot be ignored as the metal-emitter separation decreases past the point where the dipole approximation is valid. As a result, the intuitive CQED analogy is replaced with macroscopic QED techniques better suited to more complex systems [DKW98].

Despite these predictions there is still a strong desire to develop ways to increase the Q-factor of the plasmonic modes in order to more easily enter the strong-coupling regime. Two main strategies have been pursued. The first concentrates on reducing the damping of the material. The high confinement and long lifetimes of graphene plasmons have been proposed in this regard [KCdA11]. In the second, cavities have been incorporated into plasmonic structures. These plasmonic resonators combine the benefits of a high Q-factor and small mode volume. De Leon *et al* have proposed a plasmonic resonator composed of silver nanowires surrounded by dielectric Bragg reflectors, and demonstrated Purcell factors exceeding 75 [LSY+12].

One of the main properties that make photons attractive for transporting quantum information is that they are weakly interacting. However, it also means that they do not interact with each other very well, making it difficult to perform quantum

operations. Nonlinear materials can be used to boost this interaction, however the nonlinearity requires high light intensity. This is unattractive as single-photon interactions are needed for quantum photonic devices. A strongly coupled light-emitter system has a nonlinear energy structure that allows for photon-photon interactions at the single-photon level. In CQED this is known as the photon blockade effect [BBM+05]. An analogy has been found for plasmonics [MNdA12] and was used to devise the idea of a single-photon transistor [CSDL07].

In addition to single emitters, recent work has studied the interaction of multiple emitters mediated through a strong interaction with a plasmonic mode [DKF11]. There have been predictions of a plasmonic Dicke effect, where emitters coupled to a common plasmonic mode experience cooperative emission [PS09]. In a similar scenario, mediated interactions via a plasmonic mode generate entanglement between emitters [MCGTMM+11]. This is a powerful insight as the proposed entanglement generation is induced from dissipative processes. In this way a perceived weakness of plasmonics has been converted into a positive.

**Nanolasers, metamaterials and many-body systems**

Despite the remarkable progress in studying plasmonic-matter interactions and the development of a host of promising applications, the problem of high loss must still be resolved for plasmonics to fulfill its full potential. In 2003, Bergman and Stockman proposed a plasmonic version of a laser for providing amplification via stimulated emission [BS03]. This spaser could produce stimulated emission of SPPs by placing gain material around resonant metallic structures. The work paved the way for the creation and preservation of strong, coherent plasmonic fields at the nanoscale. Many proposals have since been put forward to exploit the spaser's novel effects, including the creation of subwavelength nanolasers, which out-couple the spaser's near-field as propagating radiation [NZB+09, OSZ+09]. Due to the Purcell enhancement, these nanolasers can display threshold-less lasing [MOS+11]. Spasers

have also been considered in the design of metamaterials to eliminate damping. As metamaterials have been brought from the microwave to the optical regime they have increasingly relied on plasmonic components [Sha07]. Incorporating gain will be essential for the practical realization of their novel effects.

One of the key successes of quantum optics over the last few decades has been the precise control of single quantum systems in a range of settings. Cold atom trapping in optical lattices, for instance, has helped shed light on a number of physical phenomena [BDN12]. However, optical lattices are not easily scalable and the lattice period is restricted to half the wavelength of the trapping laser. Plasmonics has emerged as a promising route towards investigating scalable solid-state systems for trapping atoms and molecules [CTP$^+$09, SBZ$^+$11]. Due to the strong-coupling between the emitter and the plasmonic mode, the metallic trap serves the dual purpose of trapping the atom as well as an efficient probe. The prospect of creating a plasmonic lattice with a nanometer period has been proposed [GTC$^+$12]. These lattices would serve as an interesting playground to examine many-body physics in a parameter regime that is unavailable to traditional optical lattices.

## 2.5 Future perspectives

A huge amount of progress has been made in the growing field of quantum plasmonics. However, many quantum properties of surface plasmons are still to be fully explored and a number of problems remain along the route to realizing fully functioning and reliable quantum devices that take advantage of the intense light-matter interactions that plasmonics offers. The most pressing issue is how to deal with loss. While recent work has shown that loss compensation and gain can be achieved in basic plasmonic waveguides in the classical regime [BL11], it remains to be seen how these techniques can be translated into the quantum regime and in what way noise can be accommodated. It might be, however, that hybrid quantum

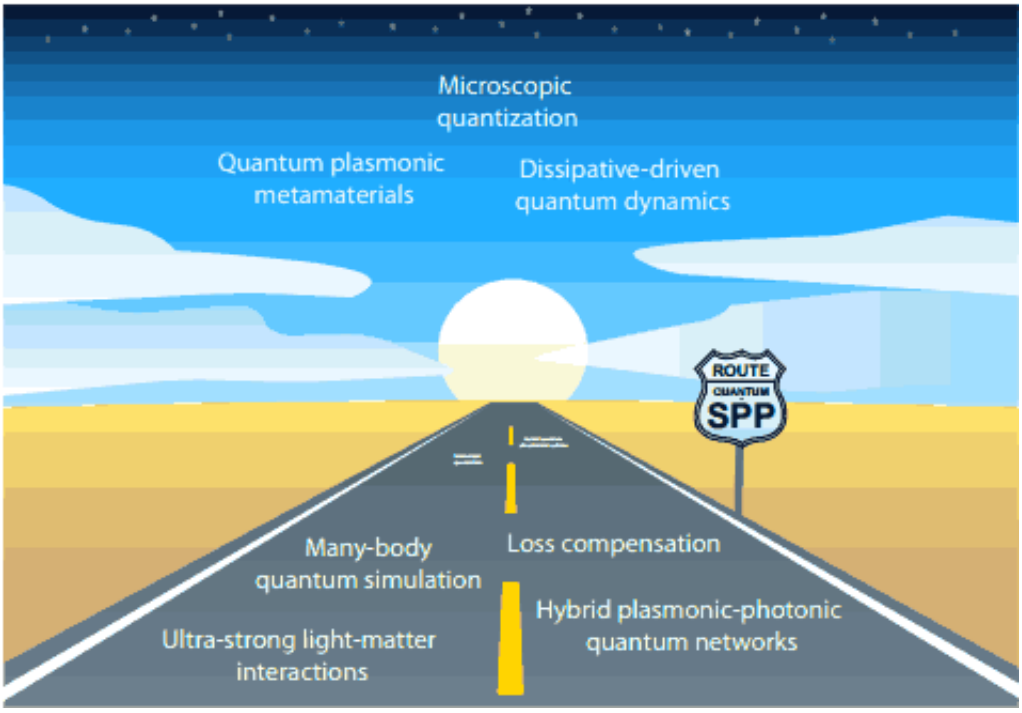


Figure 2.4: A range of topics on the horizon of the field of quantum plasmonics. Including, probing deeper into the fundamental properties of light-matter systems, such as their potential for ultrastrong quantum interactions with emitters at the nanoscale.

plasmonic-photonic systems will be the optimal solution in the trade-off between confinement and loss [CSHL06] , perhaps even exploiting the loss when needed for investigating dissipative effects in quantum systems [VWC09]. Moreover, as we start to look at miniaturizing plasmonic components further, several questions are already beginning to appear: At what scale do current quantization methods based on a macroscopic approach break down? When will non-local microscopic effects, requiring density functional theory [HLC$^+$11] combined with quantum optics, need to be considered in the design of new quantum plasmonic components? In Fig. 2.4 we highlight some exciting and unexplored topics related to these questions. Finding the answers to these and many more related questions promises to make the next stage of research in the field of quantum plasmonics a very fruitful and productive time. In the next two chapters we will outline our own efforts to exploit the promise of quantum plasmonics.

# Chapter 3

# Macroscopic response of a quantum plasmonic metamaterial

## 3.1 Introduction

In this chapter we investigate how a macroscopic collection of quantum plasmonic structures can be engineered to exhibit unusual optical responses. Specifically, we introduce a theoretical design for a quantum plasmonic metamaterial which has a tunable negative permeability. This model combines two different types of phenomenon, one taken from the field of metamaterials and the other from quantum plasmonics. The first is the use of an effective optical magnetic dipole as a unit cell in a metamaterial to produce artificial magnetism at optical frequencies. The effective magnetic dipole we use is a coplanar ring of silver metal nanoparticles (MNP) supporting localized surface plasmon modes (LSP) [ASE06, ST09, AE08]. The second phenomenon used is the Fano interference [Fan61, LZM$^+$10], which is observed when light scatters from an MNP interacting with a two-level semiconductor quantum dot (QD) in the bad cavity limit [ZGB06, RSF$^+$10, WS10]. By replacing each MNP in the coplanar ring of the unit cell with one of these MNP-QD 'metamolecules', we

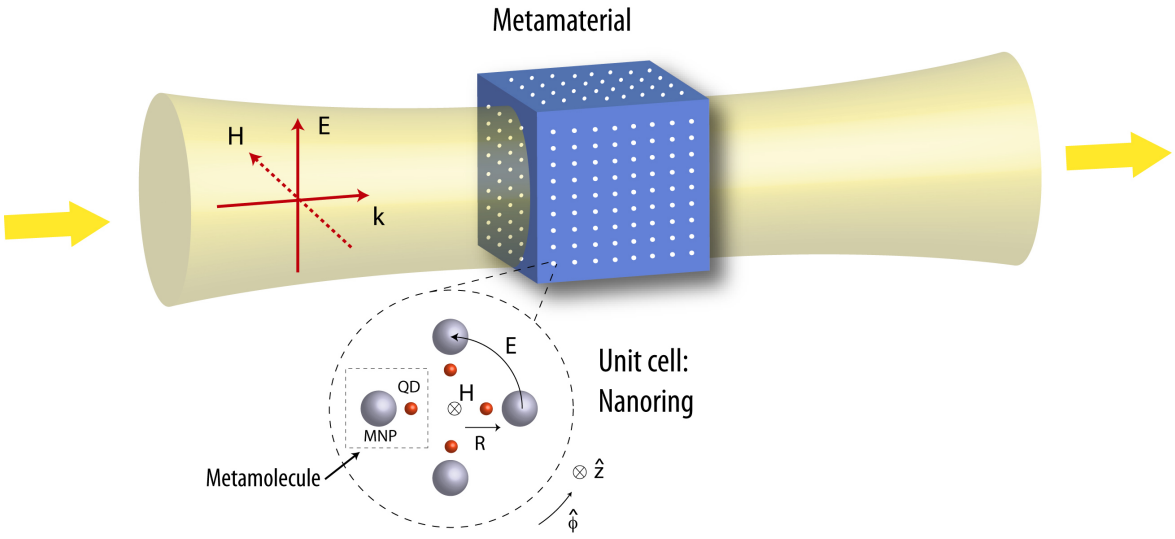


Figure 3.1: Schematic of the quantum plasmonic metamaterial. This includes a detailed sketch of one of the unit cells consisting of a MNP-QD nanoring. The unit cell has nanoscale dimensions: the radius of the MNP nanoring, QD nanoring, MNPs and QDs are 38 nm, 6nm, 16 nm and approximately 1 nm respectively. An arbitrary optical field can be injected into the metamaterial and the figure shows an example of a transverse plane wave at the center of a focused beam. The interaction between the QDs and MNP fields at each site, or 'metamolecule', cause a Fano profile to appear in the scattered magnetic field of the MNP ring. The configuration shown is for a material with a magnetic response in the $\hat{\mathbf{z}}$ direction only and the material is therefore anisotropic. To make an isotropic material with the same response in all directions, a cubic lattice consisting of three orthogonal arrays of nanorings should be used as the unit cell.

are able to transfer the Fano interference into the magnetic resonance of the ring. When the MNP-QD nanorings are then used as the unit cell of a metamaterial, the Fano interference manifests itself in the metamaterial's effective permeability $\mu_{\text{eff}}$. We exploit this interference to obtain control over the metamaterial's optical properties and , in particular, we introduce tunability and nonlinearity into $\mu_{\text{eff}}$.

We begin by reminding the reader of the basics of metamaterials which we discussed in chapter 1. We then elaborate on how metamaterials can mimic magnetism at high frequencies, how this can then be used to realise negative index materials, and what challenges need to be overcome so artificial magnetism can be brought into the optical regime. Once this background material is covered we introduce

our model in detail. First, we elaborate on the physics of the interacting MNP-QD metamolecule and show that a Fano interference profile is present in the linear polarizability ($\alpha$) of the joint system. Following this, we discuss how the 'bare' MNP nanoring acts as a magnetic resonator and we calculate the effective bulk permeability of a metamaterial composed of these nanorings. Finally, we incorporate the MNP-QD metamolecule into the nanoring and calculate the permeability of our proposed quantum plasmonic metamaterial.

## 3.2 Metamaterials

The propagation of light is modified significantly as it passes from the vacuum into materials. Common modifications include the light being reflected, refracted or its velocity being retarded. These modifications are attributed to the interaction between light and the atoms that constitute the material. Imagine, for a moment, we had the technology to build a material from the bottom up, atom by atom. If this were the case then we could create a material with whatever optical properties we desired. Unfortunately, we are limited by present technology as we do not possess the required control at the atomic level. It would seem that in our endeavour to manipulate light we are limited to materials that nature has provided for us. Recently, researchers have rejected this notion by fabricating designer materials that boast electromagnetic responses not possible in naturally occurring materials. The most important example of such a material is the metamaterial. The Greek word *meta* means beyond which highlights that these materials have properties that cannot be found naturally [SPW04, PSS06, SCC$^+$05]. These metamaterials are periodic structures whose unit cell is subwavelength size. Each unit cell is composed of an identical subwavelength structure which we will call a meta-atom. The size of the meta-atom ensures that the incoming light cannot individually discern them. As a result they, conceptually, replace the role of atoms in regular materials [CS10]. Therefore the optical response of the bulk material is governed by the response of

each individual meta-atom, over which we have full control. Crucially the optical response of these meta-atoms is based on their structure rather then the chemical properties of their component elements. The advent of metamaterials has radically altered our perception of how light can be manipulated. It has even spawned a new field of theoretical research, transformation optics, which has led to the proposal of the invisibility cloak [CCS10]. The precise light control that metamaterials provide will enable us to create technology previously thought to be the stuff of science fiction.

### 3.2.1 Macroscopic optical response parameters

As mentioned earlier, the total response of a material to light is due to the combined response of each atom. These complicated dynamics are simplified by the fact that the atoms are all much smaller then the wavelength of the incident light. This allows us to average over the effect of the atoms and define the response of the material to light with simple macroscopic parameters [Gre98]. These parameters are the permittivity ($\epsilon$) and the permeability ($\mu$) which determine the electric and magnetic response of the material respectively. We have already discussed the permittivity in chapter 2 but for completeness we present an expression for both response parameters,

$$D = \epsilon(\omega)E, \tag{3.1}$$

$$B = \mu(\omega)H, \tag{3.2}$$

where E is the electric field, D the dielectric displacement field, H the magnetic field, and B the magnetic induction field. To clarify where these parameters come from, let me restate the D field as

$$D = \epsilon_0 E + P. \tag{3.3}$$

We see that the electromagnetic field expected in the presence of a material (D field) is the original electric field as well as the polarization field which is set up within the material. The degree of polarization of the atomic ensemble in the material is given by the electric susceptibility ($\chi$), such that $P = \epsilon_0 \chi(\omega) E$. With this in mind the permittivity is more clearly defined as, $\epsilon(\omega) = 1 + \chi(\omega)$. A similar argument can be used for the magnetic response but, as we shall discuss later, one is less likely to come across naturally magnetic materials. Typically these response parameters are complex functions of frequency, where the imaginary part characterizes the light absorption of the material. The defining feature of metamaterials is that the periodicity of the unit cells is subwavelength, allowing us to define an effective permittivity ($\epsilon_{\mathsf{eff}}$) and permeability ($\mu_{\mathsf{eff}}$). This is in stark contrast to other designer materials attempting to control light. For example photonic crystals exhibit fantastic control over light due to periodic defects in their structure [Nor07]. Unfortunately, the periodicity of these defects is on the order of the light wavelength which makes it impossible to characterise these crystals with these simple, and functional, macroscopic parameters.

### 3.2.2 Artificial magnetism

In order to have complete control over light one must be able to influence both the electric and magnetic components of an electromagnetic wave. Most materials, however, interact weakly with the magnetic field, with some exceptions at lower frequencies. The weakness of magnetic effects in optical materials is directly related to the small value of the fine structure constant [SCC+05]. The ability to produce artificial magnetism at elevated frequencies has been one of the great success stories of metamaterials. This was achieved by using subwavelength magnetic resonators as meta-atoms. The first example of this was Pendry's design of two concentric split-ring resonators (SRRs) with a magnetic resonance in the microwave [PHRS99]. The SRR is analogous to an LC resonator, where the resonance

frequency is $\omega_0 \sim \sqrt{1/LC}$. The incoming magnetic field induces a circular current in the SRR which creates the effect of a magnetic dipole, while the gaps in the SRR provide a capacitance which gives the magnetic response a resonance property. The ability to produce artificial magnetism at high frequencies has already impacted on medical diagnostics, where it is used to improve MRI scans [PSS06].

### 3.2.3 Negative refractive index

Typically resonant responses, both electric and magnetic, are associated with negative real values of the permittivity and permeability. It is virtually impossible to find negative permeability materials in nature but negative permittivity materials are quite common. Many metals, such as the noble metals (gold and silver), fall into this category. The defining optical property of metals is that they are opaque to light. This is in fact characteristic of any material in which either (but not both) the permittivity or the permeability is negative. Negative permittivity materials are also associated with surface plasmon modes which make them particularly intriguing [PSS06]. The advent of metamaterials has allowed us to investigate what would happen if a material had negative real values for *both* the permittivity and permeability. In fact this question has long since been theoretically tackled. Veselago pondered what the refractive index of such a material would be [Ves68]. The refractive index

$$\eta = \sqrt{\epsilon\mu}, \tag{3.4}$$

is a useful parameter to study the propagation of light through a material, where the imaginary component is associated with absorption, while the real part governs the phase velocity of light through the material ($v_{\mathsf{phase}} = \frac{c}{\eta}$). Veselago found that the real part of $\eta$ can be made negative in a material with a negative permittivity and permeability. A negative index of refraction is something that cannot be found in

nature. For a student well versed in conventional optics these materials have some astonishing fundamental properties. Perhaps the most significant of these is that the phase velocity of light is directed against its energy flow in a negative index material. Also at an interface with a positive index material, light bends in the 'wrong' way as defined by Snell's law. Finally the vectors **E**, **H** and wave vector **k** are arranged in accordance to a left hand rule as opposed to the usual right hand rule [SK00]. What's more, standard optical phenomena are strangely modified in these materials. For example the Doppler shift is reversed and Cerenkov radiation [Cer] is radiated in a cone directed behind the moving charge instead of in front. Researchers have already envisioned applications for negative index metamaterials (NIM), the most interesting of which is the idea of a perfect lens which can access the near-field of objects [Pen00, ZL08].

The first metamaterial to experimentally show both a negative electric and magnetic response over the same frequency band was devolped in 2000 [SPV+00]. This metamaterial was a composite structure based on the SRR. The magnetic resonance frequency of the SRR is lower than electric resonance frequency typically exhibited by metals. At lower frequencies the dissipation in metals drowns out the negative response. Ingeniously the electric response frequency in the SRR metamaterial was depressed by also incorporating a lattice of thin wires into the metamaterial [PHSY96]. The wires give the electrons in the metal a large effective mass which helps to reduce the electric resonance frequency, ensuring both the electric and magnetic resonance overlap. Designs are constantly improving, a notable example is the double-fishnet metamaterial which provides a broadband effective negative index of refraction at both infrared and optical wavelengths [HWTH10, ZFP+05, HPM+12].

### 3.2.4 The way forward: plasmonic metamaterials

After these early successes, the next challenge has been to develop a NIM that operates in the optical regime. The main stumbling point has been the need to find a magnetic resonator design to replace the SRR. Intuitively, it was thought that optical magnetic resonances could be achieved by scaling down the SRR to an appropriate size. However there is a lower bound to the size achievable before the metal of the SRR deviates from a perfect conductor, at this point further miniaturization of the SRR will not lead to an increase in resonance frequency [KEW$^+$06, ZKK$^+$05]. There have been many advances in this regard, particularly with metamaterials based on plasmonic components. Metallic structures supporting LSP modes resonate naturally in the optical regime, making them obvious candidates. Metamaterials of this type have shown to experimentally exhibit a negative refractive index. However there remains many challenges, such as the development of a bulk 3-D optical NIM, the need to reduce the large losses associated with plasmonic modes and the need to ensure an isotropic response [SW11].

We have highlighted the need to develop an isotropic optical magnetic resonator in order to realise a fully functional optical NIM. An example of such a design is the MNP nanoring [AE08, ASE06, ST09]. Three nanorings can be placed orthogonally in the unit cell of a metamaterial to ensure an isotropic response. This design suffers from the problem that the magnetic and electric responses don't overlap. In the remainder of the chapter we take this excellent design and introduce two-level quantum dots. The fruit of the combined labours is a dynamically tunable, nonlinear, magnetic resonator that could prove very useful in the design of future optical metamaterials.

## 3.3 The MNP-QD metamolecule

When light of a particular frequency is incident upon a MNP of subwavelength size a LSP is excited [Mai07]. Placing quantum emitters such as atoms, quantum dots and nitrogen vacancy centers within the MNP's strong near-field enhances the interaction between them [TMÖ+13]. The MNP provides an interface between the incident light and the emitter, acting much like an antenna. As a result, the coupling frequency between the MNP field and the emitter can become very large. However, due to the large ohmic and radiative damping associated with the MNP field mode, it is rarely the case that a MNP-emitter system is able to reach this regime, despite the large coupling frequency. Typically the coupling frequency, while lower than the MNP field's damping rate, is much larger than the emission rate of the emitter. In this 'bad-cavity' limit a Fano interference can occur between the incident field and the excited field in the MNP-emitter system, leading to a characteristic Fano profile in the frequency of the scattered field [ZGB06, RSF+10, WS10]. This interference is ubiquitous in wave mechanics and occurs when a discrete system interacts with a continuum [Fan61, LZM+10]. In the present case being considered, the former is the emitter and the latter is the MNP. This particular MNP-emitter type of system has been studied in depth using both a semi-classical [ZGB06] and a fully quantum mechanical model [RSF+10, WS10]. The semi-classical model is perfectly suitable to examine the Fano interference in the weak-driving field limit. However, in the strong-field limit the semi-classical model breaks down and some of the nonlinear behavior predicted is invalidated by quantum noise [WS10]. In order to study nonlinear effects in our metamaterial design our model must be able to operate in the strong-field limit. As such, our model is set up from the beginning within a quantum framework.

### 3.3.1 The MNP-QD polarizability

We focus on producing Fano interferences in a silver MNP-QD metamolecule and exploiting them in our metamaterial design. Thus, we are interested in the explicit optical response of the MNP-QD metamolecule. The response of this system to incident light is characterized by a frequency dependent polarizability, $\alpha(\omega)$ [Gre98]. For a given incident field amplitude $E_0$ it is defined as

$$\alpha(\omega) = \frac{p_{\mathsf{MNP-QD}}(\omega)}{E_0}, \tag{3.5}$$

where $p_{\mathsf{MNP-QD}}(\omega)$ is the amplitude of the metamolecule's dipole moment. The polarizability is a complex function, where the imaginary part describes the molecules ability to absorb light.

#### The quantum model

To derive the MNP-QD system's polarizability, we first define its Hamiltonian, which is given by

$$\hat{H} = \hat{H}_0 + \hat{H}_{\mathsf{int}} + \hat{H}_{\mathsf{drive}}. \tag{3.6}$$

Where the individual terms are

$$\hat{H}_0 = \hbar\omega_0 \hat{a}^\dagger \hat{a} + \hbar\omega_x \hat{\sigma}^\dagger \hat{\sigma}, \tag{3.7}$$

$$\hat{H}_{\mathsf{int}} = i\hbar g(\hat{\sigma}\hat{a}^\dagger - \hat{\sigma}^\dagger \hat{a}), \tag{3.8}$$

$$\hat{H}_{\mathsf{drive}} = -E_0\mu(\hat{\sigma}e^{-i\omega t} + \hat{\sigma}^\dagger e^{i\omega t}) - E_0(\zeta^* \hat{a} e^{-i\omega t} + \zeta \hat{a}^\dagger e^{i\omega t}). \tag{3.9}$$

Here, $\omega_0$ and $\omega_x$ are the resonance frequencies of the MNP plasmonic field mode and the QD respectively, and $\omega$ is the external driving field frequency. The MNP resonant frequency $\omega_0$ can be derived using the Frohlich condition [Mai07] and

by modeling the permittivity of silver using the Drude model, leading to the relation $\omega_0 = \frac{\omega_p}{\sqrt{\epsilon_\infty + 2\epsilon_b}}$. The plasma frequency of silver is taken as $\omega_p = 2\pi \times 2175$ THz [ASE06, AE08, ST09] and $\epsilon_\infty$ is the ultraviolet permittivity of silver, which is set to $\epsilon_\infty = 5$ [ST09]. Finally, $\epsilon_b$ is the permittivity of the background material in which the MNP-QD metamolecule is embedded.

In Eq. (3.6), the term $\hat{H}_0$ is the free energy Hamiltonian of the MNP and QD, where $\hat{a}^\dagger$ ($\hat{a}$) is the creation (annihilation) operator for the MNP plasmonic mode and $\hat{\sigma}^\dagger$ ($\hat{\sigma}$) is the raising (lowering) operator for the QD. The term $\hat{H}_{\mathsf{int}}$ describes the near-field interaction between the QD and the MNP plasmonic mode, while $\hat{H}_{\mathsf{drive}}$ accounts for the driving of the system by an external electric field $E_0$. The coupling of the MNP plasmonic mode to the QD and the driving field are characterized by $g$ and $\zeta$ respectively, and $\mu$ is the dipole moment of the QD.

The above Hamiltonians do not account for any losses the system may incur due to interactions with an external environment. The system can lose energy both radiatively to the electromagnetic vacuum, as well as due to ohmic losses in the metal. These environmental couplings can be modeled as an interaction of the system with a bath of quantized harmonic oscillators [ZGB06, RSF$^+$10, WS10]. Treating these interactions with Born-Markov approximations enables the use of a master equation in Lindblad form, $\dot{\hat{\rho}} = \hat{\mathcal{L}}(\hat{\rho})$, which gives a complete description of the system dynamics [Car99]. Here, the Lindblad operator acts as follows

$$\hat{\mathcal{L}}(\hat{\rho}) = \frac{i}{\hbar}[\hat{\rho}, \hat{H}] + \hat{L}_0 + \hat{L}_x, \tag{3.10}$$

where

$$\hat{L}_j = \frac{\gamma_j}{2}(2\hat{c}_j\hat{\rho}\hat{c}_j^\dagger - [\hat{c}_j^\dagger\hat{c}_j, \hat{\rho}]_+), \tag{3.11}$$

$j = \{0, x\}$, $\hat{c}_0$ ($\hat{c}_x$) represents $\hat{a}$ ($\hat{\sigma}$) and $[]_+$ is the notation for the anti-commutator. $\gamma_x$ is the spontaneous emission rate of the QD and $\gamma_0$ accounts for both ohmic, $\gamma_{nr}$,

and radiative damping, $\gamma_r$, of the MNP, where $\gamma_0 = \gamma_{nr} + \gamma_r$. The spontaneous emission rate of the QD is taken as $\gamma_x = 80 \times 10^9$ rad s$^{-1}$ [RSF$^+$10]. The ohmic damping of the MNP is $\gamma_{nr} = \gamma + \frac{\gamma^3(2\epsilon_b+\epsilon_\infty)}{\omega_p}$, where $\gamma$ is the damping frequency of silver which we take as $\gamma = 2.7 \times 10^{13}$ rad s$^{-1}$ [ASE06, AE08, ST09]. The radiative emission is calculated from a dipole scattering formula, $\gamma_r = \frac{2k^3\omega_0 r^3}{\epsilon_\infty+2\epsilon_b}$ [AE08], where $k$ is the wavenumber of the light. Radiative scattering dominates for larger MNPs which are more efficient antennas, while for small MNPs the ohmic damping dominates as the mean free path of the conduction band electrons decreases [BHA00].

**Solving the MNP-QD dynamics**

In order to find the dipole moment of the MNP-QD metamolecule and hence it's polarizability we need to find the expectation values of the system operators. By working in the Heisenberg picture we can calculate the equations of motion for the expectation values, *i.e.* the Maxwell-Bloch (MB) equations, which we express here in a frame rotating with the driving field frequency $\omega$,

$$\langle \dot{\hat{a}} \rangle = -(i\Delta_0 + \frac{\gamma_0}{2})\langle \hat{a} \rangle + g\langle \hat{\sigma} \rangle + \frac{i\zeta E_0}{\hbar}, \tag{3.12}$$

$$\begin{aligned} \langle \dot{\hat{\sigma}} \rangle = &-(i\Delta_x + \frac{\gamma_x}{2})\langle \hat{\sigma} \rangle - g\langle \hat{a} \rangle + 2g\langle \hat{a}\hat{\sigma}^\dagger\hat{\sigma} \rangle \\ &+ \frac{i\mu E_0}{\hbar}(1 - 2\langle \hat{\sigma}^\dagger\hat{\sigma} \rangle), \end{aligned} \tag{3.13}$$

where $\Delta_{0(x)} = (\omega_{0(x)} - \omega)$. In the general case, the above equations are difficult to solve as they are not in a closed form and thus form an infinite hierarchy of equations [Arm09]. However, we can make approximations that transform the equations into more amenable semi-classical equations. This can be done by making the assumption that the QD and the MNP field are separate systems and factoring the term $\langle \hat{a}\hat{\sigma}^\dagger\hat{\sigma} \rangle$ into its light and matter components. This is a reasonable assumption when considering that the large damping of the MNP field inhibits coherent interactions [WS10]. The MB equations can then be simplified further by assuming a

weak driving field. In this case, the excited state population of the QD, $\langle\hat{\sigma}^{\dagger}\hat{\sigma}\rangle$, is taken to be negligible [ZGB06, RSF$^{+}$10, WS10].

The MNP-QD system described above is a driven-dissipative one and therefore we are interested in calculating the polarizability when the system reaches a non-equilibrium steady state (NESS), *i.e.* when the system operators $\dot{\hat{O}} = 0$. Using the above simplifications the NESS value of the MNP plasmonic field annihilation operator can be found to be

$$\langle\hat{a}\rangle = \frac{g\langle\hat{\sigma}\rangle}{i\Delta_0 + \frac{\gamma_0}{2}} + \frac{i\zeta E_0}{\hbar(i\Delta_x + \frac{\gamma_0}{2})}. \tag{3.14}$$

To ensure the above quantum framework correctly describes the physics of the system we compare its results to those predicted by classical theory [RSF$^{+}$10]. In this way we can relate $\langle\hat{a}\rangle$ to the MNP dipole moment ($p_{\mathsf{MNP}}$) as well as expressing $g$ and $\zeta$ in terms of system variables.

**Linking the quantum and the classical models**

The coupling frequency, $g$, of the dipole interaction between the MNP field mode and the QD is defined as $\hbar g = \mu\xi$, where $i\xi\hat{a} = \hat{E}_m$ is the positive frequency part of the MNPs dipolar electric field and $\mu$ is the dipole moment of the QD. In order to derive an expression for $g$ and $\zeta$, one must equate the NESS quantum expectation value of the MNP electric field with its classically derived value, *i.e.* $\langle\hat{E}_m\rangle = E_m$. The classical NESS value is given by

$$E_m = \frac{S}{4\pi\epsilon_0\epsilon_b}\frac{p_{\mathsf{MNP}}}{d^3}, \tag{3.15}$$

where the dipole moment of the MNP is

$$\begin{aligned} p_{\mathsf{MNP}} =& \alpha_{\mathsf{MNP}}\left(E_0 + \frac{Sp_{\mathsf{QD}}}{4\pi\epsilon_0\epsilon_b r^3}\right) \\ =& 4\pi\epsilon_0\epsilon_b r^3\left(\frac{\epsilon_m(\omega)-\epsilon_b}{\epsilon_m(\omega)+2\epsilon_b}\right)\left(E_0 + \frac{Sp_{\mathsf{QD}}}{4\pi\epsilon_0\epsilon_b r^3}\right). \end{aligned} \tag{3.16}$$

Here, $S$ is a scalar parameter set to 2 (-1) for the case of the driving field being parallel (perpendicular) to the MNP-QD separation vector, $d$ is the MNP-QD separation distance, $r$ is the radius of the MNP, $E_0$ is the driving field amplitude and $p_{QD}$ is the dipole moment of the QD. From Eq. (3.16), we see that the MNP is excited by the external driving field and the QD field. The dipole moment of the QD is given by $p_{QD} = \mu\langle\hat{\sigma}\rangle$. The frequency dependent complex function, $\frac{\epsilon_m(\omega)-\epsilon_b}{2\epsilon_b+\epsilon_m(\omega)}$, determines the resonance frequency, $\omega_0$, of the MNP field, where $\epsilon_m$ is the permittivity of the metal, calculated with the Drude model. This resonance will occur when the Fröhlich condition is met, $\mathrm{Re}[\epsilon_m(\omega)] = -2\epsilon_b$ [Mai07, KV95]. A first-order Taylor expansion of $\epsilon_m(\omega)$ allows the MNPs polarizability to be approximated by a complex Lorentzian

$$\alpha_{\mathsf{MNP}} = \frac{12\pi\epsilon_0\epsilon_b^2 r^3\beta i}{i\Delta_0 + \frac{\gamma_0}{2}}. \tag{3.17}$$

The non-radiative damping, $\gamma_{nr} = \gamma + \frac{\gamma^3(2\epsilon_b+\epsilon_\infty)}{\omega_p}$ comes naturally from $\epsilon_m(\omega)$, while the radiative damping is added in phenomenologically. For brevity we use the parameter $\beta = \frac{(\gamma^2(2\epsilon_b+\epsilon_\infty)+\omega_p^2)^2}{2(2\epsilon_b+\epsilon_\infty)^{\frac{3}{2}}\omega_p^3}$. The Taylor approximation allows us to draw an analogy between the plasmonic mode and a leaky cavity mode. The NESS value for the MNPs electric field in the quantum formalism is

$$\langle\hat{E}_m\rangle = i\xi\langle\hat{a}\rangle \tag{3.18}$$

$$= \frac{i\hbar g\langle\hat{a}\rangle}{\mu}. \tag{3.19}$$

Substituting Eq. (3.14) into the above equation we find

$$\langle \hat{E}_m \rangle = \frac{i\hbar g^2 \langle \hat{\sigma} \rangle}{\mu(i\Delta_0 + \frac{\gamma_0}{2})} + \frac{-g\zeta E_0}{\mu(i\Delta_x + \frac{\gamma_x}{2})}. \tag{3.20}$$

If we substitute Eq. (3.17) into Eq. (3.16), then the subsequent expression into Eq. (3.15) and compare it with Eq. (3.20) one obtains the following expressions for $g$ and $\zeta$,

$$g = \frac{S\mu}{d^3}\sqrt{\frac{3\beta r^3}{4\pi\epsilon_0\hbar}}, \tag{3.21}$$

$$\zeta = -i\epsilon_b\sqrt{12\beta\epsilon_0\pi\hbar r^3}. \tag{3.22}$$

If we subsequently compare the NESS value of $\langle \hat{a} \rangle$ with the classical expression of $p_{\mathsf{MNP}}$ (Eq. (3.16)), we see that

$$p_{\mathsf{MNP}} = \zeta^* \langle \hat{a} \rangle. \tag{3.23}$$

**The Fano profile**

Using Eq. (3.23), an expression for the polarizability of the joint MNP-QD metamolecule system can be derived as

$$\alpha(\omega) = \frac{\zeta^* \langle \hat{a} \rangle + \mu \langle \hat{\sigma} \rangle}{E_0}. \tag{3.24}$$

Then, by solving the MB equations, Eqs. (3.12) and (3.13), in the steady state, an analytic expression for the system's polarizability is found to be

$$\begin{aligned} \alpha(\omega) \;=\; & \frac{i\mu^2}{\hbar(i\Delta_x + \frac{\gamma_x}{2} + \frac{g^2}{i\Delta_0 + \frac{\gamma_0}{2}})} + \frac{i|\zeta|^2}{\hbar(i\Delta_0 + \frac{\gamma_0}{2} + \frac{g^2}{i\Delta_x + \frac{\gamma_x}{2}})} \\ & + \frac{i\mu g(\zeta^* - \zeta)}{\hbar((i\Delta_x + \frac{\gamma_x}{2})(i\Delta_0 + \frac{\gamma_0}{2}) + g^2)}. \end{aligned} \tag{3.25}$$

In Fig. 3.2 (a) and (b) we show the imaginary and real parts of the metamolecule's polarizability for a range of driving field frequencies, when the resonant frequency of the MNP and QD set to be equal. Here, the dipole moment radius of the QD, $r_0 = \frac{\mu}{e}$, is taken as $r_0 = 0.9$ nm (corresponding to 43.22 Debye) [RSF$^+$10] and the background permittivity is $\epsilon_b = 2.2$. One can clearly see the Fano interference profile due to the MNP-QD interaction. In addition, looking closer at the imaginary part of the polarizability in Fig. 3.2 (d), one can see that the interference suppresses light absorption at the resonance frequency. The real part of the polarizability is used to calculate the dispersion of the MNP-QD metamolecule. The frequency regions either side of the resonance are governed by anomalous dispersion where the polarizability decreases with increasing frequency, whereas at resonance there is a sharp increase in polarizability with increasing frequency, *i.e.* normal dispersion. This effect is also seen in EIT systems where it is responsible for slow light propagation [FIM05].

The Fano interference effect can be amplified by increasing the MNP-QD coupling frequency g. In the above example, g is quite strong due to the small separation distance chosen, $g/\omega_0 = 5\times10^{-4}$. However, if the QD is placed too close to the MNP, then higher-order multipoles are excited in the MNP and the dipole approximation breaks down [YZD$^+$08]. This should be avoided if we wish to use this scatterer in a metamaterial design using dipole formulae. The QD must also be placed further than 1 nm from the MNP surface in order to avoid electron tunneling [ZPN09]. We have placed the QD at a distance of $2r$ which is sufficient for higher order multipoles to be negligible [YZD$^+$08] as well as to avoid tunneling effects [ZPN09].

## 3.4 The MNP nanoring metamaterial

Let us now consider a ring of identical MNPs in a specific configuration that has recently been studied for its application as a magnetic resonator in the visible regime [ASE06, ST09, AE08, SML$^+$13]. The goal of this section is to describe

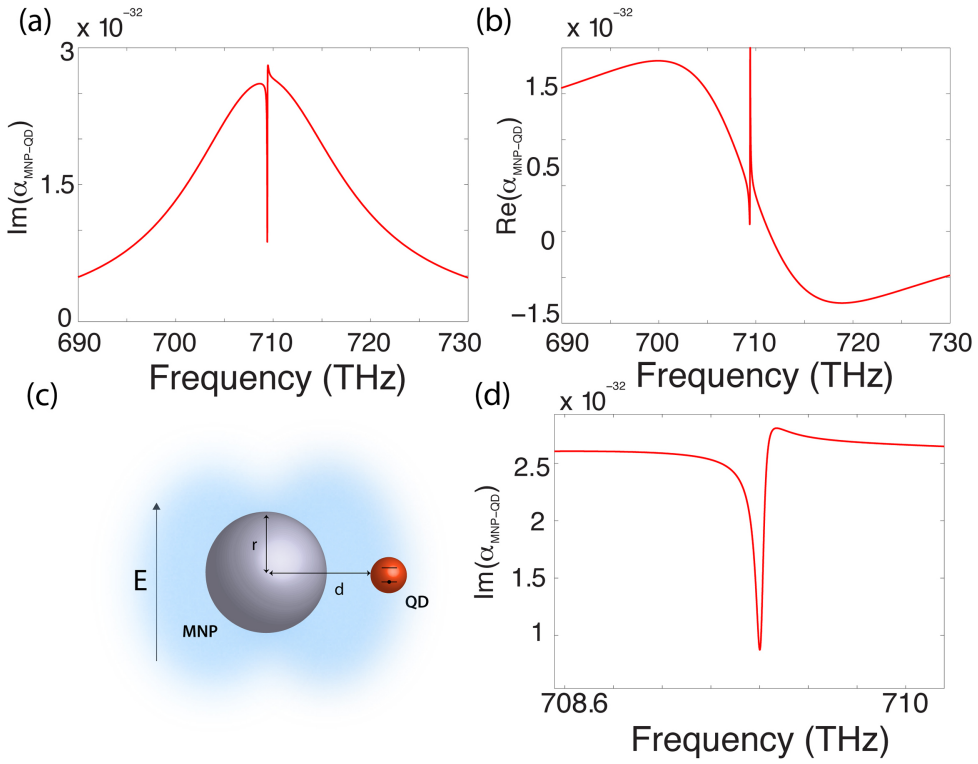


Figure 3.2: Imaginary (**a**) and real (**b**) parts of the polarizability of a MNP-QD metamolecule, whose individual dipole radii are 16 nm and 0.9 nm respectively, and whose separation distance is 32 nm. The MNP and QD are resonant in this example and they couple transversely ($S = -1$). The system is encased in a background medium of permittivity $\epsilon_b = 2.2$ and is driven weakly, $E_0\mu = 0.0001$ meV, where $\frac{E_0\mu}{\hbar}$ is the coupling frequency between the QD and the driving field. In (**c**) a sketch of the system shows that the MNP and QD are transversely coupled. In (**d**) we show the imaginary polarizability around the resonance frequency, highlighting the Fano dip.

this 'bare' system quantum mechanically so that later we can incorporate the metamolecule from the previous section.

In order to calculate the permittivity or permeability of a metamaterial, it is common practice to isolate either its electric or magnetic response with a particular type of incident field. Despite the permittivity and permeability being calculated using a special type of excitation method, these characteristic functions of the metamaterial approximate well the response of the metamaterial to an arbitrary form of incident field [ILKJ03, ASE06]. Thus we will concentrate on isolating the magnetic response

of the ring. To achieve this, we direct a high frequency magnetic field along the ring's normal axis [AE08], as shown in Fig. 3.1. The MNPs thus feel the following electric field

$$\mathbf{E_0} = \frac{i\omega\mu_0 R H_0}{2}\hat{\boldsymbol{\phi}}, \tag{3.26}$$

induced by the time varying incident magnetic field $\mathbf{H} = H_0 e^{-i\omega t}\hat{\mathbf{z}}$. Here, $R$ is the radius of the ring, $\omega$ is the frequency of the driving field, and $\hat{\boldsymbol{\phi}}$, and $\hat{\mathbf{z}}$ are unit vectors in the cylindrical coordinate system $(\hat{\mathbf{R}}, \hat{\boldsymbol{\phi}}, \hat{\mathbf{z}})$. The displacement field induced in each MNP is also directed along the azimuthal direction. Due to this symmetry, there is no net electrical response and we are therefore able to isolate the magnetic response of the system. A circular displacement field current is set up which acts as a magnetic dipole, whose magnitude is given by [ASE06]

$$m = \frac{-i\omega p_{\mathsf{MNP}} N R}{2}, \tag{3.27}$$

where $N$ is the number of electric dipoles in the ring and $p_{\mathsf{MNP}}$ is the dipole moment of a single MNP. In Fig. 3.1 the ring configuration we consider is shown for a material with a magnetic response in the $\hat{\mathbf{z}}$ direction only. Thus, the material is anisotropic. To make an isotropic material with the same response in all directions, a cubic lattice consisting of three orthogonal arrays of nanorings should be used. This can be achieved in a face-centered cubic lattice, where up to four different nanoring orientations can be included in a single unit cell [ASE06]. Furthermore, in our calculations we concentrate on the case of $N$=4 as it is the minimum number of MNPs in the ring such that the magnetic dipolar response dominates higher-order multipoles [AE08]. This is essential for the validity of characterizing the metamaterial's magnetic response with the permeability parameter, $\mu_{\mathsf{eff}}$, which we now derive [Sim11].

### 3.4.1 The permeability of a MNP nanoring metamaterial

#### The quantum model

We start by calculating the dipole moment of one of the MNP inclusions using a quantum framework. Although, strictly speaking, this approach is not required as the process is essentially classical, we set up the quantum formalism now so that it can be used when we integrate MNP-QD metamolecules into the ring in the next section. The equations of motion derived using this framework are also valid in the classical regime. The Hamiltonian of the bare system is as follows

$$\hat{H} = \hat{H}_0 + \hat{H}_{\mathsf{int}} + \hat{H}_{\mathsf{drive}}, \tag{3.28}$$

where the individual terms are

$$\hat{H}_0 = \sum_{n=0}^{N-1} \hbar\omega_0 \hat{a}_n^\dagger \hat{a}_n, \tag{3.29}$$

$$\hat{H}_{\mathsf{int}} = \sum_{n,m=0}^{N-1} \hbar J_{nm} (\hat{a}_n^\dagger \hat{a}_m + \hat{a}_m^\dagger \hat{a}_n) \quad n \neq m \tag{3.30}$$

$$\hat{H}_{\mathsf{drive}} = -E_0 \sum_{n=0}^{N-1} (\zeta^* \hat{a}_n e^{-i\omega t} + \zeta \hat{a}_n^\dagger e^{i\omega t}). \tag{3.31}$$

Here, the inter-MNP coupling frequency is given by $J_{nm}$, which for nearest neighbor coupling we denote as $J_1$ and for next-nearest neighbor coupling as $J_2$.

#### The effective permeability

Now, let's turn our efforts to calculate the effective permeability of a (classical) MNP nanoring metamaterial using our quantum formalism. In the Heisenberg picture, using the full system Hamiltonian, the equation of motion for the expectation value of the annihilation operator of each MNP field mode, $\langle \hat{a}_n \rangle$, can be found and for

$N = 4$ they can be written as

$$\langle \dot{\hat{a}}_n \rangle = -(i\Delta_0 + \frac{\gamma_0}{2})\langle \hat{a}_n \rangle - iJ_1\langle \hat{a}_{n+1} \rangle - iJ_1\langle \hat{a}_{n-1} \rangle - iJ_2\langle \hat{a}_{n+2} \rangle + \frac{i\zeta E_0}{\hbar}, \tag{3.32}$$

where the indices are written in modulo 4. This set of coupled equations can be solved in a straightforward manner in the steady state as the system's symmetry means that the expectation value of each dipole is the same. By incorporating Eq. (3.22) and Eq. (3.23) into the solution of Eq. (3.32) the dipole moment of a single MNP can be written as

$$p_{\mathsf{MNP}} = \left( \frac{-|\zeta|^2 \omega \mu_0 R H_0}{2\hbar(i\Delta_0 + \frac{\gamma_0}{2})} \right) \left( 1 + \frac{i(2J_1 + J_2)}{i\Delta_0 + \frac{\gamma_0}{2}} \right)^{-1}. \tag{3.33}$$

Then, using Eq. (3.27) we can calculate the magnetic polarizability of a single nanoring, $\alpha_m = \frac{m}{H_0}$. The effective permeability of the macroscopic composite system (metamaterial) can be calculated using the Maxwell-Garnett mixing formula [CS10, Sim11],

$$\mu_{eff} = 1 + \frac{1}{N_d^{-1}(\alpha_m^{-1} + i\frac{k^3}{6\pi}) - \frac{1}{3}}, \tag{3.34}$$

where $N_d$ is the volume concentration of nanorings in the metamaterial. The imaginary term in the denominator is only necessary when the rings are part of a regular three dimensional array. In this case, the radiative damping of the magnetic dipole is cancelled out [AE08]. Let us pause here, for a moment, in order to explicitly derive the values of the MNP-MNP coupling frequencies. This will allow us to plot the permeability and extract information from the results.

**Deriving the MNP-MNP coupling frequency**

In order to calculate the inter-MNP coupling frequencies we repeat the procedure used in section 3.3. The dipole moment of the nth MNP, $p_{\mathsf{MNP,n}}$, in an $N = 4$ nanoring

using classical theory is given by

$$p_{\mathsf{MNP,n}} = \frac{12\pi\epsilon_0\epsilon_b^2 r^3\beta i}{i\Delta_0 + \frac{\gamma_0}{2}}(E_0 + Q_1 p_{\mathsf{MNP,n+1}} + Q_1 p_{\mathsf{MNP,n-1}} + Q_2 p_{\mathsf{MNP,n+2}}), \tag{3.35}$$

where $Q_{1(2)}$ are scalar interaction terms that account for nearest (next-nearest) neighbour MNP-MNP interactions in the ring. The above expression takes into account the Lorentzian approximation for the MNP resonance that was used in section 3.3. Using Eq. (3.32) the NESS dipole moment in the quantum framework is given by

$$\begin{aligned}\zeta^*\langle\hat{a}_n\rangle =& \frac{i|\zeta|^2 E_0}{\hbar(i\Delta_0 + \frac{\gamma_0}{2})} - \frac{iJ_1\zeta^*(\langle\hat{a}_{n+1}\rangle + \langle\hat{a}_{n-1}\rangle)}{i\Delta_0 + \frac{\gamma_0}{2}} \\ & - \frac{iJ_2\zeta^*\langle\hat{a}_{n+2}\rangle}{i\Delta_0 + \frac{\gamma_0}{2}}.\end{aligned} \tag{3.36}$$

By comparing Eqs. (3.35) and (3.36) expressions for $J_1$ and $J_2$ are found to be

$$J_{1(2)} = -12\pi\epsilon_0\epsilon_b^2 r^3\beta Q_{1(2)}. \tag{3.37}$$

The value of $Q_j$ is found from the general scalar interaction terms $Q_{j\ell}$, where $Q_1 = Q_{j\ell}$ for $j$ and $\ell$ nearest neighbors and $Q_2 = Q_{j\ell}$ for $j$ and $\ell$ next-nearest neighbors. In the case of the magnetic response excitation, $Q_{j\ell}$ can be defined as the azimuthal component of the electric field at site $j$ due to the azimuthally directed dipole at site $\ell$ [AE08]. The interaction term is therefore calculated from the standard form of a dipolar electric field [Gre98]

$$\mathbf{E} = \frac{e^{ikr''}}{4\pi\epsilon_0\epsilon_b}[k^2(\mathbf{r''}\times\mathbf{p})\times\frac{1}{r''^3} + (3\mathbf{r''}(\mathbf{p}\cdot\mathbf{r''}) - \mathbf{p}\mathbf{r''^2})(\frac{\mathbf{1}}{\mathbf{r''^5}} - \frac{\mathbf{i}}{\mathbf{r''^4}})], \tag{3.38}$$

where $\mathbf{r''}$ is the distance vector between the receiving dipole $j$ at coordinates ($z = 0, R = R_{ring}, \phi = \frac{2\pi j}{N}$) and the source dipole $\ell$ at coordinates ($z' = 0, R' = R_{ring}, \phi' = \frac{2\pi\ell}{N}$). Using the definition of $Q_{j\ell}$ and Eq. (3.38) we derive the expression [AE08,

ST09],

$$Q_{j\ell} = \frac{e^{ikr''}}{4\pi\epsilon_0\epsilon_m r''^5} \times[(kr'')^2(2R^2\cos(\phi'-\phi) - R^2\cos^2(\phi'-\phi) - R^2) + (3R^2\sin(\phi'-\phi))(1-ikr'') - (r''^2\cos(\phi'-\phi))(1-ikr'')]. \tag{3.39}$$

Explicitly we have

$$Q_1 = \frac{e^{i\sqrt{2}kR}}{16\sqrt{2}\pi\epsilon_0\epsilon_b R^5}(-2k^2R^4 + 3R^2(1-ik\sqrt{2}R)), \tag{3.40}$$

$$Q_2 = \frac{e^{i2kR}}{128\pi\epsilon_0\epsilon_b R^5}(-16k^2R^4 + 4R^2(1-i2kR)), \tag{3.41}$$

where $k$ is the wave vector of the light, $k = \omega\sqrt{\mu_0\mu_b\epsilon_0\epsilon_b}$, where $\mu_0$ is the free space permeability and $\mu_b$ is the relative permeability of the background medium.

**Plotting the effective permeability**

In Fig. 3.3 we plot the effective permeability of a metamaterial with nanorings that have 2, 3 and 4 MNP inclusions. As mentioned earlier, only for $N = 4$ is the effective permeability physically meaningful. It is, however, informative to plot $N = 2$ and 3, as they show the effect the inter-MNP coupling has on red-shifting the nanoring's magnetic resonance from the electric resonance of a single MNP (vertical dashed line). In both Fig. 3.3 (a) and (b) one can see the material's resonance properties, including negative real values in panel (b). For the MNP nanoring we use the parameters of Ref. [ASE06], see Fig. 3.3. Apart from a slightly smaller, and more realistic, volume concentration of $N_d = (96\text{nm})^{-3}$, all other parameters are the same.

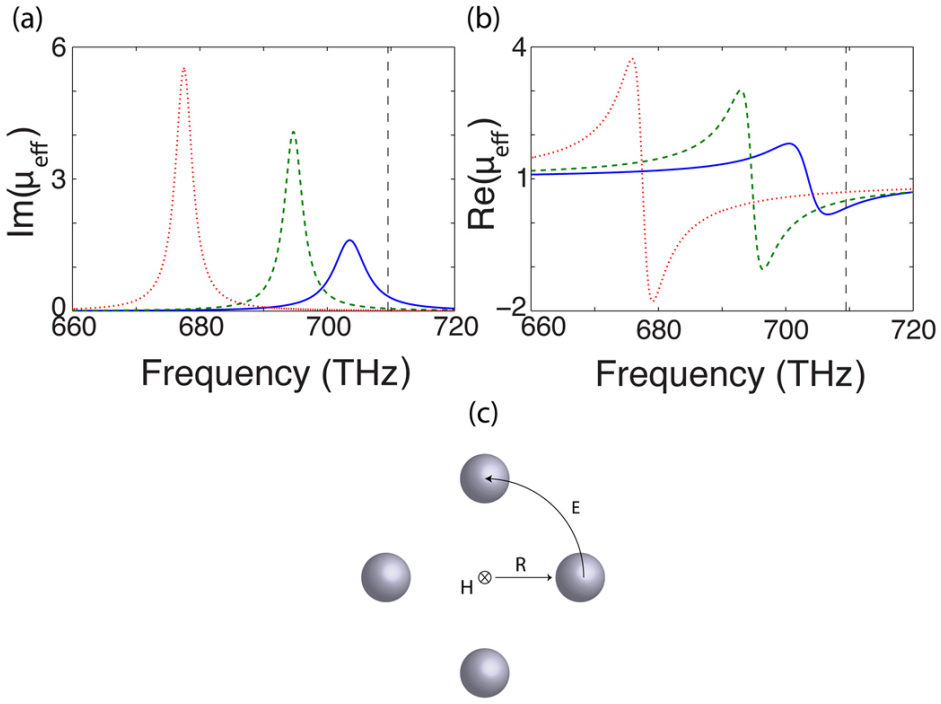


Figure 3.3: Imaginary (**a**) and real (**b**) parts of the effective permeability of an MNP nanoring metamaterial. The ring radius, $R$, and MNP radius, $r$, are 38nm and 16nm respectively. The MNPs are encased in a material with permittivity $\epsilon_b = 2.2$ and permeability $\mu_b = 1$. We plot the effective permeability for three values of $N$ in each nanoring, $N = 2$ (blue line), $N = 3$ (green dashed line) and $N = 4$ (red dotted line), where $N_d = (96\text{nm})^{-3}$. The vertical dashed line corresponds to the electric resonance of a single MNP. In (**c**) we show a sketch of the nanoring system.

## 3.5 The MNP-QD nanoring metamaterial

### 3.5.1 The weak-field limit

We now take the nanoring design from the previous section and replace each MNP with the MNP-QD metamolecule from section 3.3, as shown in Fig. 3.4 (c). In this case there are two magnetic dipoles excited by the incident magnetic field; one set up by the ring of MNPs and the other by the QD ring. We use Eq. (3.34) again to calculate the effective permeability of a metamaterial composed of these MNP-QD nanorings. However, in this case we must deal with two magnetic dipole excitations, as well as taking into account MNP-QD interactions. The Hamiltonian

for the system is

$$\hat{H} = \hat{H}_0 + \hat{H}_{\mathsf{int}} + \hat{H}_{\mathsf{drive}}, \tag{3.42}$$

where the individual terms are

$$\hat{H}_0 = \sum_{n=0}^{N-1} \hbar\omega_0 \hat{a}_n^\dagger \hat{a}_n + \sum_{n=0}^{N-1} \hbar\omega_x \hat{\sigma}_n^\dagger \hat{\sigma}_n, \tag{3.43}$$

$$\begin{aligned}\hat{H}_{\mathsf{int}} = &\sum_{n,m=0}^{N-1} \hbar J_{nm}(\hat{a}_n^\dagger \hat{a}_m + \hat{a}_m^\dagger \hat{a}_n) \quad n \neq m \\ &+ \sum_{n,m=0}^{N-1} \hbar I_{nm}(\hat{\sigma}_n^\dagger \hat{\sigma}_m + \hat{\sigma}_m^\dagger \hat{\sigma}_n) \quad n \neq m \\ &+ \sum_{n,m=0}^{N-1} i\hbar g_{nm}(\hat{a}_n^\dagger \hat{\sigma}_m + \hat{a}_n \hat{\sigma}_m^\dagger),\end{aligned} \tag{3.44}$$

$$\begin{aligned}\hat{H}_{\mathsf{drive}} = &-E_0 \sum_{n=0}^{N-1} (\zeta^* \hat{a}_n e^{-i\omega t} + \zeta \hat{a}_n^\dagger e^{i\omega t}) \\ &- E_0 \mu \sum_{n=0}^{N-1} (\hat{\sigma}_n e^{-i\omega t} + \hat{\sigma}_n^\dagger e^{i\omega t}).\end{aligned} \tag{3.45}$$

First we will calculate the effective permeability in the weak-field limit. In this case we can derive steady state MB matrix equations accounting for each site

$$\mathbf{A}\bar{a} = \mathbf{B}\bar{\sigma} + \bar{c} \tag{3.46}$$

$$\mathbf{D}\bar{\sigma} = -\mathbf{B}\bar{a} + \bar{e} \tag{3.47}$$

Where $\bar{a}$ and $\bar{\sigma}$ are vectors which represent the expectation values for $\hat{a}$ and $\hat{\sigma}$ at each site in the ring, given as

$$\bar{a} = \begin{pmatrix} \langle \hat{a}_1 \rangle \\ \langle \hat{a}_2 \rangle \\ \langle \hat{a}_3 \rangle \\ \langle \hat{a}_4 \rangle \end{pmatrix}, \bar{\sigma} = \begin{pmatrix} \langle \hat{\sigma}_1 \rangle \\ \langle \hat{\sigma}_2 \rangle \\ \langle \hat{\sigma}_3 \rangle \\ \langle \hat{\sigma}_4 \rangle \end{pmatrix}. \tag{3.48}$$

The matrix **A** represents the MNP-MNP interactions in the nanoring, given as

$$\mathbf{A} = \begin{pmatrix} i\Delta_0 + \frac{\gamma_0}{2} & iJ_1 & iJ_2 & iJ_1 \\ iJ_1 & i\Delta_0 + \frac{\gamma_0}{2} & iJ_1 & iJ_2 \\ iJ_2 & iJ_1 & i\Delta_0 + \frac{\gamma_0}{2} & iJ_1 \\ iJ_1 & iJ_2 & iJ_1 & i\Delta_0 + \frac{\gamma_0}{2} \end{pmatrix}, \tag{3.49}$$

where the MNP-MNP coupling frequency $J_n$ was defined in the previous section. The matrix **D** represents the QD-QD interactions in the nanoring, given as

$$\mathbf{D} = \begin{pmatrix} i\Delta_x + \frac{\gamma_x}{2} & iI_1 & iI_2 & iI_1 \\ iI_1 & i\Delta_x + \frac{\gamma_x}{2} & iI_1 & iI_2 \\ iI_2 & iI_1 & i\Delta_x + \frac{\gamma_x}{2} & iI_1 \\ iI_1 & iI_2 & iI_1 & i\Delta_x + \frac{\gamma_x}{2} \end{pmatrix}, \tag{3.50}$$

where $I_1$ and $I_2$ are the nearest neighbor and next-nearest neighbor QD-QD coupling frequencies, given by

$$I_{1(2)} = \frac{\mu^2}{\hbar} Q_{1(2)}. \tag{3.51}$$

The matrix **B** is the MNP-QD coupling matrix, given as

$$\mathbf{B} = \begin{pmatrix} g_1 & 0 & -g_2 & 0 \\ 0 & g_1 & 0 & -g_2 \\ -g_2 & 0 & g_1 & 0 \\ 0 & -g_2 & 0 & g_1 \end{pmatrix}. \tag{3.52}$$

Here, the coupling frequency $g_1$ is for same-site MNP-QD interactions, while $g_2$ is for an MNP coupling with its next-nearest QD neighbor. From Fig 3.4 (c) we can see that the same-site and next-nearest neighbor interactions are transverse (S = -1). Due to the azimuthal external electric field exciting the ring, the same-site QD and next-nearest neighbour QD relative to each MNP are driven in opposite directions.

As such they are out of phase, this is represented by the minus signs in the matrix. We find that the next-nearest neighbour QD works to reduce the influence of the same-site QD on each MNP. Fortunately due to the stronger same-site interaction frequency the Fano interference still occurs. Similarly both nearest neighbour QDs relative to an MNP are also out of phase, however in this case their interaction frequency is the same and their effect on the MNP is cancelled out. Finally, the vectors $\bar{c}$ and $\bar{e}$ represent the external driving of the MNPs and the QDs by the induced electric field,

$$\bar{c} = \frac{\zeta\omega\mu_0 R_1 H_0}{2\hbar}\begin{pmatrix}1\\1\\1\\1\end{pmatrix}, \bar{e} = \frac{\mu\omega\mu_0 R_2 H_0}{2\hbar}\begin{pmatrix}1\\1\\1\\1\end{pmatrix}, \tag{3.53}$$

where we have taken into account the differing radii of the MNP ($R_1$) and QD ($R_2$) nanorings. We can solve these equations to calculate the dipole moment of each MNP and QD within the nanoring,

$$p_{\mathsf{MNP}} = \zeta^*\bar{a}_1 = \zeta^*(\mathbf{A} + \mathbf{B}(\mathbf{D}^{-1})\mathbf{B})^{-1}(\mathbf{B}(\mathbf{D}^{-1})\bar{e} + \bar{c}), \tag{3.54}$$

$$p_{\mathsf{QD}} = \mu\bar{\sigma}_1 = \mu(\mathbf{D} + \mathbf{B}(\mathbf{A}^{-1})\mathbf{B})^{-1}(\mathbf{B}(\mathbf{A}^{-1})\bar{c} + \bar{e}). \tag{3.55}$$

Due to the symmetry of the system the dipole moment is the same on each site for the MNPs and also for the QDs. Following the procedure in section 3.3 we calculate the magnetic dipole of both the MNP and QD rings. The total magnetic polarizability of the MNP-QD nanoring can be found using the relation $\alpha_m = \frac{m_{\mathsf{MNP}}+m_{\mathsf{QD}}}{H_0}$ and Eq. (3.34) can be used to calculate the effective permeability of a metamaterial made from the MNP-QD nanorings. The effective permeability ($\mu_{\mathsf{eff}}$) of the metamaterial is shown in Fig. 3.4 (a) and (b). Due to the red-shift of the magnetic resonance of the MNP ring, as shown in section 3.4 ( *c.f.* Fig. 3.3), the QD resonances have

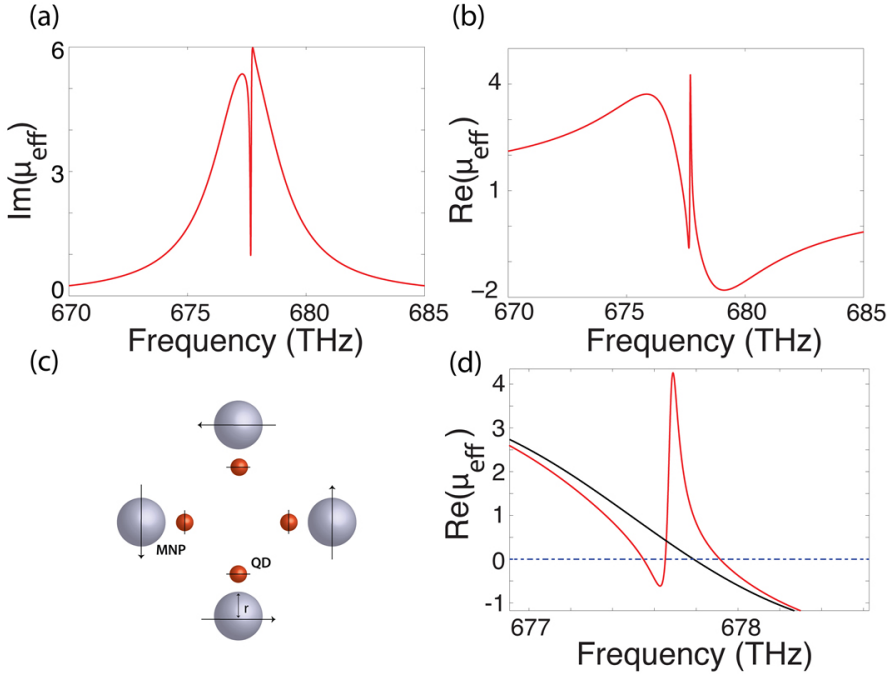


Figure 3.4: Imaginary (**a**) and real (**b**) parts of $\mu_{\text{eff}}$ for a QD-MNP nanoring metamaterial. The parameters of the system are chosen to be the same as in Figs. 3.2 and 3.3, with a MNP-QD detuning $\Delta = (\omega_0 - \omega_x) = 0.195 \times 10^{15}$ rad s$^{-1}$. In (**c**) a sketch of the system is shown, where the unit cell now consists of two interacting rings, the MNP ring and the QD ring. The arrows on the MNPs show the electric field direction at each MNP and their direction also represents their adjacent QD's dipole orientation. In (**d**) we examine the difference between Re($\mu_{\text{eff}}$) with (red) and without (black) QDs in the nanoring.

been red-shifted in order to ensure Fano interference. The MNP ring has a radius of $R_1 = 38$ nm, while the QD ring has a radius of $R_2 = 6$ nm. Thus the same site MNP-QD separation is $d = 32$ nm, as was the case for the MNP-QD molecule investigated in section 3.3.

We can see that the Fano interference present in the effective permeability is more prominent than that observed in the polarizability of an individual MNP-QD molecule (*c.f.* Fig. 3.2). This is due to multiple QDs in the nanoring interacting with each MNP either directly or mediated through MNP-MNP interactions. In Fig. 3.4 (d) we show how the introduction of the QDs in the nanoring design changes the real part of the permeability from positive to negative through the Fano interference.

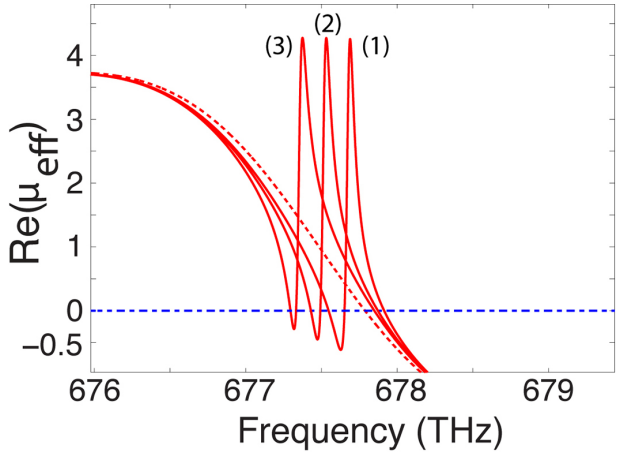


Figure 3.5: Tunability of the MNP-QD nanoring metamaterial. The real part of $\mu_{\text{eff}}$ for different MNP-QD detunings. We plot: (1) $\Delta = 0.195$, (2) $\Delta = 0.196$, and (3) $\Delta = 0.197$. All detunings are in units of $10^{15}$ rad s$^{-1}$. The dashed red line shows the bare MNP nanoring in the absence of QDs.

The magnitude of $\text{Re}(\mu_{\text{eff}})$, when negative, is not very large. This is related to the strength of the magnetic resonator. In our proof-of-principle calculations we have confined the MNP-QD nanoring to only four sites. In practice the strength of the resonance can be easily amplified by simply increasing the number of sites in the ring [AE08].

From the above analysis, one can see that the integration of QDs in the MNP nanoring has transferred the Fano line-shape of the metamolecule to the effective permeability of the metamaterial. This provides an extra degree of control over the metamaterial's response. An example of this is the ability to tune the frequency at which negative permeability occurs. From Fig. 3.4 (d) one can see that the Fano dip causes a negative real permeability at the QD resonance frequency. Thus, by dynamically shifting the resonance frequency of the QDs, one can shift the frequency at which the metamaterial has a negative permeability, as shown in Fig. 3.5. However, the trade-off for this tunability is that as the QDs are detuned away from the magnetic resonance the bandwidth narrows. The bandwidth, $\delta$, of the dip varies from 0.05 THz to 0.01 THz as we detune the QD away from the MNP

nanoring's resonance. This still compares favourably to the bandwidth found in EIT experiments with cold rubidium atoms, where a dip bandwidth of $\delta = 50$ MHz is observed [WZJZ03].

### 3.5.2 The strong-field limit: nonlinear effects

So far, all calculations have been confined to the weak driving field limit. If we want to study the nonlinear properties of the nanoring metamaterial we need to consider a strong driving field. Driving the MNP-QD metamolecule strongly can dramatically modify how light scatters from it. The two-level QD becomes saturated by the driving field and its interaction with the MNP field disappears, and with it any Fano interference. This nonlinear Fano effect cannot be predicted by classical or semi-classical theory, and has been studied previously in isolated MNP-QD systems and recently observed in quantum-well structures [ZG11, MdAN11, KGR$^+$08]. In Fig. 3.6 the parameters used in our study are chosen in order to show this effect for a single MNP-QD system of the nanoring. The MNP and the QD are driven by the same external field, and one can see that as the intensity of the field increases (from the top row to the bottom row), the Fano dip in the metamolecule's polarizability is washed out by the saturation of the QD's population. These results have been computed by solving the full master equation numerically. The numerical approach involves solving the eigenproblem,

$$\hat{\mathcal{L}}(\hat{\rho}_{SS}) = 0, \tag{3.56}$$

where $\hat{\rho}_{SS}$ is the NESS density matrix of the system. The difficulty here lies in the unbounded dimensions of the bosonic MNP field mode, whose Hilbert space is infinite. To proceed, we must truncate the dimension of the MNP field's Hilbert space. In order to capture the non-classical behavior we ensure that we allow for a dimension of at least 15. This problem is well suited to the quantum optics toolbox

developed by Tan [Tan99].

Our nanoring contains a minimum of four MNPs which makes its combined Hilbert space very large. Thus while the formalism we have developed and studied in this work is now in place, it is unfortunately too computationally intensive at present to study the saturation of the nanoring. However, logically if the QD is saturated in the MNP-QD metamolecule it will also be saturated when coupled to the MNPs in the nanoring. We know the addition of the QDs into the MNP nanoring cause the material's permeability to become negative at their resonance frequency, as seen in Fig. 3.4 and Fig. 3.5. Thus, if the QD was saturated by a separate control field then the permeability could be controlled and varied with the light intensity between positive and negative values. In future work, techniques from many-body quantum systems [GCJA13] may be used together with our formalism in order to make the computation accessible.

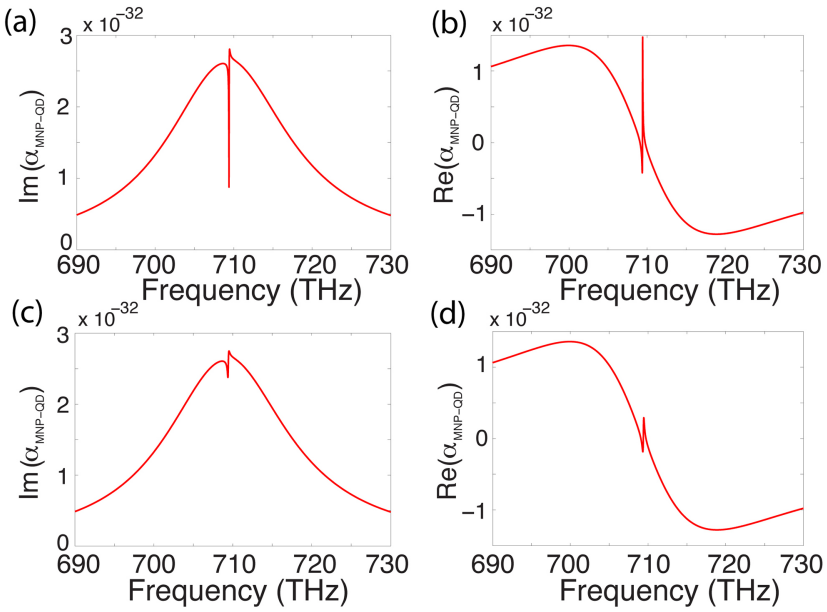


Figure 3.6: Nonlinear response of the MNP-QD metamolecule. A comparison of the imaginary ((**a**) and (**c**)) and real ((**b**) and (**d**)) parts of the polarizability for a weak external driving field (top row) with $E_0\mu = 0.0001$ meV, and a strong driving field (bottom row) with $E_0\mu = 0.1$ meV. The MNP-QD detuning is $\Delta = 0.195 \times 10^{15}$rad $s^{-1}$.

## 3.6 Remarks

In this chapter we have developed a quantum optical model to describe the dynamics of a negative permeability metamaterial integrated with two-level QDs. Using this model we found that the Fano interference of a MNP-QD metamolecule can manifest itself in the macroscopic magnetic response of a metamaterial consisting of MNP-QD nanorings. We have shown that this effect can be used to tune the properties of the metamaterial. Our model is also useful to study nonlinear effects that arise when the metamaterial is driven strongly. We showed an example of this by studying how the nonlinear Fano effect can affect our nanoring.

Importantly, we must ask can this design support a negative refractive index? While each MNP has its own electric response, the frequencies at which the MNP nanoring metamaterial has a negative permeability and the frequencies at which it has a negative permittivity do not overlap. Even with inclusion of the QDs this problem remains. Unfortunately the Fano profile in the electric and magnetic scattered fields cannot be tuned independently in our scheme. Without this ability it is not possible to ensure a frequency overlap. Instead, in future work we intend to investigate how to incorporate the magnetic nanoring resonators with a broadband negative permittivity background [CS10], using various types of lattice configuration. In this way by dynamically tuning the magnetic response, we may also be able to control the metamaterial's refractive index. However, even for a material that has only a negative permeability, recent work has shown interesting quantum dynamics can be observed in the spontaneous emission interference of an emitter placed in close proximity [ZXY11]. The ability to tune and saturate the magnetic response in this scenario may open up new additional features.

Another direction of future work would be to exam how fluorescence quenching of the QD by the MNP would affect our system. In our parameter space we do not

expect quenching to be a major factor [AB10], however it would be interesting to quantify at what point this approximation no longer holds for the system we have studied.

Furthermore, in our calculations we have used similar parameters to previous studies [ASE06, ST09, AE08]. However, it has been noted recently that the ohmic damping used for the MNP fields may well be an underestimation [MS10], resulting from the discrepancy between the Drude model used theoretically and experimental results at higher frequencies. Using more realistic damping it has been shown that rings with spherical MNPs no longer have a strong enough magnetic resonance to achieve $\mathrm{Re}(\mu_{\mathsf{eff}}) < 0$. However, this problem may potentially be resolved using MNP's with embedded gain material [HPM$^+$12] or different type of nanostructures in place of the MNPs. Indeed, by considering more complex, strongly polarized plasmonic nanostructures within the ring [MS10, MS11], negative permeability has been shown to be possible, whilst ensuring damping is correctly accounted for. Here, Morits and Simovski have explored the use of dimers [MS10] and nanoprisms [MS11], with the latter providing negative permeability in the visible regime. In both cases only dipole interactions are considered, therefore the basic theoretical model we have developed in this work using MNPs can be transferred to these more complex nanostructures in a straightforward manner, with the qualitative results of our analysis remaining valid.

# Chapter 4

# Microscopic response in the ultrastrong-coupling regime

## 4.1 Introduction

In the previous chapter we examined how a macroscopic collection of quantum plasmonic structures responds to light. Specifically, we showed that interacting MNP-QD systems could be used favourably in a negative permeability metamaterial design. In this chapter, we step away from dealing with large complex systems. Instead we focus on how smaller systems interact. In particular we are interested in a single light mode interacting with a collection of two-level quantum emitters when the interaction strength is extremely large. This model has a particular relevance to quantum plasmonics as we know plasmonic modes couple very strongly with quantum emitters. With the fast pace of experimental advances, it is certainly possible in the years ahead that a collection of quantum emitters interacting with a plasmonic mode will reach the ultrastrong-coupling regime (USC). This, less than subtle, name is used by quantum opticians to describe the situation in which the coupling frequency between two systems is comparable to or greater than the sys-

tem's resonance frequency [Bra11]. In this regime the rotating wave approximation (RWA) used by theoreticians to simplify light-matter dynamics becomes invalid. It is a fascinating regime that displays unique behaviour that should prove very fruitful in developing future quantum technologies. We are motivated to understand how to correctly model such systems in order to provide a solid platform for future experimental work in quantum plasmonics.

We begin this chapter by giving a brief description of the USC regime and how such systems interact with their surrounding environment. We place an emphasis on the latter point. We are interested in how USC systems can be externally probed and thus we must understand how they radiate into the environment. Following this we outline the main work of this chapter, the investigation of the emission radiated after the coupling between a large number of two-level emitters and a single mode cavity field is non-adiabatically switched on. Counter-rotating terms as well as the so-called diamagnetic – or $A^2$ – term are included in the light-matter interaction, where $\mathbf{A}$ is the vector potential. Under typical conditions, the system relaxes to the new ground state by radiating into two spectrally resolved output modes. We find that the Thomas-Reiche-Kuhn (TRK) sum rule, associated with the emitters, enforces qualitative constraints on the quantum statistics of this radiation. For ideal two-level emitters the populations of the two modes are always found equal. This result cannot be recovered if the $A^2$ term is neglected, or even if it is partially included via renormalization of the light mode frequency. For imperfect two-level emitters, featuring residual couplings to higher levels, we show that it is instead possible to circumvent this constraint, and that a naive application of the two-level approximation would give the wrong predictions. We discuss when an effective two-level description can be recovered in this regime. Our work in this chapter illustrates how the $A^2$ term, TRK rules, and the failure of the two-level approximation can play a crucial role as soon as the RWA is dropped.

## 4.2 Ultrastrong-coupling

Quantum technologies based on optics exploit intense interactions between light and matter degrees of freedom [Mon02], and it is a typical experimental goal in this context to maximize the coupling between the two. The strength of light-matter interactions is restricted by interaction times as well as the volume of the given light mode. Traditional cavity QED setups exploit high quality cavity mirrors to boost interaction times, yet the resulting coupling frequency remains only a tiny fraction of that of the system components. Experimental advances, for example in semiconductor microcavities and circuit QED, have pushed the strength of light-matter interactions into the ultrastrong-coupling regime [NDH$^+$10, MAK$^+$11, ALT$^+$10, TAC$^+$12, SHGE11]. This regime is characterized by interactions where the coupling frequency ($g$) is comparable to the bare frequencies of the light and matter modes. The theoretical description of the USC demands the inclusion of terms that do not conserve the excitation numbers of the individual components — the so-called 'counter-rotating terms' — making the application of the RWA invalid [Bra11, CBC05]. This regime has been studied extensively due to the lure of exotic phenomena such as the existence of virtual excitations in the ground state [CBC05], dynamical Casimir effects [LGCC09], and quantum phase transitions [NC10, EB04].

### Bloch-Siegert regime

To understand the limits of the RWA, let us briefly examine the Rabi model which describes a two-level atom interacting with a single light mode,

$$H_{\mathsf{Rabi}} = \omega_a \hat{a}^\dagger \hat{a} + \omega_x \hat{\sigma_z} + g(\hat{a} + \hat{a}^\dagger)(\hat{\sigma} + \hat{\sigma}^\dagger). \tag{4.1}$$

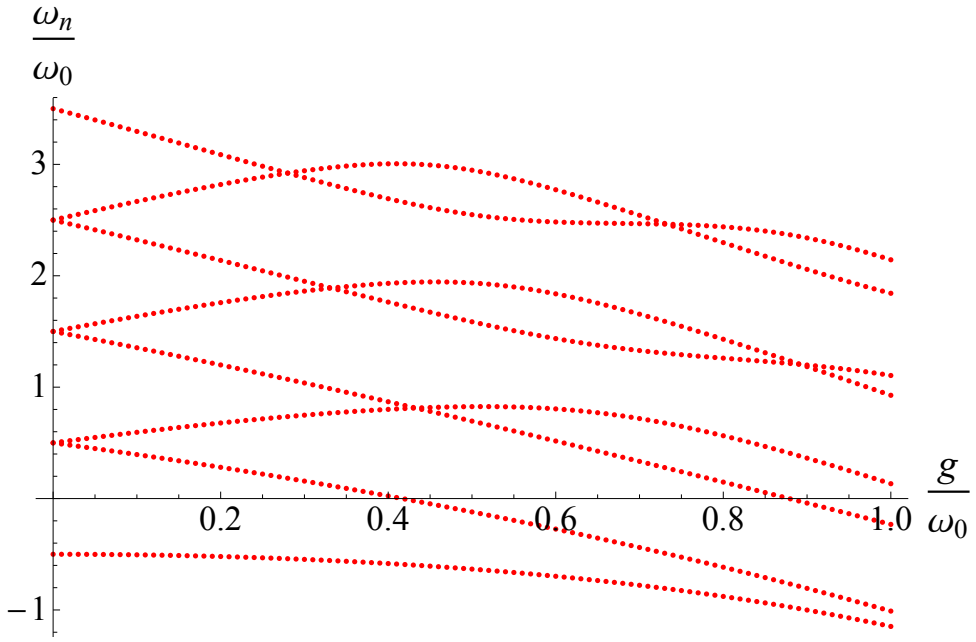


Figure 4.1: The dressed state energy levels of the resonant Rabi Hamiltonian ($\omega_a = \omega_x = \omega_0$) as a function of coupling frequency normalized to the resonance frequency $g/\omega_0$. This spectrum is characterized by the oscillating behaviour of the energy levels and is markedly different to the spectrum of the Jaynes-Cummings Hamiltonian.

Invoking the RWA is equivalent to neglecting the terms, $\hat{a}\hat{\sigma}^\dagger$ and $\hat{a}^\dagger\hat{\sigma}$. This leads to the Jaynes-Cummings Hamiltonian [WM08, Aga12]

$$H_{\mathsf{JC}} = \omega_a \hat{a}^\dagger \hat{a} + \hat{\omega}_x \hat{\sigma}_z + g(\hat{a}\hat{\sigma}^\dagger + \hat{a}^\dagger \hat{\sigma}). \tag{4.2}$$

In this model the total number of excitations is a good quantum number, allowing $H_{\mathsf{JC}}$ to be diagonalized exactly. However when $g$ gets large, the quantum excitations are no longer conserved and the Jaynes-Cumming model becomes obsolete. To get a better idea of when exactly this occurs let us perform the unitary transformation [BGB11]

$$U = e^{\Lambda(\hat{a}\hat{\sigma}^\dagger - \hat{a}^\dagger\hat{\sigma}) + \frac{g}{2\omega_a}(\hat{a}^2 - \hat{a}^{\dagger 2})\hat{\sigma}_z} \tag{4.3}$$

on $H_{\mathsf{Rabi}}$, where $\Lambda = \frac{g}{\omega_a+\omega_x}$. If we restrict the transformation to second order in $\Lambda$, we arrive at the Bloch-Siegert Hamiltonian [BGB11]

$$H_{\mathsf{BS}} = (\omega_a + \frac{g^2}{\omega_a+\omega_x}\hat{\sigma}_z)\hat{a}^\dagger\hat{a} + (\hat{\omega}_x + \frac{g^2}{\omega_a+\omega_x})\hat{\sigma_z} + g(\hat{a}\hat{\sigma}^\dagger + \hat{a}^\dagger\hat{\sigma}). \tag{4.4}$$

We see that $H_{\mathsf{BS}}$ is similar to $H_{\mathsf{JC}}$, however in $H_{\mathsf{BS}}$ there is a frequency shift for both components proportional to $\frac{g^2}{\omega_a+\omega_x}$. Obviously this shift becomes important when this parameter becomes non-negligible. Thus, taking into account acceptable errors, we can gauge that the RWA approximation is valid up to $\frac{g}{\omega_a+\omega_b} \sim 0.1$. Any system with a value of $g$ greater than this is adjudged to be in the USC regime. The Bloch-Siegert is a sub-regime of the USC, $H_{\mathsf{BS}}$ remains valid only for lower values within the USC regime. However it has proved a useful example to show how crucial the relative magnitudes of $g, \omega_a$, and $\omega_b$ are to discern the validity of the RWA.

## 4.3 Open systems in the ultrastrong-coupling regime

In order to examine how information leaks from USC systems it is essential to clarify a proper dissipative theory for this regime. One can always employ a Fano-type diagonalization technique, where the entire system-environment Hamiltonian is exactly diagonalized, which quantifies the true system-environment eigenstates regardless of the coupling strength [Fan61]. This approach has been used to understand quantum electrodynamics in dielectrics, where the matter is represented by a bosonic polarization field [HB92]. The calculations required, however, can be quite involved compared to approximate quantum optics methods such as the Markovian master equation [BP02] or input-output theory [CG84, GZ04]. On the other hand, these approximate methods, when applied naively, can predict unphysical results in the USC regime [BO12]. The naivety we allude to is the perception that the system should dissipate into the ground state of its individual components. This is exactly what happens if the formalism is derived from a dissipative model in which

each system component interacts with an infinite bath of harmonic oscillators in the vacuum. This model is satisfactory for a weakly-coupled system, however in the USC system the ground state of the individual components is not the collective system's true ground state. In order to ensure that the theory predicts dissipation to the true ground state the interaction between the system and the environment must be expressed in terms of eigenstates that diagonalize the system Hamiltonian [CC06, ARH12, BGB11].

Furthermore, these standard methods often make a Markovian approximation, meaning the coupling between the system and the environment is assumed to be frequency-independent. In a weakly-coupled system, where the transitions are very closely spaced, this is a reasonable approximation. However if the transitions are widely spaced, as is the case in even resonant USC systems, one can no longer neglect the coloured nature of the environment without error. Including the full spectral density of the environment is cumbersome and precludes many calculations. There is, fortunately, an intermediate approximation. If the transitions are spaced far apart, and their decay rates small enough, such that they are well distinguishable then we can approximate each transition decaying into an independent environment [BGB11]. In this case we can apply a markovian approximation for each transition, this independent-transition approximation has the advantage that each transition can have a unique coupling frequency to the environment.

### 4.3.1 The model

The system under examination consists of a confined photonic mode of bare frequency $\omega_a$ and annihilation operator $\hat{a}$ (cavity mode for brevity), and a collection of $n$ two-level emitters with ground state $|g\rangle$ and excited state $|e\rangle$, separated by a frequency $\omega_b$, and identically coupled to the cavity mode via electric dipole interactions. For convenience we introduce the collective operator $\hat{b} = n^{-1/2} \sum_{k=1}^{n} |g\rangle_k\langle e|_k$

(matter mode for brevity), and consider the Holstein-Primakoff regime $n \gg 1$, where $[\hat{b}, \hat{b}^\dagger] \simeq 1$ [HP40]. The cavity mode is weakly coupled to a continuum of external modes $\hat{\alpha}_\omega$ where it can radiate. To simplify the discussion we shall neglect losses in the matter system, and assume that the modes $\hat{\alpha}_\omega$ are fully accessible for measurement. While we are adopting a terminology typical of polaritonic systems, our treatment may be applied to other scenarios. The components of the total Hamiltonian, $H_{\mathsf{tot}} = H_{\mathsf{sys}} + H_{\mathsf{ext}}$, read ($\hbar = 1$)

$$H_{\mathsf{sys}} = \omega_a \hat{a}^\dagger \hat{a} + \omega_b \hat{b}^\dagger \hat{b} + g(\hat{a}+\hat{a}^\dagger)(\hat{b}+\hat{b}^\dagger) + D(\hat{a}+\hat{a}^\dagger)^2, \tag{4.5}$$

$$H_{\mathsf{ext}} = \int d\omega\, \omega \hat{\alpha}_\omega^\dagger \hat{\alpha}_\omega + \int d\omega\, J(\omega)(\hat{a} + \hat{a}^\dagger)(\hat{\alpha}_\omega + \hat{\alpha}_\omega^\dagger) \tag{4.6}$$

The cavity mode interacts with the external continuum through a frequency dependent coupling strength $J(\omega)$. The term proportional to D originates from the squared vector potential term ($A^2$) in the minimal coupling Hamiltonian. For a collection of ideal two-level emitters, the TRK sum rule for the ground state dictates that [Tho25, Wan99, Kuh25]

$$D = \frac{g^2}{\omega_b}. \tag{4.7}$$

We shall leave D implicit, however, to allow us to study the impact of the $A^2$ term on the system dynamics. To allow ultrastrong-coupling we include the counter-rotating terms $\hat{a}\hat{b}$ and $\hat{a}^\dagger\hat{b}^\dagger$. When the coupling $g$ is a significant fraction of the bare frequencies $\omega_a, \omega_b$, the open dynamics of the system is more conveniently described in terms of the eigenmodes which diagonalize $H_{\mathsf{sys}}$. We shall refer to these eigenmodes as the upper (U) and lower (L) polariton. They can be expressed as linear combinations of the positive and negative frequency parts of both the light and matter modes [Hop58], i.e.

$$\hat{p}_k = \mathrm{w}_k \hat{a} + x_k \hat{b} + y_k \hat{a}^\dagger + z_k \hat{b}^\dagger. \tag{4.8}$$

Where $k \in \{L, U\}$. The Hopfield coefficients, $\{\mathrm{w}_k, x_k, y_k, z_k\}$, and the polaritonic frequencies, $\omega_k$, are determined by inserting Eq. (4.8) into $[\hat{p}_k, H_{\mathsf{sys}}] = \omega_k \hat{p}_k$ and solving the following eigenvalue problem [Hop58, CBC05]

$$\begin{pmatrix} \omega_a + 2D & g & -2D & -g \\ g & \omega_b & -g & 0 \\ 2D & g & -\omega_a - 2D & -g \\ g & 0 & -g & -\omega_b \end{pmatrix} \begin{pmatrix} \mathrm{w}_k \\ x_k \\ y_k \\ z_k \end{pmatrix} = \omega_k \begin{pmatrix} \mathrm{w}_k \\ x_k \\ y_k \\ z_k \end{pmatrix}. \tag{4.9}$$

These Hopfield coefficients are normalized by imposing the bosonic commutation relations $[\hat{p}_k, \hat{p}^\dagger_{k'}] = \delta_{kk'}$, which gives us the normalization condition

$$\mathrm{w}^*_k \mathrm{w}_{k'} + x^*_k x_{k'} - y^*_k y_{k'} - z^*_k z_{k'} = \delta_{kk'} \tag{4.10}$$

We can also express the bare bosonic modes in terms of the polaritonic modes:

$$\hat{a} = \mathrm{w}^*_L \hat{p}_L + \mathrm{w}^*_U \hat{p}_U - y_L \hat{p}^\dagger_L - y_u \hat{p}^\dagger_U \tag{4.11}$$

$$b = x^*_L p_L + x^*_U \hat{p}_U - z_L \hat{p}^\dagger_L - z_u \hat{p}^\dagger_U \tag{4.12}$$

By recasting $H_{\mathsf{tot}}$ in terms of the polaritonic operators, we obtain

$$\begin{aligned} H_{\mathsf{tot}} = &\sum_{k=L,U} \omega_k p^\dagger_k p_k + \int d\omega \omega \alpha^\dagger_\omega \alpha_\omega \\ &+ \sum_{k=L,U} \int d\omega J(\omega)(\alpha_\omega + \alpha_\omega)((\mathrm{w}^*_k - y^*_k)p_k + (\mathrm{w}_k - y_k)p^\dagger_k). \end{aligned} \tag{4.13}$$

At this point, let us reemphasise why we express $H_{\mathsf{tot}}$ in this way. A reasonable dissipative theory should demand that the interaction with the external continuum of environment modes brings the system into its true ground state, the polaritonic mode vacuum ($p_k|0\rangle_k = 0$). As mentioned in the introduction of this section, this will not be the case if the system-environment interaction is expressed in terms

of the bare modes. In this case the system will be dissipate into the bare mode vacuum ($|0\rangle_a, |0\rangle_b$). It is clear that this scenario will bring the polaritonic modes into a non-zero energy state,

$$E_0 = \sum_{k=L,U} \langle 0_a, 0_b | p_k^\dagger p_k | 0_a, 0_b \rangle = \sum_{k=L,U} (|y_k|^2 + |z_k|^2). \tag{4.14}$$

The interaction Hamiltonian in Eq. (4.13) ensures the system dissipates into its true ground state, once the RWA has been performed. This is a perfectly reasonable approximation for weak system-environment interactions and it leaves us with the total Hamiltonian,

$$\begin{aligned} H_{\mathsf{tot}} \simeq & \sum_{k=L,U} \omega_k \hat{p}_k^\dagger \hat{p}_k + \int \mathrm{d}\omega \omega \hat{\alpha}_\omega^\dagger \hat{\alpha}_\omega \\ & + \sum_{k=L,U} \int \mathrm{d}\omega J(\omega)((\mathrm{w}_k^* - y_k^*)\hat{\alpha}_\omega^\dagger \hat{p}_k + (\mathrm{w}_k - y_k)\hat{\alpha}_\omega \hat{p}_k^\dagger). \end{aligned} \tag{4.15}$$

It is important to note that the RWA must be performed after the change into the polaritonic basis, since it is the modes $p_L, p_U$ that oscillate harmonically in the interaction picture with respect to $H_{\mathsf{sys}} + H_{\mathsf{ext}}$ [BO14a]. In some cases, however, it may be acceptable to perform the RWA before the change of basis, followed by a rescaling of the coupling coefficients [lib14a].

### 4.3.2 Input-output theory

Having set up the correct model for the dissipation in a USC bosonic system, we must now derive equations of motion in order to extract information about the system dynamics. In this regard, we will work in the Heisenberg picture and express the system dynamics in the form of Heisenberg-Langevin equations [GZ04]. At this point, one could study the dynamics induced by Hamiltonian (4.15) for a very general class of coupling profiles $J(\omega)$, for example by Fano diagonalization [Fan61]. For our purposes, however, it shall be sufficient to deal with a simplified problem,

where a further set of approximations guided by physical intuition is made. We assume that the couplings to the continuum are sufficiently weak and smooth as to induce an (approximately) Lorentzian broadening of each resonance $\omega_k$, whose width is $\gamma_k$. The frequencies $\omega_k$ of the polaritonic modes are assumed to be well resolved, in the sense that $\gamma_L, \gamma_U \ll \omega_U - \omega_L$. All of the above amounts to a rather standard procedure in open quantum systems, where the problem is recast as a pair modes in two independent, Markovian environments. In fact, this procedure is the independent-transition approximation mentioned in the introduction of this section. Each environment corresponds to a broadband (i.e. with a width much larger than $\gamma_k$) collection of external modes $\alpha_\omega$, centred around the frequency $\omega_k$. Any finite-bandwidth effect or cross talk between these two effective environments is neglected. We can thus rephrase Eq.(4.15) as two modes in two independent environments, i.e

$$H = \sum_{k=L,U} \omega_k \hat{p}_k^\dagger \hat{p}_k + \int_k \mathrm{d}\omega \hat{\alpha}_\omega^\dagger \hat{\alpha}_\omega + \sqrt{\frac{\gamma_k}{2\pi}} \int_k \mathrm{d}\omega (\hat{p}_k \hat{\alpha}_\omega^\dagger + \hat{p}_k^\dagger \hat{\alpha}_\omega) \tag{4.16}$$

where, $\gamma_k \equiv 2\pi J^2(\omega_k)(|\mathrm{w}_k|^2 + |y_k|^2)$ has been approximated as constant in the integration range, and the suffix $k$ indicates that the integral is performed in a frequency range $\omega_k \pm \delta_k$, where $\delta_k \gg \gamma_k$ justifies a Markov approximation, but $\delta_k$ is still small enough to ensure that the ranges $\omega_k \pm \delta_k$, $\omega_{k'} \pm \delta_{k'}$ do not overlap for $k \neq k'$. We can now derive equations of motion for the system using the Heisenberg equation $\dot{\hat{A}} = i[H, \hat{A}]$,

$$\dot{\hat{p}}_k = -i\omega_k \hat{p}_k - i\sqrt{\frac{\gamma_k}{2\pi}} \int_k \mathrm{d}\omega \hat{\alpha}_\omega, \tag{4.17}$$

$$\dot{\hat{\alpha}}_\omega = -i\omega\alpha_\omega - i\sqrt{\frac{\gamma_k}{2\pi}} \hat{p}_k \tag{4.18}$$

First let us solve Eq. (4.18) for the dynamics of the environmental modes at time 't',

$$\hat{\alpha}(t) = \alpha_\omega(0)e^{-i\omega t} - i\sqrt{\frac{\gamma_k}{2\pi}}\int_0^t \hat{p}_k(t')e^{-i\omega(t-t')}\mathrm{d}t', \tag{4.19}$$

where we have specified the initial conditions of the system as $t_0 = 0$. If we now substitute Eq. (4.19) into Eq. (4.17), we can simplify the polaritonic dynamics greatly

$$\dot{\hat{p}}_k = -i\omega_k\hat{p}_k - i\sqrt{\frac{\gamma_k}{2\pi}}\int_k \mathrm{d}\omega\alpha_\omega(0)e^{-i\omega t} - \frac{\gamma_k}{2\pi}\int_k\int_0^t \hat{p}_k(t')e^{-i\omega(t-t')}\mathrm{d}\omega\mathrm{d}t'. \tag{4.20}$$

To simplify Eq. (4.20) we can define an *input field* operator,

$$\hat{p}_{k,\mathsf{in}} = -\frac{i}{\sqrt{2\pi}}\int_k \mathrm{d}\omega\alpha_\omega(0)e^{-i\omega t}, \tag{4.21}$$

which obeys the commutation rule $[\hat{p}_{k,\mathsf{in}}(t), \hat{p}^\dagger_{k',\mathsf{in}}(t')] = \delta_{kk'}\delta(t-t')$. To simplify further we can utilise the following results,

$$\int_k \mathrm{d}\omega e^{-i\omega(t-t')} = 2\pi\delta(t-t') \tag{4.22}$$

$$\int_0^t f(t')\delta(t-t')\mathrm{d}t' = \frac{f(t)}{2}, \tag{4.23}$$

which hold under our approximation that the spectrum can be assumed infinitely flat around each polaritonic mode. Taking all these results into consideration we can derive a final form for the polaritonic mode dynamics

$$\dot{\hat{p}}_k = -i\omega_k\hat{p}_k - \frac{\gamma_k}{2}\hat{p}_k + \sqrt{\gamma_k}\hat{p}_{k,\mathsf{in}}. \tag{4.24}$$

We can also derive a *time-reversed* Heisenberg-Lanegvin equation,

$$\dot{\hat{p}}_k = -i\omega_k\hat{p}_k + \frac{\gamma_k}{2}\hat{p}_k - \sqrt{\gamma_k}\hat{p}_{k,\mathsf{out}}. \tag{4.25}$$

which relates the system dynamics to the *output field* operator

$$\hat{p}_{k,\mathsf{out}} = \frac{i}{\sqrt{2\pi}} \int_k \mathrm{d}\omega \alpha_\omega(t_f) e^{-i\omega(t-t_f)}, \tag{4.26}$$

which is defined for some final time $t_f$. From Eqs. (4.24) and (4.25) we can derive the input-output relations

$$\hat{p}_{k,\mathsf{out}} = \sqrt{\gamma_k}\hat{p}_k - \hat{p}_{k,\mathsf{in}}. \tag{4.27}$$

This allows us to relate the system dynamics $\hat{p}_k$ with the output into the environment $\hat{p}_{k,\mathsf{out}}$

### 4.3.3 Propagation of quantum states into the external modes

The simplicity of our model allows us to investigate in great detail the way in which quantum states propagate from our polaritonic system and into the external field modes. In this work we shall assume that both output fields $p_{k,\mathsf{out}}$ are fully accessible; in other words, given an initial time $t_0$ and a final time $t_f$, the experimentalist may manipulate any field mode of the form $\hat{f}_k = \int_{t_0}^{t_f} \mathrm{d}t \phi_k(t) \hat{p}_{k,\mathsf{out}}(t)$, where $\int_{t_0}^{t_f} \mathrm{d}t |\phi(t)|^2 = 1$ ensures bosonic normalization. It is easy to also include non-accessible environmental modes which restrict the full collection of system information [TRPS12], but we do not include them here. Fixing $t_0 = 0$ without loss of generality, we then consider the long time limit $t_f \to \infty$, in which all the information that was present in the polaritonic system at $t = 0$ has been transferred to the external fields. Here, we are interested in the output modes that best retain such quantum information. It is then an easy exercise to show that these are given by the exponential wave-packets $\phi_k(t) = \sqrt{\gamma_k}\mathrm{e}^{i\omega_k t - \gamma_k t/2}$, yielding

$$\hat{f}_L = \hat{p}_L(0), \qquad \hat{f}_U = \hat{p}_U(0). \tag{4.28}$$

Importantly, the relations in Eq. (4.28) are expressed in the Heisenberg picture, and are valid for arbitrary initial states. Therefore, at least in principle, the experimentalist can have access to two output fields that exactly reproduce the initial system statistics.

### Initial state capture

Let us take a moment to examine in more detail how we arrived at Eq. (4.28). We wish to analyze travelling light modes of the output field that have exponential form

$$\hat{f}_k(s) = N \int_0^\infty \hat{p}_{k,\mathsf{out}} \mathrm{e}^{-st} \mathrm{d}t, \tag{4.29}$$

where $\mathrm{Re}[s] > 0$. By demanding that $f_k(s)$ respects bosonic commutation relations we impose the following normalization constant, $N = \sqrt{2\mathrm{Re}[s]}$. Allowing $s$ to be complex, we can see that this form is equivalent to a Laplace transform of $p_{k,\mathsf{out}}$. By taking the Laplace transform of Eq. (4.27) we can formulate our exponentially decaying travelling output mode in terms of the input mode and the system operator

$$\hat{f}_k(s) = N\sqrt{\gamma_k}\hat{p}_k(s) - N\hat{p}_{k,\mathsf{in}}(s), \tag{4.30}$$

where $F(s)$ is the Laplace transform of the general time dependent function F(t). If we also apply the Laplace transform on Eq. (4.24) then we can recast Eq. (4.30) in terms of the system's initial state

$$\hat{f}_k(s) = N\frac{\tau_k(s)}{\sqrt{\gamma_k}}\hat{p}_k(0) + N(\tau_k(s) - 1)\hat{p}_{k,\mathsf{in}}, \tag{4.31}$$

where $\tau_k(s) = \frac{\gamma_k}{s + i\omega_k + \frac{\gamma_k}{2}}$. $\tau_k(s)$ determines the mixture of information from $P_{k,\mathsf{in}}$ and $p_k(0)$ that will be collected by $f_k(s)$. The condition to collect the initial state

exclusively is, $\tau_k(s_0) = 1$, which is satisfied by

$$s_0^k = -i\omega_k + \frac{\gamma_k}{2}. \tag{4.32}$$

Which leaves us with,

$$\hat{f}(s_0^k) = \hat{f}_k = \hat{p}_k(0). \tag{4.33}$$

## 4.4 The importance of the $A^2$ term in the ultrastrong-coupling regime

As we have alluded to already, the counter-rotating terms may not be the only extra terms that should be taken into account in the USC regime. We must also consider the inclusion of the diamagnetic, or '$A^2$', term which becomes relevant for ultrastrong-coupling frequencies, as seen in Eq. (4.5). This term is proportional to the squared vector potential term which ensures gauge invariance in the non-relativistic minimal coupling Hamiltonian [Woo76]. There is not, however, a consensus over the correct role of this term [NC10, VGD14, BO14b]. A revealing microcosm of this disagreement is found in the research on superradiant phase transition in the Dicke model. For two-level atoms it was proved that this quantum phase transition was an artifact left by neglecting the $A^2$ term [RWZ75, RW91].

In most of the above examples the physics beyond the counter-rotating terms becomes crucial as the strength of light-matter interactions is pushed towards the extreme regime $g \sim \omega_b$. Still, for the sake of simplicity one may wonder whether there exist an intermediate USC regime in which counter-rotating terms are dominant while other effects, for example associated with $A^2$, are suppressed. In this chapter, we investigate this question for a simple polaritonic system composed of a large number of two-level emitters interacting with a single mode cavity field, and

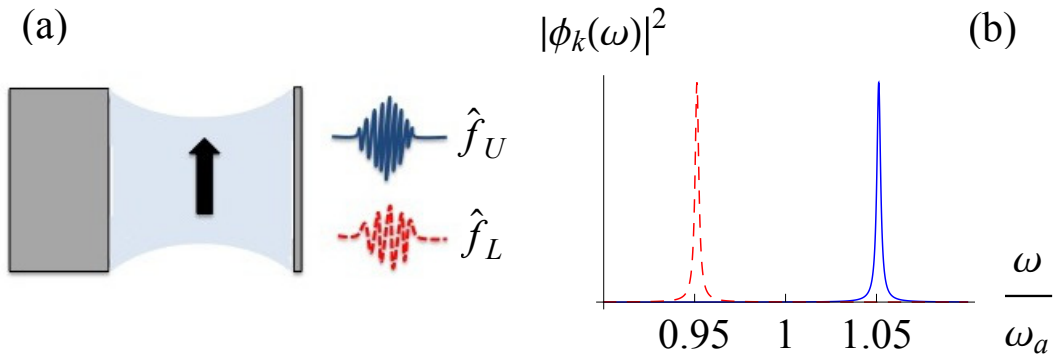


Figure 4.2: (**a**) Schematic conceptualizing the emission of the polaritonic system into the output modes $\hat{f}_U$ and $\hat{f}_L$. (**b**) Frequency distribution of the output modes $\hat{f}_U$ (blue, solid) and $\hat{f}_L$ (red, dashed), encoding the quantum statistics of the polaritons at $t_0$. We have fixed $\omega_a = \omega_b$, $g = 0.05\omega_a$, $D = g^2/\omega_b$, and chosen a frequency-independent coupling to the external modes $J(\omega) = \sqrt{\gamma/2\pi}$, where $\gamma = 0.01\omega_a$ is the decay rate of the cavity in absence of the matter mode.

find a *negative* answer. Specifically, we study the evolution of the system, initially in the bare modes vacuum, following a non-adiabatic 'switch-on' of the ultrastrong-coupling. As the system relaxes to the ground state of the coupled Hamiltonian, photons are radiated into two spectrally distinct output modes. We find that $A^2$, in combination with the TRK rules and the possibility of transitions to far detuned levels of the emitters, affect *qualitatively* the statistics of these modes. A correct description of the system beyond the RWA thus requires the inclusion of all these elements in the theoretical model. The examples we studied suggest that a correct model of the quantum emitters in the USC should include a sufficient number of transitions as to approximately saturate the TRK rule for the ground state. While in general this will result in additional theoretical difficulties for the description of the USC, we show how suitable parameter regimes can be identified in which an imperfect two-level system can be approximated by an ideal one, upon appropriately rescaling the $A^2$ term.

### 4.4.1 Non-adiabatic emission

The impact of the $A^2$ term on the emission properties of our polaritonic system can be appreciated with a simple and yet interesting example, in which the coupling $g$ is abruptly 'switched-on' from an initially negligible value. Such a modulation can be achieved, for example, in USC intersubband-cavity systems by inducing a fast change in the density of the two-dimensional electron gas [GAH+09, ATBS05, ATB+06]. Assuming the two uncoupled bare bosonic modes $\hat{a}, \hat{b}$ to be initially prepared in their vacuum state ($\hat{a}|0_a 0_b\rangle = \hat{b}|0_a 0_b\rangle = 0$), and that the coupling is non-adiabatically introduced, the system is not able to respond to the perturbation and remains in the vacuum state of the bare modes. However, for $t > 0$ the ultrastrongly coupled system will start dissipating towards the vacuum of the polaritonic modes and in order to do this it must radiate into the continuum. According to Eq. (4.28), the quantum properties of such radiation are fully captured by the output modes $\hat{f}_L, \hat{f}_U$.

Using Eqn. (4.8) and Eqn. (4.28), we can immediately recognize that the statistics of the two field modes $\hat{f}_L, \hat{f}_U$ is that of a two-mode Gaussian state of vanishing first moments. This is fully characterized by its covariance matrix, whose entries can be easily found as combinations of the Hopfield coefficients. To begin with, we turn our attention to the mean populations of the output modes, which in terms of Hopfield coefficients read

$$\langle \hat{f}_k^\dagger \hat{f}_k \rangle = n_k = |y_k|^2 + |z_k|^2. \tag{4.34}$$

A non-zero value of these quantities is perhaps the simplest signature of the influence of the counter-rotating terms on the dynamics. Figs. 4.3 and 4.4 illustrate the behaviour of $n_k$ as a function of the coupling $g$, the bare frequency difference $\omega_a - \omega_b$ and, most importantly, the parameter $D$ associated with the $A^2$ term. The TRK sum rules impose a boundary on the allowed value of D. In the case of of an electric

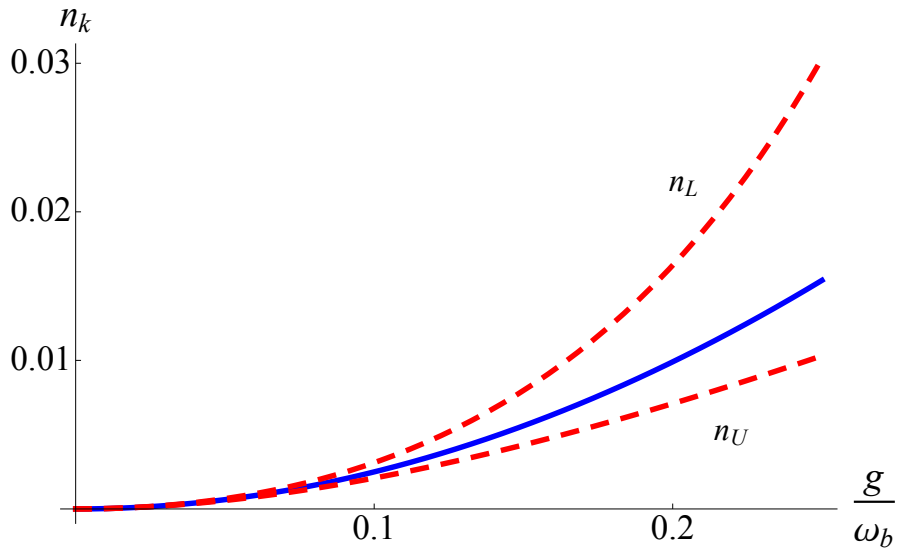


Figure 4.3: Mean population of $\hat{f}_U$ and $\hat{f}_L$ as a function of coupling strength normalized to the matter-field frequency $g/\omega_b$, when $\omega_a = \omega_b$. In this plot the blue solid line refers to $D = g^2/\omega_b$, while the red dashed line refers to $A^2$ being neglected ($D = 0$). We see that for $D = g^2/\omega_b$ the populations are distributed equally, while for $D = 0$, $n_L$ is larger.

dipole interaction between a two-level emitter and a light mode the TRK sum rule imposes [NC10]

$$D = \frac{g^2}{\omega_b}. \tag{4.35}$$

When this correct value for a two-level system is taken, we observe that the excitations are distributed equally between $\hat{f}_U$ and $\hat{f}_L$, in all the explored range of the remaining parameters $g, \omega_a, \omega_b$. Setting instead $D = 0$, which corresponds to neglecting $A^2$ but not the counter-rotating terms, results in a higher population being predicted for the lower frequency mode $\hat{f}_L$. We note that, as far as the population of the two modes is not negligible (which would correspond to the RWA), the two models are never in agreement.

### 4.4.2 Bare mode resonance

We now move on to clarify the above findings for the special case of bare mode resonance $\omega_a = \omega_b \equiv \omega_0$, where a thorough analytical understanding of the problem

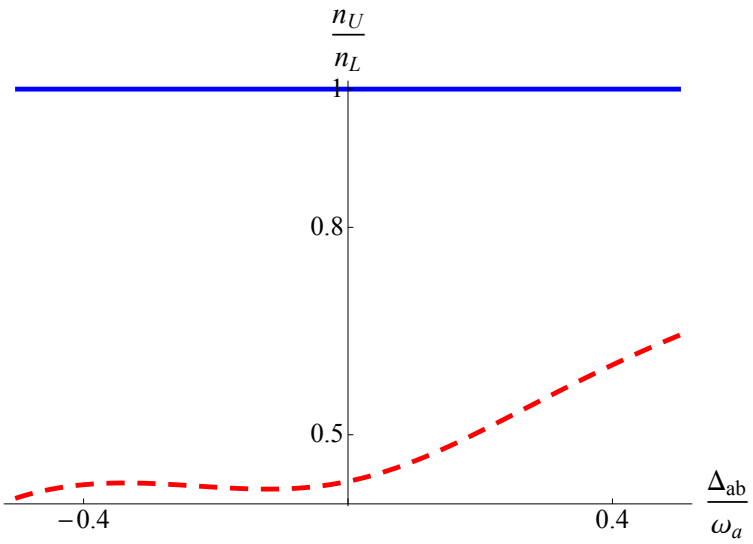


Figure 4.4: Ratio $n_U/n_L$ of the mean populations of $\hat{f}_U$ and $\hat{f}_L$ as a function of bare mode detuning $\Delta_{ab} = \omega_b - \omega_a$ for fixed coupling $g = 0.2\omega_a$. The blue solid line refers to $D = g^2/\omega_b$, while the red dashed line refers to $A^2$ being neglected ($D = 0$).

is possible. In addition, we fully characterize the output state for this case as a product of two single-mode squeezed vacuum states for the modes $\hat{f}_U, \hat{f}_L$. To do this, we explicitly diagonalize $H_{\mathsf{sys}}$, from Eq.(4.5), in two simple steps. First, consider the following 'number-conserving' transformation

$$\hat{a} = \cos\theta\hat{r}_U - \sin\theta\hat{r}_L, \quad \hat{b} = \cos\theta\hat{r}_L + \sin\theta\hat{r}_U, \tag{4.36}$$

where $\hat{r}_U, \hat{r}_L$ are independent bosonic modes that annihilate the same state as $\hat{a}, \hat{b}$. With the choice $\theta = \frac{1}{2}\tan^{-1}(g/D)$, we can recast

$$H_{\mathsf{sys}} = \sum_{k=U,L} \omega_0 \hat{r}_k^\dagger \hat{r}_k + \frac{\eta_k}{2}(\hat{r}_k + \hat{r}_k^\dagger)^2, \tag{4.37}$$

where,

$$\eta_U = D + \sqrt{g^2 + D^2}, \tag{4.38}$$

$$\eta_L = D - \sqrt{g^2 + D^2}. \tag{4.39}$$

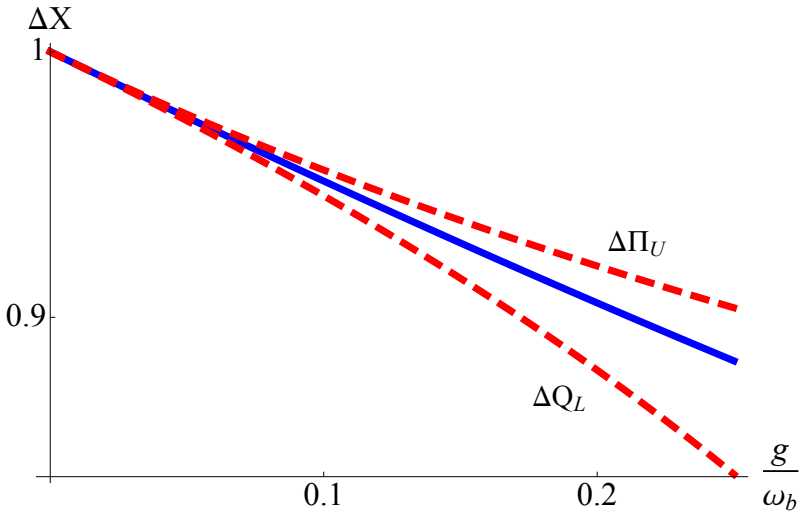


Figure 4.5: Uncertainty of the squeezed quadratures $\Delta X$, as a function of coupling strength $g$, when $\omega_a = \omega_b$. $X \in \{Q_L, \Pi_U\}$ and $\hat{Q}_L = \hat{f}_L + \hat{f}_L^\dagger, \hat{\Pi}_U = i(\hat{f}_U^\dagger - \hat{f}_U)$. We define the uncertainty as $\Delta X = \sqrt{\langle X^2\rangle - \langle X\rangle^2}$, in our case any value of uncertainty below 1 indicates squeezing. The blue solid line refers to $D = g^2/\omega_b$, while the red dashed line refers to $A^2$ being neglected ($D = 0$). We observe that for $D = g^2/\omega_b$ the output modes are squeezed equally, while for $D = 0$, $\hat{f}_L$ is more squeezed.

Note that $\eta_U > 0$ while $\eta_L < 0$. The $\hat{r}_U, \hat{r}_L$ modes do not interact, and are intimately related to the polaritonic modes $\hat{p}_U$ and $\hat{p}_L$ respectively. To complete the diagonalization we consider the squeezing transformation

$$\hat{r}_k = \cosh\xi_k \hat{p}_k - \sinh\xi_k \hat{p}_k^\dagger, \quad k = U, L, \tag{4.40}$$

which, choosing $\xi_k = \frac{1}{4}\log\left(1 + \frac{2\eta_k}{\omega_0}\right)$, reduces $H_{\text{sys}}$ to the diagonal form employed in Eq. (4.15), with the polaritonic frequencies given by $\omega_k = \sqrt{\omega_0(\omega_0 + 2\eta_k)}$. We finally note that $\omega_U > \omega_L$ and $\xi_U > 0$, while $\xi_L < 0$, signifying that $\hat{p}_U$ and $\hat{p}_L$ are obtained by squeezing the modes $\hat{r}_U$ and $\hat{r}_L$ in orthogonal quadratures. Eq. (4.40) illustrates that the vacuum states of $\hat{a}, \hat{b}$ (hence of $\hat{r}_U, \hat{r}_L$) corresponds to a product of single-mode squeezed states for $\hat{p}_L, \hat{p}_U$, and hence for the output modes $\hat{f}_L, \hat{f}_U$. This is shown in Fig. 4.5, where the behaviour of the uncertainties of the quadratures of the two output modes is illustrated as a function of the normalized coupling frequency $(g/\omega_b)$. We find that $\hat{f}_U$ and $\hat{f}_L$ are squeezed equally when the $A^2$ term

is included. If, however, it is neglected then we find that $\hat{f}_L$ is squeezed more than $\hat{f}_U$. This corresponds to our observations of the mean population in Fig. 4.3. This can be fully clarified by noting that the degree of squeezing and population of each mode is a monotone function of $|\xi_k|$. It is then useful to calculate

$$|\xi_U| - |\xi_L| = \frac{1}{4}\log\left[1 + \frac{4}{\omega_0}\left(D - \frac{g^2}{\omega_0}\right)\right], \tag{4.41}$$

which proves in a transparent manner that the two modes are squeezed equally, and thus have equal mean populations, when $D$ assumes the TRK value for a two-level system. On the other hand, the correct behaviour of squeezing and populations can never be reproduced if $D$, hence $A^2$, is neglected. We note that this result holds *for any value of the coupling* $g$, suggesting once again that counter-rotating effects, no matter how weak, cannot be properly accounted for without the inclusion of a suitable diamagnetic term in the light-matter interaction.

### 4.4.3 Imperfect two-level emitters

As anticipated, a further commodity that may need to be given up beyond the RWA is the two-level approximation. To investigate this issue in our context we enrich the structure of each emitter by considering, in addition to the levels $|g\rangle, |e\rangle$, the existence of higher excited states $|e'_j\rangle$. For simplicity, we shall keep the assumption of bare mode resonance between $\hat{a}$ and $\hat{b}$. Each transition $|g\rangle \leftrightarrow |e'_j\rangle$ has a frequency $\omega_j > \omega_0$ and is dipole coupled to the cavity field. We neglect the possibility of dipole transitions between excited states. Again, we consider collective operators $\hat{c}_j = n^{-1/2}\sum_{k=1}^{n} |g_k\rangle\langle e'_j|_k$, which together with $\hat{b}$ describe a set of mutually independent annihilation operators in the limit $n \gg 1$. Thus, the system Hamiltonian in Eq. (4.5) is modified as

$$H'_{\mathsf{sys}} = H_{\mathsf{sys}} + \sum_j \omega_j \hat{c}_j^\dagger \hat{c}_j + g_j(\hat{c}_j + \hat{c}_j^\dagger)(\hat{a} + \hat{a}^\dagger), \tag{4.42}$$

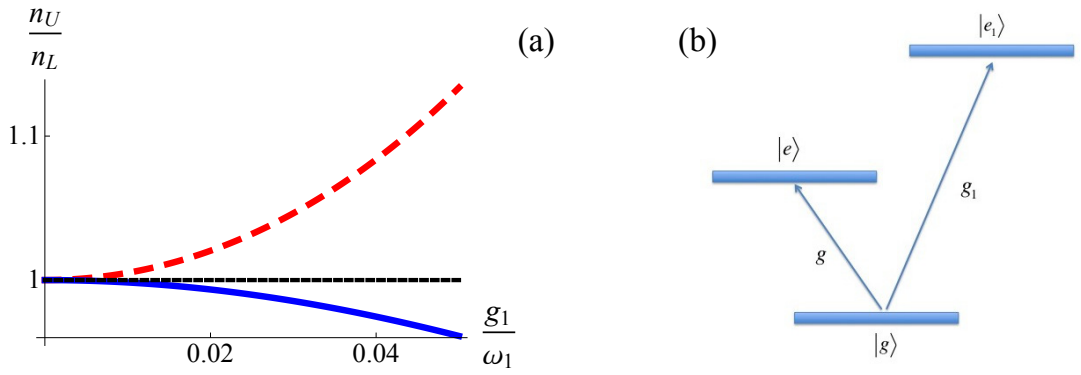


Figure 4.6: (**a**) Ratio $n_U/n_L$ of the mean populations of $\hat{f}_U$ and $\hat{f}_L$ in the case of (**b**) three-level emitters, where the third level is weakly coupled to the light mode ($g_1/\omega_1 \ll 1$). $n_U/n_L$ is plotted as a function of the third-level coupling frequency normalized to the the third-level transition frequency $g_1/\omega_1$. The blue solid line represents the model in which the full three-level system is accounted for. The red dashed line represents a two-level approximation which naively incorporates the third level in the $A^2$ term. We also include the model for a perfect two-level system as a qualitative comparison (black dotted line). We see that the deviation from the ideal two-level result, as $g_1$ is increased, is qualitatively incorrect in the naive treatment, as well as being overestimated in magnitude. Parameters: $g/\omega_0 = 0.1$ and $\omega_1/\omega_0 = 2.5$

where $g_j$ are the coupling strengths of the newly introduced transitions. Note that the TRK sum rule for the ground state now imposes a larger weight for the coefficient of $A^2$, that is $D = g^2/\omega_0 + \sum_j g_j^2/\omega_j$. The construction of the normal modes of $H'_{\text{sys}}$ in terms of bare operators, and the determination of the output fields statistics following a non-adiabatic introduction of the coupling, follow the same lines as before. We shall again focus on the statistics of the output operators $\hat{f}_L, \hat{f}_U$, being in this case defined as the two output modes with the lowest ($L$), and second-lowest ($U$) carrier frequency, respectively.

We are interested here in regimes where $g_j \ll \omega_j$, such that transitions to the higher levels are suppressed and each emitter can be expected to approximate a two-level system. Thus it may be tempting at this point to simply neglect the modes $\hat{c}_j$ and recover the Hamiltonian in Eq (4.5), valid for two-level emitters, with the only difference that $D > g^2/\omega_0$, since the $|g\rangle \leftrightarrow |e\rangle$ transition does not saturate

the sum rule anymore [NC10]. This, for example, would predict a slightly higher population and squeezing in the output mode $\hat{f}_U$ according to Eq. (4.41). It is, however, dangerous to make inconsistent, partial, approximations. For this partial approximation the higher levels are included in the $A^2$ term, but aside from this the two-level approximation persists. In Fig. 4.6 we compare this partial approximation with the full calculation employing Hamiltonian (4.42), for the simplest case in which only one extra mode $\hat{c}_1$ is considered. We find qualitative discrepancies whenever the difference of the populations is non-negligible: we can indeed observe that the full Hamiltonian can result in $n_L > n_U$. This suggests the partial inclusion of the higher levels in the $A^2$ term is erroneous.

Indeed, a naive two-level approximation cannot explain multi-level behaviour without violating the TRK sum rule, as Eq. (4.41) requires $D < g^2/\omega_0$ to achieve a higher population in the lower frequency mode. Still, in the regime $D \gtrsim g^2/\omega_0$, one may be content to neglect the fine details associated to the modes $\hat{c}_j$, and ask whether a refined two-level approximation can be found. This is indeed the case, as can be seen by adiabatically eliminating the modes $\hat{c}_j$ from Hamiltonian (4.42) [GJ10, Rr12]. This yields

$$H'_{\mathsf{sys}} \simeq H_{\mathsf{sys}} - \sum_j \frac{g_j^2}{\omega_j}(\hat{a} + \hat{a}^\dagger)^2, \tag{4.43}$$

where the contribution of higher levels is effectively removed from the $A^2$ term, such that $D \to D_{\mathsf{eff}} = g^2/\omega_0$, the TRK value for an ideal two-level system. This exactly corresponds to neglecting the difference in populations for the two output modes and this behaviour is seen for small third-level coupling frequencies in Fig. 4.6. A similar line of reasoning can be adopted if one is interested in simplifying the model by only including a small number of extra modes $\hat{c}_j$, in which case the sum in Eq. (4.43) will extend only to those modes that are neglected. This indicates that, in a consistent description of two- or multi-level emitters beyond the RWA, one should remove from the $A^2$ term the contributions of any neglected transitions.

### 4.4.4 Two mode properties

Up to this point we have specified how, by studying single mode observables, emitted by a polaritonic system after a non-adiabatic switch-on of the ultrastrong-coupling, we can gain insight into the role of the $A^2$ term. Can we do the same for two mode observables? We investigate, for the case of perfect two-level emitters, the entanglement between the two polaritonic ouput modes ($\hat{f}_U$ and $\hat{f}_L$). We plot the log-negativity ($E_N$), as a measure of entanglement [VW02, Ple05, LKPL00], versus the bare-mode detuning in the cases of the inclusion and exclusion of the $A^2$ term (*c.f* Fig. 4.7). We observe that at resonance the output modes are not entangled, regardless of whether the $A^2$ term is included or not. We find the greatest discrepancy occurs when $\omega_b > \omega_a$. In this case, we find that by neglecting the $A^2$ one would wrongly predict a greater amount of entanglement then if the $A^2$ was correctly accounted for. Entanglement is an important resource in many quantum technologies, thus it is important to know how the $A^2$ term affects this particular entanglement generation procedure.

#### Log Negativity

We construct the two-mode covariance matrix for the modes $\hat{f}_U$ and $\hat{f}_L$ in order to investigate the correlations that exist between them. As we are dealing with Gaussian states in this scenario (vacuum states), whose behaviour is completely determined by the second-order moments of the annihilation operator, knowledge of the covariance matrix is sufficient for all our calculations [Aga12]. We shall write the Gaussian two-mode state of the output modes in terms of the quadratures $Q_L$, $Q_U$, $\Pi_L$ and $\Pi_U$, defined as $Q_k = \frac{(f_k + f_k^\dagger)}{\sqrt{2}}$ and $\Pi_k = \frac{(f_k - f_k^\dagger)}{\sqrt{2}i}$, $k = L, U$. Notice that we have normalized these quadratures slightly differently to those used to quantify single-mode squeezing. The reason for this was for convenience of having a non-squeezed

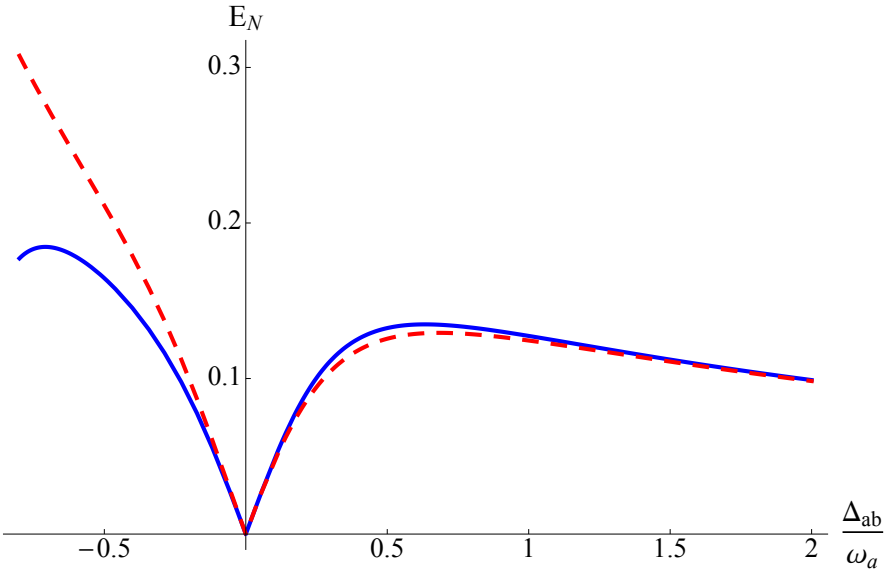


Figure 4.7: In the case of ideal two-level emitters, we plot the log-negativity ($E_N$) between $\hat{f}_U$ and $\hat{f}_L$ as a function of the normalized matter-light detuning $\Delta_{ab}/\omega_a$, for different values of D. The blue solid line represents $D = g^2/\omega_b$ and the red dashed line represents $D = 0$. Parameters: $g/\omega_a = .2$.

minimal uncertainty of 1. Now, let us a define a row vector $R$,

$$R = \begin{pmatrix} Q_L & \Pi_L & Q_U & \Pi_U \end{pmatrix}. \tag{4.44}$$

Using this vector we can construct the covariance matrix,

$$\sigma_{i,j} = \frac{1}{2}\langle R_i R_j + R_j R_i \rangle - \langle R_i \rangle \langle R_j \rangle. \tag{4.45}$$

We now have a matrix in the block form,

$$\sigma = \begin{pmatrix} \alpha_L & \gamma \\ \gamma^T & \alpha_U \end{pmatrix}. \tag{4.46}$$

Using Eqn. (4.8), the covariance matrix for the two output modes can be expressed in terms of the bare modes. Assuming that the bare modes are initially in the vacuum state we can express the covariance matrix in terms of the Hopfield coefficients. We

can now calculate the log-negativity ($E_N$) as a measure of the entanglement,

$$E_N = \max[0, -\ln(2v_-)]. \tag{4.47}$$

Where $v_-$ is defined as the smaller of the two symplectic eigenvalues of $\sigma$,

$$v_\pm = \sqrt{\frac{\widetilde{\Delta}(\sigma) \pm \sqrt{\widetilde{\Delta}(\sigma)^2 - 4\mathrm{Det}[\sigma]}}{2}}, \tag{4.48}$$

where $\widetilde{\Delta}(\sigma) = \mathrm{Det}[\alpha_L] + \mathrm{Det}[\alpha_U] - 2\mathrm{Det}[\gamma]$.

## 4.5 Remarks

By probing the emission of a simple polaritonic system in the USC regime, we have highlighted a companionship between the counter-rotating terms, $A^2$ term, and the failure of the two-level approximation. Our results indicate that a consistent description of physics beyond the RWA should display a balance between the weight of the $A^2$ term and the number of dipole transitions that are included when modeling the quantum emitters. Whenever an allowed transition is neglected, its corresponding contribution to $A^2$ should be removed from the Hamiltonian.

We remark that our results are based on a number of assumptions, on top of the dipole and Holstein-Primakoff approximations. One of these is the single-mode treatment of the field. This should hold at low enough light-matter coupling, in particular if the emitters are placed in the middle of a Fabry-Perot cavity, where the next allowed field mode vanishes. The model can be expected to show its limitations as $g$ is increased to higher and higher values [Lib14b]. Furthermore, we have neglected the possibility of dipole transitions between the excited states. By applying the TRK rules to states other than the ground state, however, one finds that some of these transitions must necessarily be allowed. Their effect may be safely

neglected if one assumes that the emitters, while in large numbers, are sufficiently diluted in space [VvDM11]. We believe that future studies trying to address one or more of these limitations will greatly benefit the understanding of the USC regime.

Finally, we note that our study concerns emitters obeying the TRK sum rules, and we have assumed that their ground–to–first excited state transition plays the major role in the light-matter interaction. Systems that do not conform to these rules, for example involving USC between a cavity field and transition between excited states [CN12], will require a separate treatment. t

# Chapter 5

# Conclusion

## 5.1 Summary of thesis achievements and outlook

In this thesis we have studied the role of quantum plasmonics in light matter-interactions on both a macroscopic and microscopic scale. We began by providing a comprehensive review on the field of quantum plasmonics, with particular attention given to the the study of plasmonic modes interacting with quantum emitters.

Following this, we examined the possibility of integrating two-level quantum dots (QD) into a plasmonic metamaterial that has a negative permeability. The unit cell of the metamaterial is a ring of plasmonic metal nanoparticles (MNP), each of which supports an electric dipole. We theoretically examined the prospect of interchanging each MNP in the ring with a MNP-QD metamolecule. Light scattered from such a metamolecule exhibits a Fano interference effect. We proved that this Fano interference effect can be manifested into the magnetic response of the metamaterial. Finally we showed that we can exploit the Fano interference to introduce dynamic tunability and nonlinearity into the metamaterial's magnetic response.

We also examined the model of a single mode of light interacting ultrastrongly

with a collection of quantum emitters, which we treat as a polaritonic system in the Holstein-Primakoff approximation. We were motivated to study this by the prospect of such a regime being attained in a quantum plasmonic setting. In particular we examined the role of the diamagnetic, or $A^2$, term in the light-matter dynamics. This term is derived from the fundamental minimal coupling Hamiltonian yet it is regularly neglected in the effective Hamiltonians used in quantum optics. We studied the relevance of the $A^2$ term by examining the emission from our system after a non-adiabatic switch-on of the light-matter coupling. This emission is split into two separate output modes, relating to the upper and lower polaritonic modes of the system. We find that the mean population will be distributed equally in each output mode if we account for the $A^2$ term. If, however, we naively neglect the $A^2$ term then we find that the population distribution is unequal. These results were verified by also examining the single mode squeezing of the output modes. The conclusion drawn from this chapter is that the $A^2$ term is *qualitatively* important in the USC and this holds true for both two-level and multi-level emitters.

In this thesis we show that the study of quantum emitters interacting with plasmonic structures is a diverse and fertile area of research. We have given examples of both fundamental results and possible real world applications. However this thesis only takes the first step. There is still much work to be done. As regards our quantum plasmonic metamaterial, the next step is to use quantum emitters to provide dynamic tunability in a negative refractive index metamaterial. We envisage two ideal milestones in this regard. The first is the deisgn of a metamaterial that combines our MNP-QD nanoring with a broadband negative permittivity background, which ensures the electric and magnetic responses overlap. In this way the negative refractive index is controlled via the magnetic response of our MNP-QD nanoring. The ultimate goal, however, would be to build upon the ideas presented in chapter 3 to combine quantum emitters and plasmonic structures in the unit cell of a metamaterial in such a way that the electric and magnetic responses could be tuned

*independently*. We believe this endeavour is a practical synergy of quantum optics, plasmonics and metamaterials, which could provide rich rewards in the future.

One of the greatest challenge for quantum plasmonics is to reduce the large amounts of dissipation associated with plasmonic modes. Until this is overcome it will be difficult to enter the USC in a practical plasmonic setting and hence the effects of the $A^2$ term will not be relevant. However, as I have mentioned in chapter 2, there are many reasons to be hopeful in this regard. The work we have presented in chapter 4 is still of fundamental importance and is relevant to a wide range of physical settings. For future work we would like to further explore the impact multi-level systems have on the $A^2$ term in the USC regime, as it is both a fundamentally intriguing *and* experimentally relevant problem.

# Appendix A

# The $A^2$ term

In this appendix we elaborate on the details used in the study of the $A^2$ term in chapter 4. Specifically, we wish to show how the system Hamiltonian used in Eq. 4.5 is derived from the minimal coupling Hamiltonian ($H_{\mathsf{mc}}$). To do so we adopt a slightly different notation to the one used in the main body of the thesis. In the main text, we found convenient to use a non-uniform notation in which the symbols $|g\rangle, |e\rangle$ denoted the ground and first excited state of a single emitter, assumed to take central role in the dynamics of interest, while the remaining levels were indicated as $|e'_j\rangle$. The corresponding bosonic modes were also grouped as $\hat{b}$, associated with the $|g\rangle \leftrightarrow |e\rangle$ transition, and $\hat{c}_j$ associated with $|g\rangle \leftrightarrow |e'_j\rangle$. For the purposes of this appendix, however, it shall be more convenient to adopt a uniform notation where we label all levels as $|\varepsilon_l\rangle$ through a single discrete index $l \geq 0$. It is assumed that the corresponding energies $\varepsilon_l$ are non-decreasing in $l$, with $l = 0$ labelling the ground state. Similarly, the collective operator associated with $|\varepsilon_0\rangle \leftrightarrow |\varepsilon_l\rangle$ shall be indicated as $\hat{b}_l$. This has the advantage of rendering the derivations to follow more compact. It is straightforward to recover the notation of the main text by associating $|g\rangle \equiv |\varepsilon_0\rangle$, $|e\rangle \equiv |\varepsilon_1\rangle$ and $\hat{b} \equiv \hat{b}_1$.

## A.1 The minimal coupling Hamiltonian

To begin we will take the case of a single emitter that can be described as a collection of non-relativistic particles, of mass $m_j$ and charge $q_j$, that are subject to a potential $\hat{V}$ which includes both trapping forces as well as inter-particle interactions. Such a system can be described by the minimal coupling Hamiltonian ($\hbar = 1$)

$$H_{\mathsf{mc}} = H_{\mathsf{field}} + \sum_j \frac{(\hat{\mathbf{p}}_j - q_j\hat{\mathbf{A}})^2}{2m_j} + \hat{V}(\hat{\mathbf{x}}_1, \hat{\mathbf{x}}_2, ...). \tag{A.1}$$

Where $H_{\mathsf{field}}$ accounts for the free field dynamics. $\hat{\mathbf{x}}_j$ is the position operator of the j-th particle and $\hat{\mathbf{p}}_j$ is it's momentum operator. We will make the dipole approximation, as such we can assume that the vector potential operator $\hat{\mathbf{A}}$ is spatially independent. Under this approximation $\hat{\mathbf{A}}$ commutes with all the particle operators, allowing us to expand the Hamiltonian as follows

$$H_{\mathsf{mic}} = H_{\mathsf{field}} + H_{\mathsf{emitter}} + H_{\mathsf{int}} + H_{\mathsf{diam}}, \tag{A.2}$$

$$H_{\mathsf{emitter}} = \sum_j \frac{\hat{\mathbf{p}}_j^2}{2m_j} + \hat{V}, \tag{A.3}$$

$$H_{\mathsf{int}} = -\sum_j \frac{q_j\hat{\mathbf{p}}_j \cdot \hat{\mathbf{A}}}{m_j}, \tag{A.4}$$

$$H_{\mathsf{diam}} = \sum_j \frac{q_j^2}{2m_j}\hat{\mathbf{A}}^2. \tag{A.5}$$

To connect this microscopic description to the effective models which are expressed in terms of emitter energy levels, we assume that $H_{\mathsf{emitter}}$ gives rise to a discrete level structure:

$$H_{\mathsf{emitter}} = \sum_l \varepsilon_l |\varepsilon_l\rangle\langle\varepsilon_l|. \tag{A.6}$$

Using the canonical commutation relations, we can express $\hat{\mathbf{p}}_j = i\, m_j[H_{\mathsf{emitter}}, \hat{\mathbf{x}}_j]$ and thus rewrite the interaction Hamiltonian as

$$H_{\mathsf{int}} = i \sum_{ll'} (\varepsilon_l - \varepsilon_{l'}) \langle \varepsilon_l | \hat{\mathbf{d}} \cdot \hat{\mathbf{A}} | \varepsilon_{l'} \rangle |\varepsilon_l\rangle\langle\varepsilon_{l'}|. \tag{A.7}$$

We have introduced the dipole operator as $\hat{\mathbf{d}} = \sum_j q_j \hat{\mathbf{x}}_\mathbf{j}$. To reduce $H_{\mathsf{mc}}$ into a more recognisable form we make the following approximations. We assume that there are no transitions between excited states. We also set the ground state energy $\varepsilon_0$ to zero, thus $\varepsilon_l$ now corresponds to the transition frequency of the $|\varepsilon_0\rangle \leftrightarrow |\varepsilon_l\rangle$ transition. We also introduce the notation

$$\hat{\sigma}_l = |\varepsilon_0\rangle\langle\varepsilon_l|, \tag{A.8}$$

$$\hat{\sigma}_l^\dagger = |\varepsilon_l\rangle\langle\varepsilon_0|. \tag{A.9}$$

Finally we also consider a single-mode quantized field ($H_{\mathsf{field}} = \omega_0 \hat{a}^\dagger \hat{a}$), whose vector potential can be written $\hat{\mathbf{A}} = \mathbf{A_0}(\hat{a} + \hat{a}^\dagger)$. By introducing the abbreviations $G_l \equiv \varepsilon_l |\langle \varepsilon_l | \hat{\mathbf{d}} \cdot \hat{\mathbf{A}} | \varepsilon_0 \rangle|$ for the light-emitter coupling frequency and $\alpha \equiv \sum_j \frac{q_j^2}{2m_j} \mathbf{A}_0^2$, we can write the effective Hamiltonian

$$H_{\mathsf{eff}} \simeq \sum_l \left[ \varepsilon_l \hat{\sigma}_l^\dagger \hat{\sigma}_l + G_l(\hat{\sigma}_l + \hat{\sigma}_l^\dagger)(\hat{a} + \hat{a}^\dagger) \right] + \omega_0 \hat{a}\hat{a}^\dagger + \alpha(\hat{a} + \hat{a}^\dagger)^2. \tag{A.10}$$

The TRK rule for the ground state [Wan99] can now be used to derive a strict relationship between the couplings $G_l$, the transition frequencies $\varepsilon_l$, and the coefficient $\alpha$, characterizing the strength of the diamagnetic term. One has

$$\sum_l \varepsilon_l \left| \langle \varepsilon_l | \hat{\mathbf{d}} \cdot \mathbf{A}_0 | \varepsilon_0 \rangle \right|^2 = \sum_j \frac{q_j^2}{2m_j} \mathbf{A}_0^2 \tag{A.11}$$

which is easily seen to correspond to the equality

$$\sum_l \frac{G_l^2}{\varepsilon_l} = \alpha. \tag{A.12}$$

## A.2 The bosonization of many emitters

Having established the key parameters of single emitters that emerge from the microscopic model, we can move on to the description of a large number $n \gg 1$ of these that interact with the same field. Following the same steps as before, the corresponding microscopic Hamiltonian can be written as

$$H_{\mathsf{eff}}^n \simeq \sum_{l,k} \left[\varepsilon_l \hat{\sigma}_{l,k}^\dagger \hat{\sigma}_{l,k} + G_l(\hat{\sigma}_{l,k} + \hat{\sigma}_{l,k}^\dagger)(\hat{a}+\hat{a}^\dagger)\right] + \omega_0 \hat{a}\hat{a}^\dagger + \alpha(\hat{a}+\hat{a}^\dagger)^2. \tag{A.13}$$

where $D \equiv n\,\alpha$ and the dummy index $k$ labels the individual emitters, which we have assumed identically coupled to the field $\hat{a}$ for simplicity. We can exploit the symmetries of Eq. (A.13) to define the collective operators

$$\hat{b}_l \equiv \frac{1}{\sqrt{n}} \sum_k \hat{\sigma}_{l,k}, \tag{A.14}$$

allowing us to rewrite

$$H_{\mathsf{eff}}^{(n)} = \sum_l \left[\varepsilon_l \hat{b}_l^\dagger \hat{b}_l + g_l(\hat{b}_l + \hat{b}_l^\dagger)(\hat{a}+\hat{a}^\dagger)\right] + D(\hat{a}+\hat{a}^\dagger)^2, \tag{A.15}$$

where $g_l \equiv \sqrt{n} G_l$. It is simple to see that this Hamiltonian is the multi-level generalization of Eq. (4.5). Comparing the definitions of $g_l$ and $D$ with Eq. (A.12), we find that the TRK sum rule translates in this case to

$$\sum_l \frac{g_l^2}{\varepsilon_l} = D \tag{A.16}$$

which in the two-level case reduces to

$$D = \frac{g^2}{\omega_b}, \tag{A.17}$$

as defined in the main body of the thesis.

# Bibliography


[AB10] R. D. Artuso and G. W. Bryant. Strongly coupled quantum dot-metal nanoparticle systems: exciton-induced transparency, discontinuous response, and suppression as driven quantum oscillator effects. *Phys. Rev. B*, 82(195419), 2010.

[ABN06] P. Anger, P. Bharadwaj, and L. Novotny. Enhancement and quenching of single molecule fluorescence. *Phys. Rev. Lett.*, 96(113002), 2006.

[AE08] A. Alù and N. Engheta. Dynamical theory of artificial optical magnetism produced by rings of plasmonic nanoparticles. *Phys. Rev. B*, 78(085112), 2008.

[Aga12] G. S. Agarwal. *Quantum optics*. Cambridge university press, 2012.

[ALT+10] A. A. Anappara, S. De Liberato, A. Tredicucci, C. Ciuti, G. Biasiol, L. Sorba, and F. Beltran. Ultrastrong light-matter coupling regime with polariton dots. *Phys. Rev. Lett.*, 105(196402), 2010.

[AMY+07] A. V. Akimov, A. Mukherjee, C. L. Yu, D. E. Chang, A. S. Zibrov, P. R. Hemmer, H. Park, and M. D. Lukin. Generation of single optical plasmons in metallic nanowires coupled to quantum dots. *Nature*, 450(402-406), 2007.

[ARH12] S. Savasta A. Ridolfo, M. Leib and M. J. Hartmann. Photon blockade in the ultrastrong coupling regime. *Phys. Rev. Lett.*, 109(193602), 2012.

[Arm09] M. Armen. *Bifurcations in single atom cavity QED.* PhD thesis, California Institute of Technology, 2009.

[ASE06] A. Alù, A. Salandrino, and N. Engheta. Negative effective permeability and left-handed materials at optical frequencies. *Opt. Express*, 14(1557), 2006.

[ATB+06] A. A. Anappara, A. Tredicucci, F. Beltram, G. Biasiol, and L. Sorba. Tunnel-assisted manipulation of intersubband polaritons in asymmetric coupled quantum wells. *Appl. Phys. Lett.*, 89(171109), 2006.

[ATBS05] A. A. Anappara, A. Tredicucci, G. Biasiol, and L. Sorba. Electrical control of polariton coupling in intersubband microcavities. *Appl. Phys. Rev. Lett.*, 87(051105), 2005.

[AvEW02] E. Altewisher, M. P. van Exter, and J. P. Woerdman. Plasmon-assisted transmission of entangled photons. *Nature*, 418:304–306, 2002.

[BBM+05] K. M. Birnbaum, A. Boca, R. Miller, A. D. Boozer, T. E. Northup, and H. J. Kimble. Photon blockade in an optical cavity with one trapped atom. *Nature*, 436:87–90, 2005.

[BDN12] I. Bloch, J. Dalibard, and S. Nascimbene. Quantum simulations with ultracold quantum gases. *Nature Physics*, 8:267–276, 2012.

[BGB11] F. Beaudoin, J. M. Gambetta, and A. Blais. Dissipation and ultrastrong coupling in circuit qed. *Phys. Rev. A*, 84(043832), 2011.

[BH83] C. F. Bohren and D. R. Huffman. *Absorption and scattering of light by small particles*. Wiley, 1983.

[BHA00] M. L. Brongersma, J. W. Hartman, and H. A. Atwater. Electromagnetic energy transfer and switching in nanoparticle chain arrays below the diffraction limit. *Phys. Rev. B*, 62(R16356), 2000.

[BL11] P. Berini and I. De Leon. Surface plasmon-polariton amplifiers and lasers. *Nature Photonics*, 6:16–24, 2011.

[BO12] M. Bamba and T. Ogawa. Dissipation and detection of polaritons in the ultrastrong-coupling regime. *Phys. Rev. A*, 86(063831), 2012.

[BO14a] M. Bamba and T. Ogawa. Reply to "comment on 'system-environment coupling derived by maxwell's boundary conditions from the weak to the ultrastrong light-matter-coupling regime' ". *Phys. Rev. A*, 89(017802), 2014.

[BO14b] M. Bamba and T. Ogawa. Stability of polarizable materials against superradiant phase transition. *arXiv:1406.2420*, 2014.

[BP02] H. P. Breuer and F. Petruccione. *The theory of open quantum systems*. Oxford University Press, 2002.

[Bra11] D. Braak. Integrability of the Rabi model. *Phys. Rev. Lett.*, 107(100401), 2011.

[BS03] D. J. Bergman and M. I. Stockman. Surface plasmon amplification by stimulated emission of radiation: quantum generation of coherent surface plasmons in nanosystems. *Phys. Rev. Lett.*, 90(027402), 2003.

[Car99] H. J. Carmicheal. *Statistical methods in quantum optics 1: master equations and Fokker-Plank equations*. Springer, Berlin, 1999.

[CBC05] C. Ciuti, G. Bastard, and I. Carusotto. Quantum vacuum properties of the intersubband cavity polariton field. *Phys. Rev. B*, 72(115303), 2005.

[CC06] C. Ciuti and I. Carusotto. Input-output theory of cavities in the ultrastrong coupling regime: the case of time-independent cavity parameters. *Phys. Rev. A*, 74(033811), 2006.

[CCS10] H. Chen, C. T. Chan, and P. Sheng. Transformation optics and metamaterials. *Nature Materials*, 9(5):387–396, 2010.

[Cer] P. Cerenkov. Visible radiation produced by electrons moving in a medium with velocities exceeding that of light. *Phys. Rev.*, 52:378–379.

[CG84] M. J. Collett and C. Gardiner. Squeezing of intracavity and traveling-wave light fields produced in parametric amplification. *Phys. Rev. A*, 30(1386), 1984.

[CN12] C. Ciuti and P. Nataf. Comment on "superradiant phase transitions and the standard description of circuit QED". *Phys. Rev. Lett.*, 109(179301), 2012.

[CS10] W. Cai and V. Shalaev. *Optical metamaterials: fundamentals and applications*. Springer, Dordecht, 2010.

[CSDL07] D. E. Chang, A. S. Sorenson, E. A. Demler, and M. D. Lukin. A single-photon transistor using nanoscale surface plasmons. *Nature Physics*, 3:807–812, 2007.

[CSHL06] D. E. Chang, A. S. Sorenson, P. R. Hemmer, and M. D. Lukin. Quantum optics with surface plasmons. *Phys. Rev. Lett.*, 97(053002), 2006.

[CTP+09] D. E. Chang, J. D. Thompson, H. Park, V. Vuletic, A. S. Zibrov, P. Zoller, and M. D. Lukin. Trapping and manipulation of isolated atoms using nanoscale plasmonic structures. *Phys. Rev. Lett.*, 103(123004), 2009.

[CVT+10] A. G. Curto, G. Volpe, T. H. Taminiau, M. P. Kreuzer, R. Quidant, and N. F. van Hulst. Unidirectional emission of a quantum dot coupled to a nanoantenna. *Science*, 329:930–933, 2010.

[CWrK11] Y. Chen, M. Wubs, J. Mørk, and A. F. Koenderink. Coherent single-photon absorption by single emitters coupled to one-dimensional nanophotonic waveguides. *New. J. Phys.*, 13(103010), 2011.

[DKB+05] J. Dintinger, S. Klein, F. Bustos, W. L. Barnes, and T. W. Ebbesen. Strong coupling between surface plasmon-polaritons and organic molecules in subwavelength hole arrays. *Phys. Rev. B*, 71(035424), 2005.

[DKF11] D. Dsotjan, J. Kaestel, and M. Fleischhauer. Dipole-dipole shift of quantum emitters coupled to surface plasmons of a nanowire. *Phys. Rev. B*, 84(075419), 2011.

[DKW98] H. Dung, L. Knoll, and D. Welsch. Three dimensional quantization of the electromagnetic field in dispersive and absorbing inhomogeneous dielectrics. *Phys. Rev. A*, 57:3931–3942, 1998.

[EB04] C. Emary and T. Brandes. Phase transitions in generalized spin-boson (Dicke) models. *Phys. Rev. A*, 69(053804), 2004.

[Fan61] U. Fano. Effects of configuration interaction on intensities and phase shifts. *Phys. Rev.*, 124(1866), 1961.

[FIM05] M. Fleischhauer, A. Imamoglu, and J. P. Marangos. Electromagnetically induced transparency: optics in coherent media. *Rev. Mod. Phys.*, 77:633–673, 2005.

[FRM+05] S. Fasel, F. Robin, E. Moreno, D. Erni, N. Gisin, and H. Zbinden. Energy-time entanglement preservation in plasmon-assisted light transmission. *Phys. Rev. Lett.*, 94(110501), 2005.

[GAH+09] G. Gunter, A. A. Anappara, J. Hees, A. Sell, G. Biasiol, L. Sorba, S. De Liberato, C. Ciuti, A. Tredicucci, A. Leitenstorfer, and R. Huber. Sub-cycle switch-on of ultrastrong light–matter interaction. *Nature (London)*, 458(178), 2009.

[GB10] D. K. Gramotnev and S. I. Bozhevolnyi. Plasmonics beyond the diffraction limit. *Nature Photonics*, 4:83–91, 2010.

[GCJA13] T. Grujic, S. R. Clark, D. Jaksch, and D. G. Angelakis. Repulsively induced photon superbunching in driven resonator arrays. *Phys. Rev. A*, 87(053846), 2013.

[GFDHM11] V. Giannini, A. L. Fernández-Dominguez, S. C. Heck, and S. A. Maier. Plasmonic nanoantenas: fundamentals and their use in controlling the radiative properties of nanoemitters. *Chem. Rev.*, 111:3888–3912, 2011.

[GJ10] O. Gamel and D.F.V. James. Time-averaged quantum dynamics and the validity of the effective Hamiltonian model. *Phys. Rev. A*, 82(052106), 2010.

[GMK75] L. Genzel, T. P. Martin, and U. Kreibig. Dielectric function and plasma resonances of small metal particles. *Z. Physik B*, 21:339–346, 1975.

[Gre98] W. Greiner. *Classical electrodynamics*. Springer, New York, 1998.

[GTC+12] M. Gullans, T. G. Tiecke, D. E. Chang, J. Feist, J. D. Thompson, J. I Cirac, P. Zoller, and M. D. Lukin. Nanoplasmonic lattices for ultracold atoms. *Phys. Rev. Lett.*, 109(235309), 2012.

[GV07] Y. Gong and J. Vuković. Design of plasmon cavities for solid-state cavity quantum electrodynamics applications. *Appl. Phys. Lett.*, 90(033133), 2007.

[GZ04] C. W. Gardiner and P. Zoller. *Quantum noise*. Springer, 2004.

[Hal86] W. P. Halperin. Quantum size effects in metal particles. *Rev. Mod. Phys.*, 58:533–606, 1986.

[HB92] B. Huttner and S. M. Barnett. Quantization of the electromagnetic field in dielectrics. *Phys. Rev. A*, 46(4306), 1992.

[HFJGVZ13] T. Hummer, L. Martín-Moreno F. J. García-Vidal, and D. Zueco. Weak and strong coupling regimes in plasmonic-QED. *Phys. Rev. B*, 87(115419), 2013.

[HKSA11] A. Huck, S. Kumar, A. Shakoor, and U. L. Andersen. Controlled coupling of single nitrogen-vacancy center to a silver nanowire. *Phys. Rev. Lett.*, 106(096801), 2011.

[HLC+11] N. J. Halas, S. Lal, W-S. Chang, S. Link, and P. Nordlander. Plasmons in strongly coupled metallic nanostructures. *Chem. Rev.*, 111:3913–3961, 2011.

[Hop58] J. J. Hopfield. Theory of the contribution of excitons to the complex dielectric constant of crystals. *Phys. Rev.*, 112(1555), 1958.

[HP40] T. Holstein and H. Primakoff. Field dependence of the intrinsic domain magnetization of a ferromagnet. *Phys. Rev.*, 58(1098), 1940.

[HPM+12] O. Hess, J. B. Pendry, S. A. Maier, R. F. Oulton, J. M. Hamm, and K. L. Tsakmakidis. Active nanoplasmonic metamaterials. *Nature Materials*, 11(572), 2012.

[HS10] A. Hatef and M. R. Singh. Plasmonic effect on quantum coherence and interference in metallic photonic crystals doped with quantum dots. *Phys. Rev. A*, 81(063816), 2010.

[HWTH10] J. M. Hamm, S. Wuestner, K. L. Tsakmakidis, and O. Hess. Theory of light amplification in active fishnet metamaterials. *Phys. Rev. Lett.*, 107(167405), 2010.

[ILKJ03] A. Ishimaru, S. W. Lee, Y. Kuga, and V. Jandhyala. Generalized constitutive relations for metamaterials based on the quasi-static lorentz theory. *IEEE. Trans. Antennas Propag.*, 51(2550), 2003.

[JKWB08] Y. C. Jun, R. D. Kekatpure, J. S. White, and M. L. Brongersma. Nonresonant enhancement of spontaneous emission in metal-dielectric-metal plasmon waveguide structures. *Phys. Rev. B*, 78(153111), 2008.

[JS11] Z. Jacob and V. M. Shalaev. Plasmonics goes quantum. *Science*, 334:463–464, 2011.

[KCdA11] F. H. L. Koppens, D. E. Chang, and F. J. García de Abajo. Graphene plasmonics: a platform for strong light-matter interactions. *Nano Lett.*, 11:370–377, 2011.

[KEW+06] M. Klein, C. Enkrich, M. Wegener, C. M. Soukoulis, and S. Linden. Single split ring resonators at optical frequency: limits of size scaling. *Optic Letters*, 31:1259–1261, 2006.

[KGB+09] R. Koselov, B. Grotz, G. Balasubramanian, R. J. Stohr, A. A. L. Nicholet, P. R. Hemmer, F. Jelezko, and J. Wrachtrup. Wave-particle duality of single surface plasmons polaritons. *Nature Physics*, 5:470–474, 2009.

[KGR+08] M. Kroner, A. O. Govorov, S. Remi, B. Biedermann, S. Seidl, A. Badolato, P. M. Petroff, W. Zhang, R. Barbour, B. D. Gerardot, R. J. Warburton, and K. Karrai. The nonlinear Fano effect. *Nature*, 451(311), 2008.

[KHRS06] S. Kuhn, U. Hakanson, L. Rogobete, and V. Sandoghdar. Enhancement of single-molecule fluorescence using a gold nanoparticle as an optical nanoantenna. *Phys. Rev. Lett.*, 97(017402), 2006.

[Kuh25] W. Kuhn. *Z. Phys.*, 33(408), 1925.

[KV95] U. Kreibig and M. Vollmer. *Optical properties of metal clusters*. Springer berlin, 1995.

[KXB93] O. Keller, M. Xiao, and S. I. Bozhevolnyi. Optical diagmagnetic polarizability of a mesoscopic metallic sphere: transverse self-field approach. *Opt. Commin.*, 102:238–244, 1993.

[LGCC09] S. De Liberato, D. Gerace, I. Carusott, and C. Ciuti. Extracavity quantum vacuum radiation from a single qubit. *Phys. Rev. A*, 80(053810), 2009.

[lib14a] S. De liberato. Comment on "System-environment coupling derived by Maxwell's boundary conditions from the weak to the ultrastrong light-matter-coupling regime". *Phys. Rev. A*, 89(117801), 2014.

[Lib14b] S. De Liberato. Light-matter decoupling in the deep strong coupling regime: the breakdown of the Purcell effect. *Phys. Rev. Lett.*, 112(016401), 2014.

[LKPL00] J. Lee, M. S. Kim, Y. J. Park, and S. Lee. Partial teleportation of entanglement in the noisy environment. *J. Mod. Opt*, 47(2151), 2000.

[lMLWX09] l. Mao, Z. Li, B. Wu, and H. Xu. Effects of quantum tunneling in metal nanogap on surface-enhanced raman scattering. *Appl. Phys. Lett.*, 94(243102), 2009.

[LSY+12] N. P. De Leon, B. J. Shields, C. L. Yu, D. E. Englund, A. V. Akimov, M. D. Lukin, and H. Park. Tailoring light-matter interaction with a nanoscale plasmon resonator. *Phys. Rev. Lett.*, 108(226803), 2012.

[LZM+10] B. Luk'yanchuck, N. I. Zheludev, S. A. Maier, N. J. Halas, P. Nordlander, H. Giessen, and C. T. Chong. The Fano resonance in plasmonic nanostructures and metamaterials. *Nature Materials*, 9(707), 2010.

[Mai07] S. A. Maier. *Plasmonics: fundamentals and applications*. Springer, New York, 2007.

[MAK+11] V. M. Muravev, I. V. Andreev, I. V. Kukushkin, S. Schmult, and W. Dietsche. Observation of hybrid plasmon-photon modes in microwave transmission of coplanar microresonators. *Phys. Rev. B*, 83(075309), 2011.

[MCGTMM+11] D. Martin-Cano, A. González-Tudela, L. Martín-Moreno, F. J. García-Vidal, C. Tejedor, and E. Moreno. Dissipation-driven generation of two-qubit entanglement mediated by plasmonic waveguides. *Phys. Rev. B*, 84(235306), 2011.

[MdAN11] A. Manjavacas, F. J. García de Abajo, and P. Nordlander. Quantum plexcitonics: strongly interacting plasmons and excitons. *Nano Lett.*, 11(2318), 2011.

[MNdA12] A. Manjavacas, P. Nordlander, and F. J. García de Abajo. Plasmon blockade in nanostructured graphene. *ACS Nano*, 6:1724–1731, 2012.

[Mon02] C. Monroe. Quantum information processing with atoms and photons. *Nature*, 416(238), 2002.

[MOS+09] B. Min, E. Otsby, V. Sorger, E. Ulin-Avila, L. Yang, X. Zhang, and K. Vahala. High-q surface-plasmon-polariton whispering gallery microcavity. *Nature*, 457:455–458, 2009.

[MOS+11] R. Ma, R. F. Oulton, V. Sorger, G. Bartal, and X. Zhang. Room-temperature sub-diffraction-limited plasmon laser by total internal reflection. *Nature Materials*, 10:110–113, 2011.

[MS10] D. K. Morits and C. R. Simovski. Negative effective permeability at optical frequencies produced by rings of plasmonic dimers. *Phys. Rev. B*, 81(205112), 2010.

[MS11] D. K. Morits and C. R. Simovski. Isotropic negative effective permeability in the visible range produced by clusters of plasmonic triangular nanoprisms. *Metamaterials*, 5(4):162–168, 2011.

[MTMK14a] K. R. McEnery, M. S. Tame, S. A. Maier, and M. S. Kim. Tunable negative permeability in a quantum plasmonic metamaterial. *Phys. Rev. A*, 89(013822), 2014.

[MTMK14b] K. R. McEnery, T. Tufarelli, S. A. Maier, and M. S. Kim. Non-adiabatic emission of ultrastrongly-coupled oscillators: signatures of the $a^2$ term. *arXiv:1407.7446*, 2014.

[NC10] P. Nataf and C. Ciuti. No-go theorem for superradiant quantum phase transitions in cavity QED and counter-example in circuit QED. *Nature Commun.*, 1(72), 2010.

[NDH+10] T. Niemczyk, F. Deppe, H. Huebl, E. P. Menzel, F. Hocke, M. J. Schwarz, J. J. Garcia-Ripoll, D. Zueco, T. Hümmer, E. Solano, A. Marx, and R. Gross. Circuit quantum electrodynamics in the ultrastrong-coupling regime. *Nature Physics*, 6(772), 2010.

[Nor07] D. J. Norris. Photonic crystals: a view of the future. *Nature Materials*, 6:177–178, 2007.

[NZB+09] M. A. Noginov, G. Zhu, A. M. Belgrave, R. Bakker, V. M. Shalaev, E. E. Narimanov, S. Stout, E. Herz, T. Suteewong, and U. Wiesner. Demonstration of a spaser-based nanolaser. *Nature*, 460:1110–1112, 2009.

[OSZ+09] R. F. Oulton, V. J. Sorger, T. Zentgraf, R. Ma, C. Gladden, L. Dai, G. Bartal, and X. Zhang. Plasmon lasers at deep subwavelength scale. *Nature*, 461:629–632, 2009.

[PBS06] W. J. Padilla, D. N. Basov, and D. R. Smith. Negative refractive index metamaterials. *Materials Today*, 9(28), 2006.

[Pen00] J. B. Pendry. Negative refraction makes a perfect lens. *Phys. Rev. Lett.*, 85(3966), 2000.

[PHRS99] J. B. Pendry, A. J. Holden, D. Robbins, and W. J. Stewart. Magnetism from conductors and enhanced nonlinear phenomena. *Microwave theory and technique, IEEE transactions*, 47:2075–2089, 1999.

[PHSY96] J. B. Pendry, A. J. Holden, W. J. Stewart, and I. Youngs. Extremely low frequency plasmons in metallic mesostructures. *Phys. Rev. Lett.*, 76:4773–4776, 1996.

[Ple05] M. B. Plenio. Logarithmic negativity: a full entanglement monotone that is not convex. *Phys. Rev. Lett.*, 95(090503), 2005.

[PS09] V. N. Pustovit and T. V. Shahnazyan. Cooperative emission of light by an ensemble of dipoles near a metal nanoparticle: the plasmonic Dicke effect. *Phys. Rev. Lett.*, 102(077401), 2009.

[PSS06] J. B. Pendry, D. Schurig, and D. R. Smithith. Controlling electromagnetic fields. *Science*, 312:1780–1782, 2006.

[Pur46] E. M. Purcell. Resonance absorption by nuclear magnetic moments in a solid. *Phys. Rev.*, 69(674), 1946.

[RB95] P. R. Rice and R. J. Brecha. Cavity induced transparency. *Opt. Commun.*, 126:230–235, 1995.

[RBH01] J. M. Raimond, M. Brune, and S. Haroche. Manipulating quantum entanglement with atoms and photons in a cavity. *Rev. Mode. Phys*, 73(565), 2001.

[RGH+06] X. F. Ren, G. P. Gou, Y. F. Huang, C. F. Li, and G. C. Guo. Plasmon-assisted transmission of high-dimensional orbital angular-momentum entangled state. *Europhys. Lett.*, 76:753–759, 2006.

[Rr12] F. Reiter and A. S. Sørensen. Effective operator formalism for open quantum systems. *Phys. Rev. A*, 85(032111), 2012.

[RSF+10] A. Ridolfo, O. Di Stefano, N. Fina, R. Saija, and S. Savasta. Quantum plasmonics with quantum dot-metal nanoparticle molecules: influence of the Fano effect on photon statistics. *Phys. Rev. Lett.*, 105(263601), 2010.

[RW91] K. Rzazewski and K. Wódkiewicz. Stability of matter interacting with photons. *Phys. Rev. A*, 43(593), 1991.

[RWZ75] K. Rzazewski, K. Wódkiewicz, and W. Zakowicz. Phase transitions, two-level atoms, and the $A^2$ term. *Phys. Rev. Lett.*, 35, 1975.

[SBW+10] J. A. Schuller, E. S. Barnard, W., Y. C. Jun, J. S. White, and M. L. Brongersma. Plasmonics for extreme light concentration and manipulation. *Nature Materials*, 9:193–204, 2010.

[SBZ+11] C. Stehle, H. Bender, C. Zimmermann, D. Kern, M. Fleischer, and S. Slama. Plasmonically tailored micropotentials for ultracold atoms. *Nature Photonics*, 5:494–498, 2011.

[SCC+05] V. M. Shalaev, W. Cai, U. K. Chettiar, H. Yuan, A. K. Sarychev, V. P. Drachev, and A. V. Klidishev. Negative index of refraction in optical metamaterials. *Opt. Lett*, 30(3356), 2005.

[Sha07] V. M. Shalaev. Optical negative-index metamaterials. *Nature Photonics*, 1(41), 2007.

[SHGE11] T. Schwartz, J. A. Hutchison, C. Genet, and T. W. Ebbeson. Reversible switching of ultrastrong light-molecule coupling. *Phys. Rev. Lett.*, 106(196405), 2011.

[Sim11] C. R. Simovski. On electromagnetic characterization and homogenization of nanostructured metamaterials. *J. Opt.*, 13(013001), 2011.

[SK00] D. R. Smith and N. Kroll. Negative refractive index in left-handed materials. *Phys. Rev. Lett.*, 85:2933 – 2936, 2000.

[SML+13] F. Shafiei, F. Monticone, K. Q. Le, X. X. Liu, T. Hartsfield, A. Alù, and X. Li. A subwavelength plasmonic metamolecule exhibiting magnetic-based optical Fano resonance. *Nature Nanotechnology*, 8(95), 2013.

[SPV+00] D. R. Smith, W. J. Padilla, D. C. Veir, S. C. Nemat-Nasser, and S. Schultz. Composite medium with simultaneously negative permeability and permittivity. *Phys. Rev. Lett.*, 84(4184), 2000.

[SPW04] D. R. Smith, J. B. Pendry, and M. C. K. Wiltshire. Metamaterials and negative refractive index. *Science*, 305:799–792, 2004.

[SSR+10] S. Savasta, R. Saija, A. Ridolfo, O. Di Stefano, P. Denti, and F. Borghese. Interaction nanopolaritons: Vacuum Rabi splitting with a single quantum dot in the center of a dimer. *ACS Nano*, 4:6369–6376, 2010.

[ST09] C. R. Simovski and S. A. Tretyakov. Model of isotropic resonant magnetism in the visible range based on core-shell clusters. *Phys. Rev. B*, 79(045111), 2009.

[SW11] C. M. Soukoulis and M. Wegener. Past achievements and future challenges in the development of three-dimensional photonic metamaterials. *Nature Photonics*, 5(523), 2011.

[TAC+12] Y. Todorov, A. M. Andrews, R. Colombelli, S. De Liberato, C. Ciuti, P. Klang, G. Strasser, and C. Sirtori. Ultrastrong coupling regime and plasmon polaritons in parabolic semiconductor quantum wells. *Phys. Rev. Lett.*, 108(106402), 2012.

[Tan99] S. M. Tan. A computational toolbox for quantum and atomic optics. *J. Opt. B*, 1(424), 1999.

[TH08] A. Trugler and U. Hohenester. Strong coupling between a metal nanoparticle and a single molecule. *Phys. Rev. B*, 77(115403), 2008.

[Tho25] W. Thomas. *Naturwissenschaften*, 13(627), 1925.

[TMÖ+13] M. S. Tame, K. R. McEnery, S. K. Özdemir, J. Lee, S. A. Maier, and M. S. Kim. Quantum plasmonics. *Nature Physics*, 9(329), 2013.

[TRPS12] T. Tufarelli, A. Retzker, M. B. Plenio, and A. Serafini. Input–output Gaussian channels: theory and application. *New. J. Phys.*, 14(093046), 2012.

[TYT+97] J. Takahara, S. Yamagisha, H. Taki, A. Morimoto, and T. Kobayashi. Guiding of a one-dimensional optical beam with nanometer diameter. *Opt. Lett*, 22:475–477, 1997.

[Ves68] V. G Veselago. The electrodynamics of substances with simultaneusly negative values of $\epsilon$ and $\mu$. *Sov. Phys. Usp.*, 10(509), 1968.

[VGD14] A. Vukics, T. Grieber, and P. Domokos. Elimination of the A-square problem from cavity qed. *Phys. Rev. Lett.*, 112(073601), 2014.

[VKH12] C. Van Vlack, P. T. Kristensen, and S. Hughes. Spontaneous emission spectra and quantum light-matter interactions from a strongly coupled quantum dot metal-nanoparticle system. *Phys. Rev. B*, 85(075303), 2012.

[VvDM11] O. Viehmann, J. von Delft, and F. Marquardt. Superradiant phase transitions and the standard description of circuit QED. *Phys. Rev. Lett.*, 107(113602), 2011.

[VW02] G. Vidal and R. F. Werner. Computable measure of entanglement. *Phys. Rev. A*, 65(032314), 2002.

[VWC09] F. Verstraete, M. M. Wolf, and J. I Cirac. Quantum computation and quantum-state engineering driven by dissipation. *Nature Physics*, 5:633–636, 2009.

[VWP+13] P. Vasa, W. Wang, R. Pomraenke, M. Lammera, M. Maiuri, C. Manzoni, G. Cerullo, and C. Lienau. Real time observations of ultrafast Rabi oscillations between excitons and plasmons in metal nanostructures with J-aggregates. *Nature Photonics*, 7(128-132), 2013.

[Wan99] S. Wang. Generalization of the Thomas-Reiche-Kuhn and the Bethe sum rules. *Phys. Rev. A*, 60(262), 1999.

[WM08] D. F. Walls and G. J. Milburn. *Quantum optics*. Springer, Berlin, 2008.

[Woo76] R. G. Wooley. Gauge invariance and the thermodynamics of the electromagnetic field. *J. Phys. A: Math. Gen.*, 9(L15), 1976.

[WS10] E. Waks and D. Sridharan. Cavity QED treatment of interactions between a metal nanoparticle and a dipole emitter. *Phys. Rev. A*, 82(043845), 2010.

[WZJZ03] J. Wang, Y. Zhu, K. J. Jiang, and M. S. Zhan. Bichromatic electromagnetically induced transparency in cold rubidium atoms. *Phys. Rev. A*, 68(063810), 2003.

[YPV09] V. Yannopapas, E. Paspalakis, and N. V. Vitanov. Plasmon-induced enhancement of quantum interference near metallic nanostructures. *Phys. Rev. Lett.*, 103(063602), 2009.

[YZD+08] J. Y. Yan, W. Zhang, S. Duan, X. G. Zhao, and A. O. Govorov. Optical properties of coupled metal-semiconductor and metal-molecule nanocrystal complexes: role of multipole effects. *Phys. Rev. B*, 77(165301), 2008.

[ZFP+05] Shuang Zhang, Wenjun Fan, N. C. Panoiu, K. J. Malloy, R. M. Osgood, and S. R. J. Brueck. Experimental demonstration of near-infrared negative-index metamaterials. *Phys. Rev. Lett.*, 95(137404), 2005.

[ZG11] W. Zhang and A. O. Govorov. Quantum theory of the nonlinear Fano effect in hybrid metal-semiconductor nanostructures: the case of strong nonlinearity. *Phys. Rev. B*, 84(R081405), 2011.

[ZGB06] W. Zhang, A. O. Govorov, and G. W. Bryant. Semiconductor-metal nanoparticle molecules: hybrid excitons and the nonlinear Fano effect. *Phys. Rev. Lett.*, 97(146804), 2006.

[ZKK+05] J. Zhou, Th. Koschny, M. Kafesaki, E. N. Economou, J. B. Pendry, and C. M. Soukoulis. Saturation of the magnetic response of split-ring resonators at optical frequencies. *Phys. Rev. Lett.*, 95(223902), 2005.

[ZL08] X. Zhang and Z. Liu. Superlenses to oversome the diffraction limit. *Nature Materials*, 7:435–441, 2008.

[ZPN09] J. Zuloaga, E. Prodan, and P. Nordlander. Quantum description of the plasmon resonances of a nanoparticle dimer. *Nano Lett.*, 9(2):887–891, 2009.

[ZXY11] X. Zeng, J. Xu, and Y. Yang. Spontaneous emission interference enhancement with a $\mu$-negative metamaterial slab. *Phys. Rev. A*, 84(033834), 2011.